TECHNISCHE UNIVERSITÄT MÜNCHEN

Studienfakultät Brau- und Lebensmitteltechnologie

Lehrstuhl für Brau- und Getränketechnologie

Ultrasound based PAT-concept for online monitoring of fermentative bioprocesses.

Sven Hoche

Vollständiger Abdruck der von der Fakultät Wissenschaftszentrum Weihenstephan für Ernährung, Landnutzung und Umwelt der Technischen Universität zur Erlangung des akademischen Grades eines

Doktor-Ingenieurs (Dr.-Ing.)

genehmigten Dissertation.

Vorsitzender: Prof. Dr.-Ing. Ulrich Kulozik

Prüfer der Dissertation:

1. Prof. Dr.-Ing. Thomas Becker

2. Prof. Dr.-Ing. Hermann Nirschl

Die Dissertation wurde am 24.10.2016 bei der Technischen Universität München eingereicht und durch die Fakultät Wissenschaftszentrum Weihenstephan für Ernährung, Landnutzung und Umwelt am 15.07.2017 angenommen.

Acknowledgements

I want to thank Prof. Becker for the provision of the workplace and the electronics; however, in particular for the liberty that was granted to me throughout the research project.

Especially, I want to thank the Wissenschaftsförderung der Deutschen Brauwirtschaft e.V., whose support allowed the realisation of the project ultimately. Further thanks deserve to all those scientists whose numerous trials, works and publications have created the basis for this work.

I would also like to thank all the colleagues of the Institute of Brewing and Beverage Technology for the excellent cooperation and support. In particular, mention may be made here: Dr. M. A. Hussein - stimulating discussions with him have contributed significantly to the quality of the work; Dr. Simone Mack, Daniel Krause, Dominik Ullrich Geier and Ronny Takacs - without the humorous conversation with you the time at the BGT would have been nowhere near as colorful and cheerful as it was.

Of course, I want to thank my family, especially my parents, without whose support and education I would never have reached this point in my life.

Big thanks to my wife Janine, who more than once had to postpone her or both of our interests to allow the completion of this work – and, in spite of everything, has managed over and over again that I never lose track of the really important things in life.

And finally I want to thank all the friends, with special mention of:
Frank Buchheister: Epitome of eloquence and supporter of many humanitarian establishments - thanks for the many motivational talks.
Family Wipfler - Thanks for broaden my horizon.

Publications

Peer reviewed publications

1. Hoche, S., Krause, D., Hussein, M. A., Becker, T.: Ultrasound based, in-line monitoring of anaerobe yeast fermentation: model, sensor design and process application. International Journal of Food Science and Technology 51 (2016), 710–719. DOI: 10.1111/ijfs.13027.
2. Hoche, S., Hussein, M. A., Becker, T.: Density, ultrasound velocity, acoustic impedance, reflection and absorption coefficient determination of liquids via multiple reflection method. Ultrasonics 57 (2015), 65–71. DOI: 10.1016/j.ultras.2014.10.017.
3. Hoche, S., Hussein, M. A. & Becker, T.: Critical process parameter of alcoholic yeast fermentation: speed of sound and density in the temperature range 5–30 °C. International Journal of Food Science and Technology 49 (2014), 2441–2448. DOI: 10.1111/ijfs.12566.
4. Hoche, S., Hussein, M. A., Becker, T.: Ultrasound-based density determination via buffer rod techniques: a review. Journal of Sensors and Sensor Systems 2 (2013), 103–125. DOI: 10.5194/jsss-2-103-2013.

Conference contributions

Oral presentations

1. Hoche, S.; Hussein M.A.; Becker, T.: Non-invasive, ultrasound based measurement system – The basics. EBC Symposium 2011, Copenhagen, Denmark, 2012.
2. Hoche, S.; Hussein M.A.; Becker, T.: Ultrasound based density determination via specific acoustic impedance: review and validation of methods, Vortrag; EUROPACT 2011. Glasgow, UK, 2011.
3. Hoche, S.; Elfawakhry, H.; Hussein M.A.; Becker, T.: Möglichkeiten und Grenzen der Ultraschallmesstechnik in der Brautechnologie, Vortrag; Technologisches Seminar Weihenstephan 2011. Weihenstephan, Germany, 2011.
4. Hoche, S., Hussein, M. A., Becker, T.: Ultrasonic Measurement Techniques for Process Monitoring using the Example of Concentration Monitoring of

Fermentation Fluids. Workshop: Rote und Weiße Biotechnologie: Herstellung von Substanzen mittels Fermentationsverfahren, deren Aufarbeitung und Reinigung. Hanau, Germany, 2010.

5. Hoche, S., Elfawakhry, H., Hussein, M. A., Becker, T.: Ultrasonic monitoring system for kneading control. 9th European Young Cereal Scientists and Technologists Workshop. Budapest, Hungary, 2010.

Poster presentations

6. Hoche, S.; Hussein M.A.; Becker, T.: Nicht-invasive, online Dichtebestimmung mittels ultraschallbasierender Mehrfach-Reflektions-Methode. 11. Dresdner Sensorsymposium. Dresden, Germany, 2013.
7. Hoche, S., Hussein, M. A., Becker, T.: Ultrasonic measurement techniques for process monitoring using the example of concentration monitoring of fermentation fluids. Bioprozessorientiertes Anlagendesign. Nürnberg, Germany, 2010.
8. Hoche, S., Hussein, W. B., Hussein, M. A., Becker, T.: Time of flight prediction for fermentation process in-line application. 9. Dresdner Sensor-Symposium. Dresden, Germany, 2009.

Table of Contents

Abstract

Due to the progressive application of process analytical technologies the non-destructive, real-time monitoring of fermentative bioprocesses is increasingly in the interest of science. The long-term target is to relate the monitored product qualities via critical process parameters to the performance of the entire process and thereby gain a deeper understanding overall.

Within the scope of the investigated example (anaerobe yeast fermentation) the critical quality attributes were narrowed down to the temporal characteristics of alcohol and sugar content and to determine the course of the process, the process parameters of temperature, density and ultrasonic velocity (USV) can be used. In turn, the ultrasonic measurement technology provides relevant advantages over other non-destructive methods related to the technological implementation and costs and via ultrasound based buffer methods and the reflection method the density of a medium can be determined. The Multiple Reflection Method (MRM) was evaluated as particularly advantageous for the application. The method provides the combined determination of USV and density on the basis of the amplitude and time analysis of three useful sound signals.

Previous knowledge gaps in the field have been eliminated through extensive experimental studies, particularly related to the relationships between the main component concentrations and the critical process parameters. The resulting model resulted in the following primary objective requirements concerning the error amounts of process parameters: UPS: <0.5 m/s, temperature: <0.1°C and density <0.5 kg/m³. Validation studies showed that theoretically accuracies in the range 0.5 % g/g by weight of sugar and 0.3% g/g by weight ethanol are possible which could be confirmed by the fermentation experiments. Decisive limiting factor is the limited amplitude accuracy and the resulting variations of the reflection coefficient. An improvement in the overall measurement accuracy can be achieved by the improvement of the measurement technology: a higher time resolution and the reduction of the signal-to-noise ratio.

Zusammenfassung

Die zerstörungsfreie, Echtzeitüberwachung fermentativer Bioprozesse steht aufgrund des voranschreitenden Einsatzes von Prozess-Analyse-Technologien zunehmend im Interesse der Wissenschaft. Langfristiges Ziel ist es dabei die überwachten Produktqualitäten über kritische Prozessparameter mit dem Prozessverlauf in Zusammenhang zu bringen und dadurch ein tieferes Gesamtverständnis zu erlangen.

Im Rahmen des untersuchten Beispiels (anaerobe Hefefermentation) konnten die kritischen Qualitätsattribute auf den zeitlichen Verlauf des Alkohol- und Zuckergehalt reduziert werden und um den Prozessverlauf zu erfassen, können die Prozessparameter Temperatur, Dichte und Ultraschallgeschwindigkeit (USV) herangezogen werden. Die Ultraschallmesstechnik wiederum bietet bezogen auf die technologische Implementierung und die Kosten Vorteile gegenüber anderen zerstörungsfreien Methoden und kann im Rahmen der Dämpfer-Methoden über den Reflexionskoeffizienten auch die Dichte eines Mediums erfassen. Basierend auf den Resultaten einer Literatur- und Methodenrecherche wurde die Multiple-Reflexion-Method (MRM), die basierend auf der Amplituden- und Zeitauswertung von drei Nutzsignalen die kombinierte Bestimmung von USV und Dichte ermöglicht, als bezogen auf die Anwendung besonders vorteilhaft bewertet.

Bisherige Erkenntnislücken auf dem Gebiet wurden durch weitreichende experimentelle Untersuchungen, insbesondere bezüglichen der Zusammenhänge zwischen den Hauptkomponentenkonzentrationen und den kritischen Prozessparametern, beseitigt. Das resultierende Modell ergab folgende primäre Zielanforderungen bezüglich der Fehlerbeträge der Prozessparameter: USV: < 0.5 m/s, Temperatur: < 0.1°C und Dichte < 0,5 kg/m³. Die Validierungsuntersuchungen ergaben, dass theoretisch Genauigkeiten im Bereich 0.5%g/g Masseanteil Zucker und 0.3%g/g Masseanteil möglich sind, was durch Gärversuche bestätigt werden konnte. Maßgeblich limitierender Faktor ist die begrenzte Amplitudengenauigkeit und die daraus resultierenden Schwankungen des Reflexionskoeffizienten. Eine Verbesserung der Gesamtmessgenauigkeit kann durch eine Verbesserung der Messtechnik: eine höhere Zeitauflösung und die Reduktion des Signal zu Rauschen Verhältnis, realisiert werden.

1 Introduction

1.1 Online concentration monitoring of anaerobe yeast fermentation in beverage industries

The need for reliable online measurement technology arises from the desire of producing more steadily improved product qualities and to reduce simultaneously waste and production costs. The realisation of these objectives through an improved understanding of the interrelations between physical-chemical bulk properties and molecular structure-forming properties are often confined due to the limited technological possibilities and the seasonal variations in raw materials. As a result, more attention was drawn to the monitoring of important raw materials and product properties during the production and storage which caused an increasing interest in real-time capable analysis systems, particularly in pharmaceutical, chemical and food industry. Finally, the realisation of these structures was summarised as Process Analytical Technology (PAT) end even dignified through governmental recommendations like the guidance of the U.S. Food and Drug Administration (FDA) (framework 2004). The central element of this technology is the use of various tools to characterise the relationships between process flow and product quality, ensuring an effective assessment of product quality, which again reveals the fundamental need of real-time monitoring technology. In combination with the rapidly advancing development of one-chip control systems this need entails the in-depth, application-oriented investigation of non-invasive sensor technologies. Through the employment of these technologies a deeper understanding of the process, an improved, more efficient production will be generated and will finally lead to new, innovative developments.

In this context, the present work is concerned with two central points of a PAT implementation for fermentative bioprocesses: the identification and determination of critical quality attributes (CQA) and process parameters (CPPs) and the development of a process measurement system for an in-line, real-time monitoring of the CPPs. The investigation of these points was performed process specifically on the basis of anaerobic yeast fermentation of malt based raw materials. Containing, it might be specified that the following described monitoring system is neither intended to

determine the CPPs of the overall process of beer fermentation nor to cover all of the quality attributes of the beer. A characterisation of the CQA of malt or wort and a corresponding monitoring and control of CPP has to be realised in the preceding sub-processes.

Substantial progress in nondestructive testing of foodstuffs has been made particularly with the use of infrared and nuclear magnetic resonance measurement techniques However, up to now the practical application remains limited due to the substantial costs. In comparison, the realisation of compact ultrasonic measurement systems is significantly cheaper and easier to implement, so that significant importance is attached to the use of ultrasound for non-invasive food characterisation and consequently became the focus of interest in recent decades.

Of particular importance in the development of a sensor, is the localisation and characterisation of the desired field of application. Eventually, the application specifies relevant boundary conditions and leads via a tightly interlocked decision-making chain from the measuring problem to the finished probe. The classification of the process and the specification of the measuring problem is characterised by the following summarising questions and answered subsequently by comprehensive explanations:

1. What are the important, crucial attributes for the characterisation of the sub-process anaerobic yeast fermentation in the overall process of beer production?
2. What are relevant, variable process parameters and which ones are essential with respect to the detection of critical process attributes?
3. How can the acquisition of critical process parameters be realised and what other technical boundary conditions result from the chosen method of determination?

A central part of the anaerobic yeast fermentation is the material transformation of the dissolved sugars to ethanol and CO_2 by the yeast cells. Closely related to this transformation are a number of other biochemical reactions of the energy and nutrient resources metabolism of the yeast, which inter alia contribute significantly to the aroma formation of the beer. While a small amount of the generated CO_2 is

physically bound in the liquid, the insoluble fraction rises and thereby removes volatile, partly undesirable flavor components. Nevertheless, considering the composition of the wort, the type, amount and the physiological state of the pitching yeast and the apparatus / equipment used as known, no longer modifiable start condition, then the concentrations course of the main components can be referred to as an essential attribute for the qualitative process evaluation.

If the above mentioned starting conditions clearly set out the further course of the process is significantly influenced by the technological process management - essential in the anaerobic fermentation of beer is the process control of pressure and temperature within the instrumental, technological possibilities. An on-line determination of the concentrations of main components dissolved in the liquid: sugar and ethanol, in turn, may only be realised via a relation to primary, physical properties which are directly affected by the concentration changes. Investigations on binary mixtures of water and various types of sugars (Contreras*, et al.* 1992; Gepert and Moskaluk 2007; Flood*, et al.* 1996) have shown that a unique concentration determination by viscosity, optical refractive index, density and ultrasonic velocity as a function of temperature is possible. The paper also suggested (Contreras*, et al.* 1992) that in particular the ultrasonic velocity has a high sensitivity to the particular investigated sugar type. The investigation of ternary mixtures of water with sucrose and ethanol (Schöck and Becker 2010) clearly show the opposite density sensitivity of both solvates, so that in combination with the temperature and a further characteristic quantity an unambiguous determination of the concentration proportions is possible. The use of models based on linear, proportional addition of the respective property characteristic of the pure components, such as the Urick- (Urick 1947), Natta Baccaredda- - (Natta and Baccaredda 1948) or Nomoto equation (Nomoto 1958), fail in case of associated (polar) liquids (Resa*, et al.* 2005). Even semi-empirical approaches in which the property characteristic of the water-ethanol mixture is applied as solvent and only the type of sugar is used as a solvate in terms of the above mentioned equations show an unsatisfactory accuracy (Resa*, et al.* 2005).

Studies on sound absorption confirm these fundamental problems in the description of polar liquids. While a combination of the theories for viscous and thermal

relaxation could be used successfully to describe the sound absorption of non-associated, non-polar liquids, these approaches failed in associated, polar liquids such as water and alcohol (Dukhin and Goetz 2002). Within polar liquids or mixtures of them strong intermolecular forces cause the expression of superimposed structures, which are considered in theoretical approaches through the bulk viscosity (D'Arrigo 1974; Bhatia 2012; Litovitz and Davis 1965; Kinsler 2000). Practically, however, exact values for the bulk viscosity are known for very few liquids; and even less is known about the temperature dependence or the bulk viscosity of mixtures of polar liquids. An approach for the theoretical description of the expression of the characteristics of water-sugar-ethanol mixtures based on extensive investigations of structural volume characteristics therefore appears very promising, but these approaches are unlikely to be successful when it comes to determining the component concentrations of unknown mixtures. In summary it can be said that the exact characterisation of the characteristic expressions of water-sugar-ethanol mixtures with theoretical approaches based on known data is not possible and the use of empirical data is required.

As mentioned above, the apparatus used is an essential boundary condition for the anaerobic fermentation. Here, cylindroconical tanks (CCT) are the most often built and installed large tank types in the fermentative beverage industries. Thus, the CCT's of the Research Brewery Weihenstephan represent a wide range of application-related constraints and lend themselves to practical investigations with the desired measurement system. However, due to the historical development, especially in this type of tank it has to be considered that in practice both installations exist: outdoor-types (installation, with or without insulation) and in building-types (indoor installation). Particularly with temperature-sensitive measurement methods, which the ultrasound-based buffer methods damper unquestionably belong to, variable temperature gradients (day-night cycle, yearly cycle, etc.) in this regard have to be considered as a boundary condition for the desired measurement system. The density plays a central role in the concentration determination of water-sugar-ethanol mixtures. First of all, compared with the dependencies to the component concentrations the density shows marginal, almost negligible temperature sensitivity and secondly the density shows in the relevant concentration range an opposite

sensitivity to the two solvates: decreasing density with increasing ethanol concentration and increasing density with increasing glucose concentrations. In contrast, most of the other online capable methods to determine the density (e.g.: radiometric or resonance vibration method) are uttermost unsuitable for the application in the fermentation tank. The reasons range from high security requirements, over low acceptance and high investment and maintenance costs to method inherent bypass implementations. One of the few methods that offer not only a feasible inline determination of the density but also the added benefit of a combined ultrasonic velocity determination is the ultrasound-based buffer method.

1.2 Ultrasound based buffer methods – fundamentals and simplifications

The key to the comprehension of the buffer methods is the understanding of sound propagation across planar interfaces; explained simplified in the following text for normal incidence. Any wave that encounters an interface will be partly transmitted and partly reflected (Figure 1.1 shows a simplified schematic with an incident wave traveling in positive direction, +x). The ratios which describe the two parts with respect to the incident wave are the reflection and the transmission coefficients.

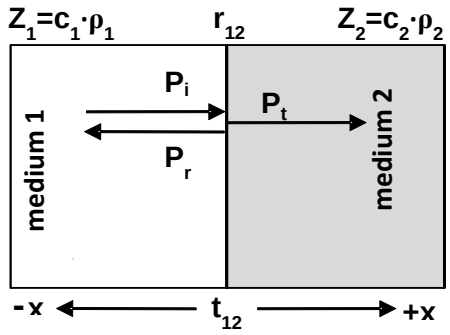

Figure 1.1: Simplified reflection and transmission of a plane wave normally incident on a planar interface; p… pressure; c… sound velocity; ρ… density; r… reflection coefficient; t… transmission coefficient; indices: 1,2,… medium specifics; i… incident; r… reflected; t… transmitted

Pressure description of the incident wave:

$$\mathrm{P_i} = p_i e^{j(\omega t - kx)} \quad (1)$$

, the transmitted wave:

$$\mathrm{P_t} = p_t e^{j(\omega t - kx)} \quad (2)$$

, and the reflected wave:

$$\mathrm{P_r} = p_r e^{j(\omega t + kx)} \quad (3)$$

, with the complex pressure amplitude p, the circular frequency ω, the wave number k and the axial dimension x.

According to conservation of energy the conditions at the interface can be derived by the continuity of pressure, P (equal pressure on both sides of the boundary) and the continuity of the normal components of velocity, v (equal normal components of the particle velocities on both sides of the boundary), leading to:

$$P_i + P_r = P_t$$
$$v_i + v_r = v_t \quad (4)$$

and the ratio

$$\frac{P_i + P_r}{v_i + v_r} = \frac{P_t}{v_t} \quad (5).$$

Further on the specific acoustic impedance, Z of a homogenous plane wave is defined as ratio of pressure and particle velocity or as product of density, ρ_m and sound velocity of a medium, c_m:

$$\mathrm{Z} = \frac{P}{v} = \rho_m \cdot c_m \quad (6).$$

For the above described interphase example (6) leads to:

$$\mathrm{Z}_1 = \frac{P_i}{v_i} = -\frac{P_r}{v_r} \qquad \mathrm{Z}_2 = \frac{P_t}{v_t} \quad (7).$$

Equation (5) combined with the relations of (7) results in:

$$Z_1 \frac{P_i + P_r}{P_i - P_r} = Z_2 \quad (8)$$

, and leads to the well-known description of the pressure reflection coefficient:

$$\mathrm{r}_{12} = \frac{P_r}{P_i} = \frac{\mathrm{Z}_2 - \mathrm{Z}_1}{\mathrm{Z}_2 + \mathrm{Z}_1} \quad (9).$$

The fundamental concept of all buffer methods is the determination of the acoustic reflection coefficient at an interphase. The formation of single sound pulses can be specified based upon the plane wave propagation. And by constituting ratios of certain pulse specifications, unknown parameters of the pulse specifications can be eliminated resulting in a simple amplitude description of the reflection coefficient (see chapter 2.2.1).

The determination of the density via the buffer methods is up to the knowledge of the properties of at least one interface material, the buffer. Knowing the buffer's acoustic impedance and the reflection from the amplitude description offers the impedance determination of the unknown interphase partner via equation (9). Further on, being able to measure the sound velocity of the unknown medium provides the calculation of the medium density via equation (6).

Up to this point the density determination via buffer-rid techniques seems to be mounted upon two simple cornerstones. Indeed, the preceded description illustrate that the foundation of the buffer methods structure is the plane wave propagation, an idealised simplification of the reality. In the following sections the different steps of

simplification will be specified to show weather the negligence for the measurement application is feasible or not.

The first level of simplification is the assumption that the specific acoustic impedance, fundamentally defined as ratio of excess pressure to particle velocity, satisfies the density – sound velocity product (see equation (6)). Technically speaking this relation is only satisfied for the plane wave simplification in the acoustic far field which is defined as the region beyond the Fresnel distance, $z_0 = a^2/\lambda$ (Cheeke 2012), whereby a is the radius of a circular plane radiator and λ the wavelength. Within the far field the difference between observation point to source center point distance, r and distance to the true source area, r' becomes small and negligible (compare Figure 1.3 & 1.4),

Indeed the quotient of acoustic pressure and particle velocity results in a complex representation and can be derived from the displacement of a particle in a plane sound wave:

$$u(x,t) = u_0 \cdot e^{(-\alpha x)} \cdot e^{i(\omega t - \varphi)} \tag{10}$$

, whereby u_0 is the peak particle velocity amplitude, $\varphi = kx$ is the phase, $k = 2\pi/\lambda$ the wavenumber, $\omega = 2\pi f$ the circular frequency, f the frequency, and α the damping coefficient (in Np/m). Thereby one obtains following equation:

$$u(x,t) = u_0 \cdot e^{\left[i\frac{2\pi}{\lambda}\left(c_m t - x\left(1 - i\frac{\lambda\alpha_m}{2\pi}\right)\right)\right]} \tag{11}.$$

According to Hooke's law and the definition of the acoustic pressure one obtains for a longitudinal wave:

$$\mathrm{P} = \frac{F}{A} = -K\frac{\partial u}{\partial x} \tag{12}$$

, and with $\mathrm{c} = \sqrt{K/\rho}$

$$\mathrm{P} = -\rho_m \cdot {c_m}^2 \frac{\partial u}{\partial x} = -\rho_m \cdot {c_m}^2 i\frac{2\pi}{\lambda}\left(1 - i\frac{\lambda\alpha_m}{2\pi}\right)u(x,t) \tag{13}$$

, whereby F is the vertical force acting on a surface element, A the area of the surface element and K the compression or bulk modulus. The particle velocity is the first time derivative of the particle displacement.

$$\mathrm{v} = \frac{\partial u(x,t)}{\partial t} = i\frac{2\pi c_m}{\lambda}u(x,t). \tag{14}$$

Therefore the ratio of acoustic pressure and particle velocity results in:

$$\frac{P}{v} = \rho_m \cdot c_m(1 - i\frac{\alpha_m \lambda}{2\pi}) \quad (15)$$

, which reveals the relation between the complex sound velocity, c_c and the medium sound velocity c_m:

$$c_m = c_c \cdot \frac{1}{(1 - i\frac{\alpha_m \lambda}{2\pi})} = c_c \cdot CF \quad (16)$$

For simplicity, further on the relating term will be called complex factor CF. The characteristic for varying absorption regions as well as relevant sound velocities and frequencies is shown in Figure 1.2.

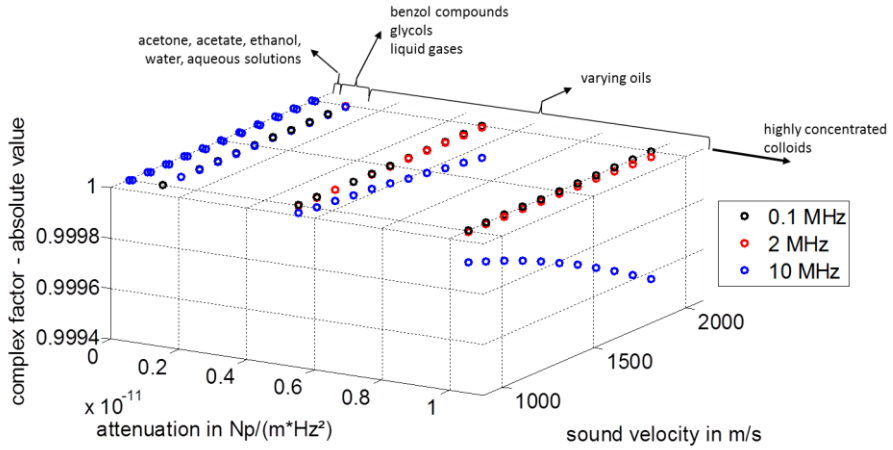

Figure 1.2: Absolute representation of the complex factor for liquid typically attenuation and sound velocity regions for the frequencies 0.1, 2 and 10 MHz.

The valuation shows that for relevant liquids and frequencies the expected difference between complex sound velocity and “far field” sound velocity is in the range < 1%. Only for very high frequencies and highly attenuating fluids significant deviations can be expected. For aqueous solutions as they are relevant within this work, the deviations are in the range < 2ppb. So, the simplification represented by equation (6) is feasible. Anyway, in case of dramatically higher frequencies or a significant higher attenuation, a reconsideration of the relations is appropriate.

The second level of simplification is the assumption of the planar wave propagation in general. Finally, the wave is generated by a real transducer whose dimensions are as limited as it is the energy of the generated wave. One of the most fundamental properties of plane waves is the constancy of the amplitude and phase of each acoustic property on each plane perpendicular to the propagation direction. For real acoustic wave fronts of real acoustic transducer with limited radiating surface, however, this applies only approximately and even in very large distances

from the wave origin only. The clearest mathematical illustration of this simplification can be obtained from the spherical wave propagation. Again, the acoustic impedance is derived from the quotient of sound pressure and particle velocity. With $v = \frac{U_0}{r\rho_m c_m}\left[1 - \frac{i}{rk}\right] e^{i(\omega t - kr)}$ and $P = \frac{U_0}{r} e^{i(\omega t - kr)}$ one derives (see Cheeke (2012)):

$$\mathrm{Z} = \frac{P}{\mathrm{v}} = \rho_m c_m \left(\frac{k^2 r^2}{(1 + k^2 r^2)} + i \frac{kr}{(1 + k^2 r^2)} \right) \quad (17).$$

The absolute value of the acoustic impedance is:

$$|\mathrm{Z}| = \left|\frac{P}{\mathrm{v}}\right| = \rho_m c_m \frac{kr}{\sqrt{1 + k^2 r^2}} = \rho_m c_m \cos\theta \quad (18)$$

, whereby θ is the phase angle between real and imaginary part. This makes clear that for kr >> 1 (which is another description of the far field region), the difference between real and imaginary component becomes negligible and the assumption of a plane wave is feasible. In contrast, the sound field description of a real sound source is significantly more complex. It is assumed that each infinitesimal surface element of the source vibrates uniformly with the speed $v = V_0 \exp(j\omega t)$ normal to the surface and emits the same elementary spherical wave (see Cheeke (2012), Kinsler (2000)):

$$p(r,t) = \frac{i\rho c V_0}{\lambda r} e^{i(\omega t - kr)} \quad (19)$$

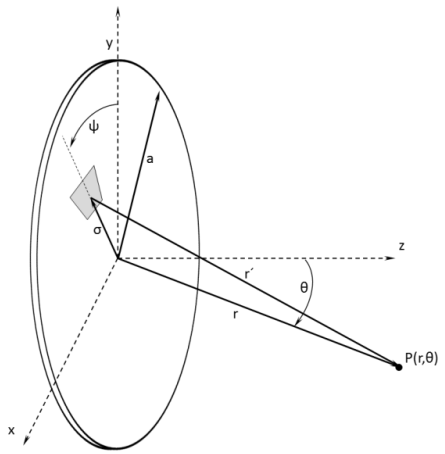

Figure 1.3: Illustration of the geometrical variables of the acoustic pressure distribution of a circular, plane sound source; a… transducer radius, σ, r, ψ, θ… circular coordinates to describe geometrically the infinitesimal surface area and the observation point; P(r, θ)… acoustic property at the observation point defined through r and θ; r'… distance between surface area and P.

In any, geometrically unique defined point of observation each acoustical property can be described according to the Huygens principle as a superposition of all wavelets. According to the illustration of the geometrical terms in Figure 1.3, the following equation results to calculate the sound pressure distribution of a circular, flat sound source:

$$\mathrm{P}(\mathrm{r},\theta) = \frac{i\rho c k}{2\pi} V_0 \int_0^a \sigma d\sigma \int_0^{2\pi} \frac{e^{i(\omega t - k\acute{r})}}{\acute{r}} d\psi \quad (20)$$

, whereby V_0 is the velocity peak amplitude of the transducer surface and r' the distance between observation point and surface element.

$$\acute{r} = \sqrt{r^2 + \sigma^2 - 2r\sigma sin\theta cos\psi} \quad (21)$$

A general, closed-form solution of this integral is too complex for practical use (Zemanek 1971; Weyns 1980a; Weyns 1980b), so generally numerical integration methods are used to derive a solution effectively. However, simple, closed-form solutions are possible for the central acoustic axis (z-axis: r'= (r² + σ²) ½) and sufficiently large distances from the sound source (far-field solution: r >> a). A comparison of the different solutions is shown in Figure 1.4. The systematic fluctuations within the near field, which is confined by the last characteristic maximum at zλ/a², can be identified clearly. Further on, the difference between far field solution and the actual characteristics of the pressure amplitude is presented. Even at a distance of twice the near field, significant deviations are identifiable. Thus, the feasibility of simplifications for the acoustic far field even at distances beyond the near field is restricted. Other interesting aspects become apparent upon the consideration of the transverse pressure amplitude distributions. In deed the distribution in the near field is also axisymmetric but by no means homogeneous Also in the transverse direction characteristic, local minima and maxima appear (compare Figure 1.4).

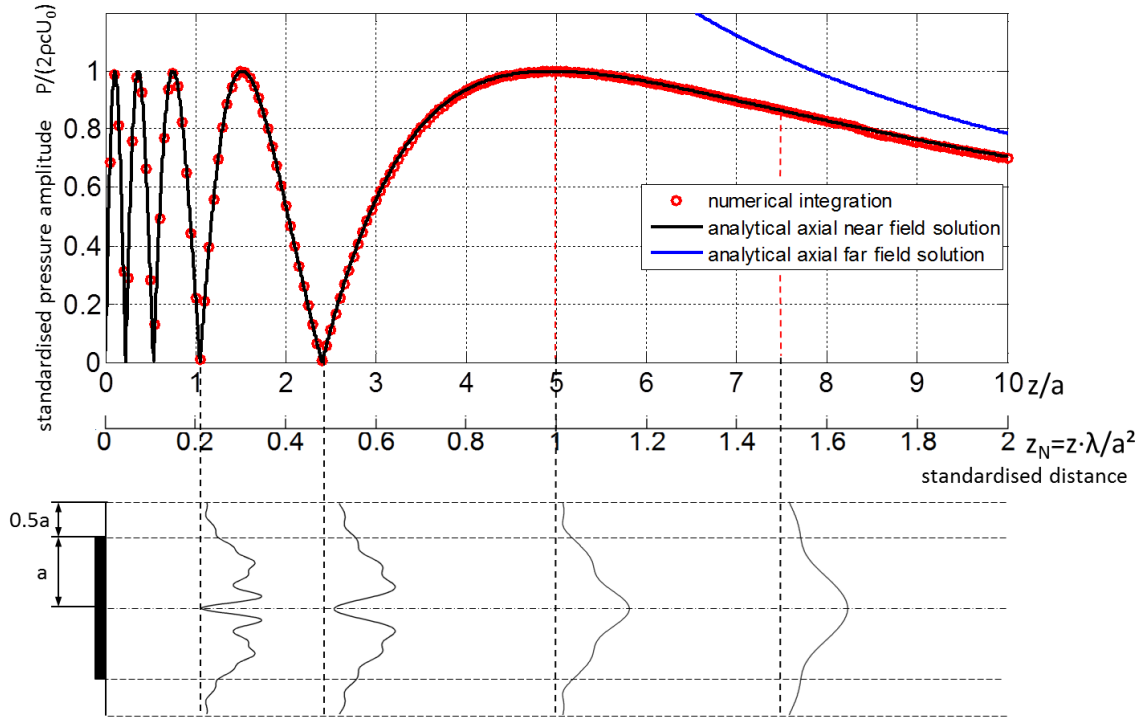

Figure 1.4: Comparison of analytical, numerical and far field solution. Top: Axial distributions of the standardised acoustic pressure ($P/2\rho c_0 U_0$; whereby U_0 is the velocity amplitude at x=0, c_0 the sound velocity and ρ the density of the medium) along the central propagation axis, z generated by an acoustic source with circular surface with radius a defined through the ratio a/λ=5. Below: transverse distribution of the numerical integration for the distances: 0.22, 0.5, 1 and 1.5 z_N.

In particular for the application of the buffer methods the wave diffraction is of importance which deviates from the assumed plane wave propagation. Due to the spherical propagation of the elementary waves some of the signal energy is radiated into regions, which is beyond the detectable corridor of a transducer of similar size. Is the pulse-echo method applied or a receiver of similar size in terms of the sender-receiver principle is used, disproportionately high signal losses are determinable in relation to the initial deflection and compared with the expected, exponential signal attenuation. The comparison of normalised sound fields for different transducer radius to wavelength ratios clearly shows the strong dependence of the near field characteristics on the acoustic constraints. With increasing ratio coefficient (a/λ), the number of the fluctuations increases dramatically, while in the region >1 NAA (normalised axial distance NAA = zλ / a²) changes are hardly perceptible.

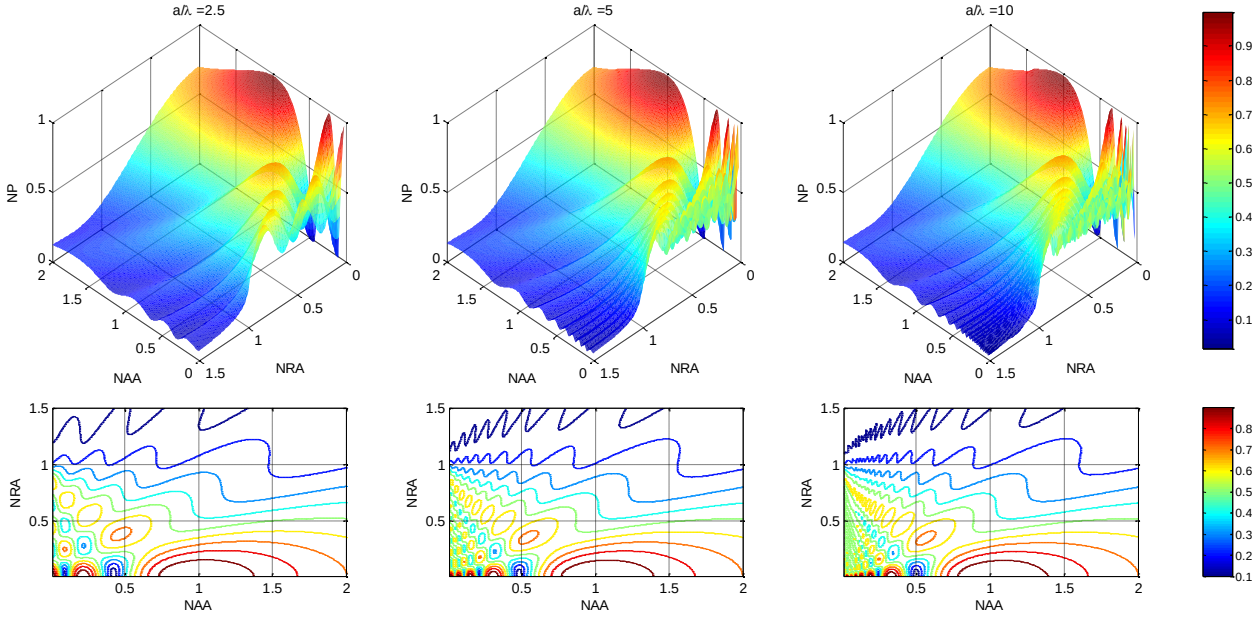

Figure 1.5: Results of numerical sound field calculations displayed in surface and contour-line plots for the transducer radius to wavelength ratios: 2.5, 5, and 10; NP… normalised pressure amplitude ($P/2\rho c_0 U_0$; whereby U_0 is the velocity amplitude at x=0); NAA… normalised axial distance ($z\lambda/a^2$); NRA… normalised, radial distance (x/a).

Whether the differences between theoretical real and ideal, plane wave (following called diffraction) can be neglected for the ultrasound-based density determination or not, in turn, is highly dependent on the applied method to determine the reflection coefficient and the selected materials and methods. By reviewing relevant publications in the field of ultrasound buffer methods, the classification in four key subcategories was possible (see 2.2.1): the multiple-reflection method (MRM), the

reference reflection method (RRM), the transmission method (TM) and the angular reflection method (ARM). All four categories use the plane wave propagation as the basic concept and are subject to the above described method immanent limitations in a real application. In two of the four sub-categories: RRM and ARM, it is potentially possible to determine the reflection coefficient irrespective of a diffraction correction. In either case, signals might be evaluated that are received at similar standardised distance to the sound source. Both methods, however, were excluded for the intended application due to the following listed reasons:

- Depending on implementation only a separate or inaccurate determination of ultrasound speed is possible.
- At least the RRM requires the determination of reference values.
- For the intended application, moreover, significant and potentially variable temperature gradients have to be considered as boundary conditions. The consideration of all potential gradients would involve extensive calibrations.

In case of applying the transmission method with low accuracy requirements one can abstain from diffraction correction when choosing ideal dimensions and an optimum reference medium. This is not valid in cases in which signal with different distances to the sound source are evaluated, as the TMOR of Henning*, et al.* (2000) or the R_echo12_12 Methode of Bjørndal and Frøysa (2008). Due to the complex sensor designs by the receiver implementation, the often not negligible sound attenuation in the liquid, and the not to be underestimated calibration effort the TM was excluded for the intended application.

Eventually, the MRM was identified as the optimal method for the determination of relevant parameters to determine component concentrations during the anaerobic yeast fermentation in cylindroconical fermentation tanks (CCT). A method immanent realisation of ultrasonic velocity determination can be realised comparatively simple. The determination of all relevant result parameters is possible within a single ultrasound signal, without further reference signals, and methods-based the attenuation can be neglected. Thus, a large part of temperature gradient caused effects can be neglected, which may represent an immense source of error in all reference methods (RRM, ARM). However, the amplitude evaluation of at least three

user signals with different distances from the sound source is necessary for the determination of the reflection coefficient. Thus, diffraction correction is a basic requirement for accurate results. To compensate the diffraction effects a method was chosen, which calculates the average pressure amplitude, P of a circular transducer-equivalent surface at a defined distance from the sound source in relation to the average pressure amplitude of an equidistant ideal plane wave, P_0 of similar size (Khimunin 1972). However, the diffraction correction implies a homogeneous medium and does not consider any additional phase boundaries. For this reason, the normalised distances are calculated first by combining the wavelengths of the involved materials and the associated dimensions (Papadakis*, et al.* 1973) to further on calculate the compensation factor for an arbitrary material. With this factor the amplitude results of the individual sound pulses can be corrected and the exact reflection coefficient can be calculated in accordance with the basic concept of plane wave propagation. The following figures offer valuable clues on the impact of the application-specific variation of individual parameters on the pressure amplitude ratio $|P/P_0|$. Although the comparative analysis usually is executed via the normalised axial distance to the source and only for multiples of k·a, but this rarely results in a clear picture of the impact in the real application. Particularly for transducer radius variations which don't necessarily entail changes of the axial dimensions of the entire sensor system, the normal form of representation is useful to clarify real differences (see Figure 1.6).

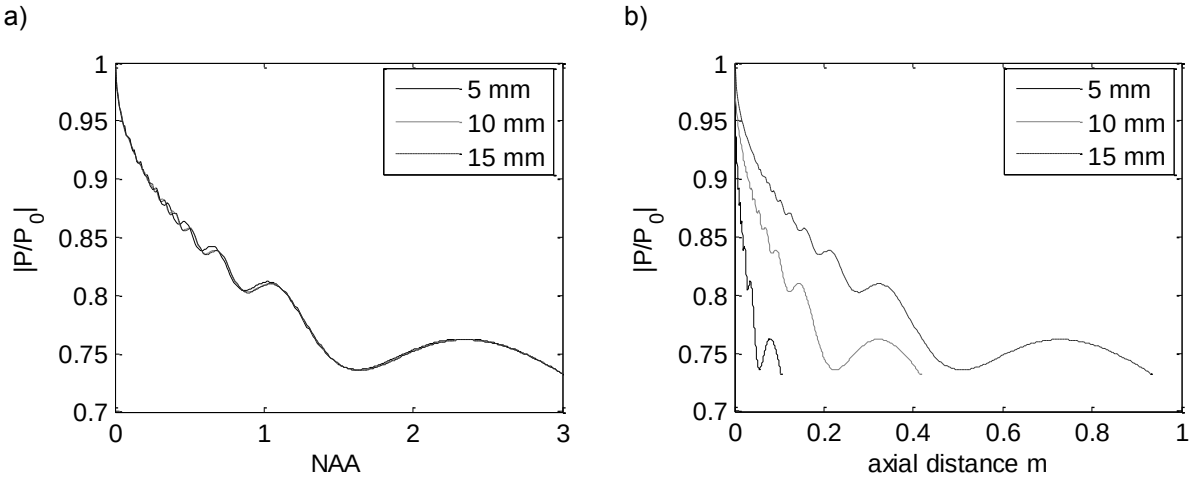

Figure 1.6: Ratio of pressure amplitudes according to Khimunin (1972) for varying transducer radii, a sound velocity of 1450 m/s and a frequency of 2 MHz; a) for domain up to a normalised distance (NAA = $z\lambda/a^2$) of 3 and b) similar results but the domain presented in m to illustrate the impact in real dimension.

The smaller the transducer radius, the faster the pressure amplitude drops with increasing distance from the source. In practical terms, only radius deviations in the range << 1mm are expected, so that relevant amplitude errors amounts ought to be not more severe than in sound velocity deviations (see Figure 1.8). The changes due to in practice common variations of the transducer frequency are so distinct that the illustration in real axial domain is not necessary.

In particular, the number of inflexion points in the near field increases dramatically (see Figure 1.7 b); more drastic than one would expect from simple axial sound field observations (compare with Figure 1.4), but quite in line with expectations, arising from considerations enlarged in the plane (compare with Figure 1.5). For the actual application a constant correction frequency corresponding to the maximum frequency of the analyzed signal from the first interface, proved effective. Despite all this, if an appropriate broadband transducer is applied, or the amplitude evaluation is carried out through the determination of the spectral density of a wide frequency band in general, it ought to be examined if the consideration of all employed frequencies might be reasonable.

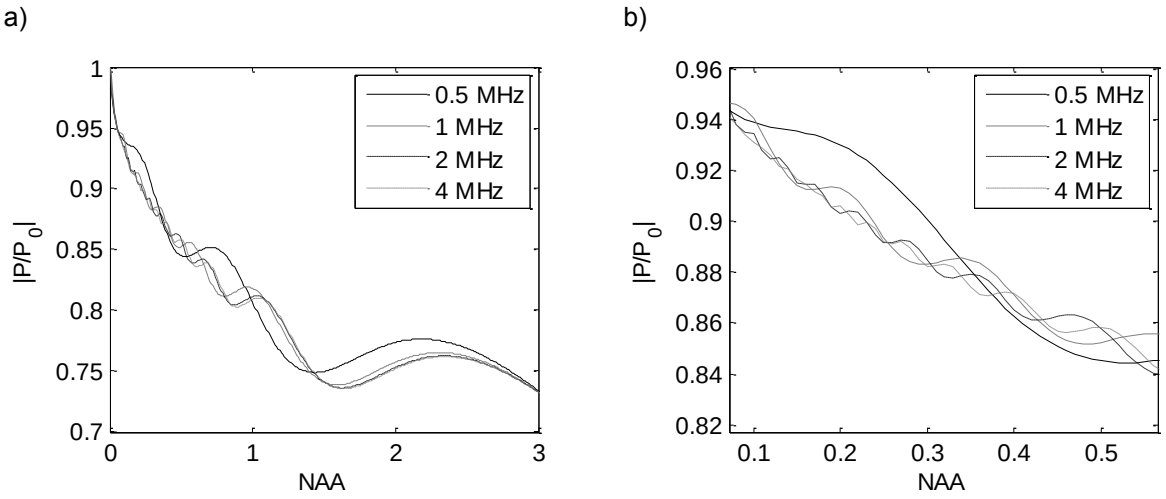

Figure 1.7: Ratio of pressure amplitudes according to Khimunin (1972) for the transducer radius 5 mm, a sound velocity of 1450 m/s and the frequencies 0.5, 1, 2, and 4 MHz; a) for domain up to a normalised distance (NAA = $z\lambda/a^2$) of 3 and b) enlarged representation to clarify the fluctuations and its variation range with frequency changes.

The impact of sound velocity changes on the pressure amplitude ratio is the most important aspect regarding the diffraction compensation. While both, the transducer radius as well as the frequency spectrum, remain relatively constant during the process, the speed of sound is subject to permanent changes. In practical, this will affect primarily the determination of the combined normalised distance. But in

principle, however, it may be equated with the compensation of ultrasonic velocities exposed to errors (compare with Figure 1.8). As shown in Figure 1.8a application relevant variations of the sound velocity hardly cause changes in the pressure amplitude ration even when surveyed with respect to the real axial distance. Due to the displacement of the local extrema, however, increasing deviations arise with increasing axial distance (see Figure 1.8b) which can be noticed as direct amplitude error magnitude in the accuracy of the reflection coefficient. The desired system accuracy requires a reflection coefficient accuracy of 0.1% and thus the demand for amplitude errors much smaller than 0.1%. Therefore, even small errors contributions should be avoided, the speed of sound changes ought to be considered and the computational expenses have to be accepted.

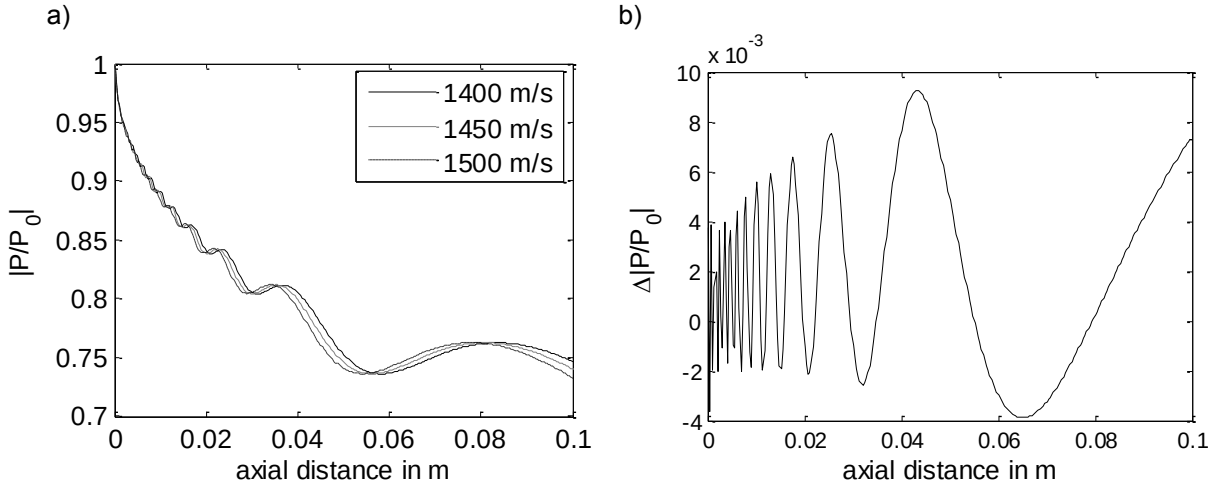

Figure 1.8: Ratio of pressure amplitudes according to Khimunin (1972) for the transducer radius 5 mm, varying sound velocities and a frequency of 2 MHz; a) for domain up to a normalised distance (NAA = $z\lambda/a^2$) of 3 and b) illustration of the pressure ratio difference at 1450 and 1500 m/s to clarify the error potential in case of ultrasonic velocities exposed to errors

1.3 Density and concentration determination via ultrasound based buffer methods

In the previous chapter essential conditions for the successful determination of the reflection coefficient, the density and ultimately the specific acoustic impedance of liquids via ultrasound based buffer methods were explained. The section below is intended light up both, the impact of these constraints on the practical implementation, as well as the possibilities and limitations that result ultimately for the determination of the component concentrations by the measured acoustic parameters.

The primary condition for correct results is the obligatory implementation of the diffraction correction. Here, the most obvious and simplest requirement is the shape of the transducer. Although sound field calculations are basically possible for other forms of sound source as well (see Weyns (1980a) and Weyns (1980b)), but when applying a different form also the development and examination of an adjusted diffraction correction is mandatory. The investigations (Weyns 1980a) even show that sector-shaped interruptions change the sound field asymmetrically leading to significant deviations in particular in the near field region (up to 1 NAA). Such sector-shaped interruptions as assumed for the sound field calculations of Weyns are typical for incomplete sound coupling between the surface of the piezoelectric ceramic and the buffer material, for instance: recesses as often provided for solder connections between the connecting wires and the electrodes. Another possible interpretation is incomplete or differing polarisations with nonstandard electrodes. State of the art in the production of piezoelectric ceramics requires the electrode metallisation prior to the polarisation, thus special electrode shapes in most cases result in a polarisation which differs from the ideal case.

Another uncertainty regarding the correction of sound field effects constitutes acoustic matching layers. Although matching layers often improve the efficiency of the transducer, but also require additional signal coupling layers and precise manufacturing technologies. A further disadvantage is the dependence of the matching layer characteristics on the sound velocity and hence on the temperature. So far, no experimental data on these subjects are known. However, based on the theoretical basic principles it is likely, that both transmission and reflection are significantly affected which would result in deviations of the buffer method’s results.

Similar discussion points which so far have been found little attention in the Science arise on closer examination of the diffraction correction. Here the "real" pressure amplitude is calculated based on the assumption of constant transducer displacement which is distributed uniformly over the surface of the transducer, deflection constant for the calculation of the. But in general, for "real" transducers this is not true. Also, the additional phase interface in buffer methods results causes additional diffraction effects in the transmitted signals parts which are not taken into account in pressure amplitude calculating up to date. In this context, additional

transmission effects due to surface roughness are of interest as well.Indeed there have been studies on the effects of intermediate, absorbing layers on the sound field expression (siehe Brand (2004)), but no comparative considerations with respect to deviations from the theoretically calculated sound fields or to sound fields without considering additional phase interface. In practical terms, however, it is generally questionable if measurement of the transducer as accurate as possible, an exact determination of all material parameters and the consideration of any additional effects in the diffraction correction actually result in a reasonable, applicable solution, especially since currently there are hardly any information on the extent of their impact. Due to limited technological possibilities the influence of these effects has not been studied separately. Instead, the constraints of the diffraction correction were satisfied as far as possible and robust, application-oriented calibration methods as a solution-oriented approach for the measurement system were chosen.

Additional boundaries to determine individual component concentrations arise from the empirical model and the experimentally evaluated data base. In order to allow a relation to the real conditions, first a brief overview of typical concentration spectra of sugar types in worts is given. These are primarily dependent on the raw materials and associated fluctuations, and the methods of manufacture, so the individual process steps in malting and mashing. Table 1-1 shows the concentration relations within a typical beer wort, whereat information may vary slightly depending on the source (compare MEBAK (2012) and Narziss and Back (2009)). Typically available sugar types are dextrins, oligosaccharides with more than four glucose units, and the yeast fermentable mono-, di- and tri-saccharides (Narziss and Back 2009). With approximately 74% the fermentable sugars maltose, maltotriose, sucrose, glucose and fructose represent the majority of the total carbohydrate content and eventually the entire convertible fraction (MEBAK 2012). According to Annemüller and Manger (2009) due to different transport processes into the cell the individual fermentable sugars types are metabolised at different, partially delayed instants of time. Other ingredients, but in much lower concentrations, are proteins, enzymes, vitamins, lipids, and minerals, inter alia.

Regarding now the hitherto known fundamentals, concentration- and temperature-dependent relationships with respect to ultrasonic velocity and density are previously

known only to binary mixtures of water with glucose, sucrose and fructose (Contreras*, et al.* 1992; Resa*, et al.* 2005). A review via validated measurement technology even showed significant variations in the range > 1 m / s speed of sound, so that a general revision of the models is recommended. For the additional component ethanol, in fact, reliable temperature-dependent data exist only for the ultrasonic velocity of the ternary mixture with sucrose (Schöck and Becker 2010).

Table 1-1: Concentration spectra of varying sugar types in a typical beer wort with an overall sugar content of 12% according to MEBAK (2012).

sugar type:	**conzentration:**	**unit:**
maltose:	54-64	g/l
maltotriose:	11-13	g/l
glucose:	8,5	g/l
sucrose:	3-5	g/l
fructose:	1,9	g/l
xylose:	70	mg/l
arabinose:	60	mg/l
galactose:	1,1-1,6	mg/l
cellobiose:	50	mg/l

Based on the situation described the necessary data has been determined experimentally (see 2.2.2), the empirical models for water-maltose-ethanol mixtures were developed (see 2.2.2 & 2.2.4), and finally applied as a simplified model for the fermentation fluid (see 2.2.4). In fact, it can be assumed that maltose as the major sugar in malt-based fermentation fluids represents the overall characteristics in terms of sound velocity and density in wide range. In addition, glucose, fructose and sucrose are metabolized preferably and quickly by the yeast which decreases their influence with progressing fermentation time. As well, the individual sugars show pretty different variations in relation to maltose, so that the effects are partially compensated. Despite this, any deviation from the assumed, ideal composition causes a potential bias and this refers to all ingredients; not only the sugar types.

Besides the ingredients deviating from the ideal case, there are other factors which are not considered by the model, in particular the yeast cell count and the pressure. Regarding the temperature-specific pressure dependence, numerous works were published in the past (Kell 1975 ; Kell 1977; Wilson 1959; Fine and Millero 1973; Belogol'skii*, et al.;* Benedetto*, et al.* 2003). And although, the mentioned works are

only valid for water technically speaking and in this respect need to be adjusted additionally according to the new International Temperature Scale of 1990, in spite the data allows the estimate of the temperature-specific, pressure-caused changes of the density and sound velocity of aqueous solutions. The results of this evaluation show that the expected changes in the observed pressure range (up to 3 bar) are not relevant for the desired measuring accuracy and can be neglected. The same statement can be made for expected deviations due to yeast cell variations during the fermentation process. While process-specific variations of at most 1-50 million cells/ml are expected, the sound velocity change is approximately 0.5 m/s per 100 million yeast cell count increase (Resa*, et al.* 2009).

The above stated clearance for pressure changes in the expected range is valid in general, but does not meet the specific case 100% factual. In addition to the direct effects of pressure changes some side effects appear in case of anaerobic fermentation. Here it is supposed especially the dissolution of carbon dioxide, CO_2. Particularly at the end of fermentation when the pressure increases and the temperature is lowered to adjust the amount dissolved CO2 according to the recipe, this factor comes into effect. A consistent estimation of the interrelations can be carried out by means of the works of Rammert (1993), who has investigated the CO_2 solubility in beers, and Liu (1998), who investigated among others the influence of dissolved CO_2 on the ultrasonic velocity. Accordingly, for the expected CO_2 content of 0.5-7 gCO_2/l causes a speed of sound variation of up to 15 m/s.

1.4 Thesis concept

The previous chapters gave a deeper insight into the basic concept of the ultrasound-based buffer methods and the associated boundary conditions in which various simplifications are valid. But thereby not the full scope of the work is represented.

The experimental determination of the density and ultrasonic velocity of water-maltose-ethanol mixtures as a function of temperature and component concentration played a central role for the solution of the problem statement. On the one hand, the described relationships are a necessary precondition for an adequate reference method; on the other hand it could clearly be shown that a representation of the

relationships by means of the data base and theoretical approaches hitherto known is not possible.

The examination of the experimental data through reference data of the two-component mixtures: ethanol-water and sugar-water showed very good agreement but it some cases significant differences as well. However, the deviations could be attributed to methodological problems of reference work or real deviations corresponding to real differences (vgl. Hoche*, et al.* (2014), D'Arrigo and Paparelli (1988), Brunn*, et al.* (1974), Liley*, et al.* (1997), Vatandas*, et al.* (2007), Contreras*, et al.* (1992)).

The experimentally determined data on the one hand provided the basis for the establishment of an empirical model for the determination of the density and speed of sound as a function of temperature, the ethanol, and the sugar concentration. Further on the empirical model enabled an extensive validation of the desired buffer method (MRM) with respect to the reflection coefficient, the density, and the specific acoustic impedance (see 2.2.3). On the other hand an adequate empirical model to determine the individual component concentrations by means of temperature and acoustic parameters based on the data could be established, which is the more relevant aspect for the intended measurement system (see 2.2.4).

The overview shown in the preceding passages gives an outlook and to some extent even the answer to some basic questions that remained unanswered at the beginning of the work and are summarised in this retrospect:

- How are temperature- and concentration- caused density and sound velocity changes of the three-component mixture, water-sugar-ethanol characterised and which model provides an accurate representation of these relationships.
- Which accuracy of the relevant parameters is required in order to ensure the required accuracy in determination of the individual components concentrations?
- Which method-specific simplifications are actually feasible for the desired accuracy and which relevance do sound field effects represent for the accurate determination of the reflection coefficient using the ultrasound based buffer methods?

- What technical requirements have to be met and which signal processing steps are required to achieve the required accuracy of the target parameters?
- Is the consideration of further application-related specific characteristic mandatory?

The investigation of these basic questions will finally answer the key question whether the application for fermentation monitoring of the, since the 70's in its fundamentals well-known ultrasound based buffer methods is possible with adequate accuracy under brewing technological constraints or not.

Therewith, a tool for online fermentation monitoring for the beverage industry would be available, which on the one hand meets the hygienic standards and is CIP-suitable, whereby the manual sampling with all the associated risks of contamination is in fact superfluous in use, and on the other hand, implies significant process improvements in terms of product quality, continuity, and fermentation time, thus eventually reduces the amount of waste and production costs.

In summary, as consequent response to the above crystallised questions the following key points have been investigated in the present work:

(i) Verification of the concentration and temperature dependent data bases for the characterisation of brewing technologically relevant sugar-ethanol-water mixtures during anaerobic yeast fermentation.

(ii) Theoretical investigations of the fundamentals, constraints and requirements of the ultrasound based buffer methods to determine the density by means of reflection coefficients.

(iii) Development of a test rig for the purpose of experimental determination of the temperature and concentration-specific data field of all relevant parameters for the characterisation of brewing technologically relevant sugar-ethanol-water mixtures.

(iv) Validation of the acoustic measurement method and the experimental data by means of the results of the test equipment.

(v) Development of an optimised sensor design and a model to determine the individual component concentrations of brewing technologically relevant sugar-ethanol-water mixtures during anaerobic yeast fermentation.

(vi) Evaluation of the sensor and the model in pilot plant scale.

2 Summary of results (thesis publications)

2.1 Paper summary

Part 1 – Review

Ultrasound-based density determination via buffer rod techniques: a review

In the review all relevant publications on the subject ultrasound based buffer methods back to its origins in the 70s were surveyed with the aim to verify the results of all investigations which researched into approaches of ultrasound-based density determination. The focus was on the applied fundamentals, relevant details of the experimental realization of the method and the critical evaluation of all the technological aspects in relation to the accuracy achieved with through the reported procedure.

Based on the methodological and conceptual fundamentals a classification into four sub-categories could be carried out. Nevertheless, all subcategories possessed following commonalities: The fundamental basis of the density determination is the determination of the reflection coefficient at an interface, wherein at least the precise characterization of the material specifications: density and sound velocity, of the buffer material has to be possible based upon previously known relations. The determination of the reflection coefficient is specified by means of useful signals whose history has to be associated with the interface. And the plane wave propagation provides the physical basis for the description of the characteristics of the signals used, starting from the excitation signal.

Part 2 – Specification of the polar mixture's characteristics

Critical process parameter of alcoholic yeast fermentation: speed of sound and density in the temperature range 5–30 °C.

The development of an appropriate experimental setup for determining the ultrasonic velocity and density of liquids as a function of temperature and for varying maltose and ethanol concentrations was the key requirement to characterize the course of the fermentation by means of the aimed measurement method. Through reduction of temperature gradients, a high temperature accuracy and cyclic recalibration of the reflector distance an ultrasonic velocity accuracy of ± 0.02 m/s was achieved. A

reference measurement system based on the resonant oscillation method with separate temperature measurement was used to determine the density with an accuracy of 1E-3 g/cm³. With the described experimental setup 100 individual measurement results for each parameter and the corresponding ultrasound signals were recorded per concentration combination within for the application technologically relevant temperature and concentration ranges.

The establishment of a concentration-dependent, empirical model additionally allowed the evaluation of the results by means of published comparative data. Therewith, as has been proven a reliable data basis was available which for the first time allows the determination of the component concentrations for maltose and ethanol in ternary mixtures with water by means of various physical quantities. Likewise, the developed model allows the estimation of the course of key parameters under typical fermentation conditions.

Part 3 – Which accuracy can be reached through the applied technologies and methods?

Density, ultrasound velocity, acoustic impedance, reflection and absorption coefficient determination of liquids via multiple reflection method.

The measurement cell developed in part 2 initially was used only for the exact determination of the ultrasonic velocity within the determination of the data basis of the empirical model. At the same time the measurement cell, as well as the experiments were designed in a way that allows in addition the determination of the reflection coefficient by means of multiple reflection method with minimized fault and error conditions. Thereby, an important aspect was the recording of the original signal data in order to investigate the effect of different signal processing methods and algorithms on the amplitude accuracy and their influence on the reflection coefficient. Due to the reference density measurement in accordance with the theoretical foundations not only to validation of the accuracy of the buffer methods with respect to the reflection coefficient was possible, but also with respect to the specific acoustic impedance and the density. Simultaneously, absorption values for the determined data field of the three-component mixture could be presented for the first time.

Altogether, the chosen validation method provides a verified accuracy with respect to the technological constraints and the applied signal processing algorithms. And this

accuracy finally can be used for the estimation of the concentration accuracy of different empirical models.

Part 4 – Time for a test under real process conditions!

Ultrasound based, in-line monitoring of anaerobe yeast fermentation: model, sensor design and process application.

Based on the data of part 2 different models for the determination of the individual component concentrations based on the temperature and acoustically determined parameter were established. The validation results of part 3 provided the basis for the estimation of achievable concentration accuracies. Specifically in relation to the stability against temperature deviations the temperature - ultrasound velocity - density model achieved the best results and was considered for the process validation. Based on analysis concerning the amplitude accuracy an optimized sensor design based on the VARINLINE process access was developed for measurements in cylindroconical tanks. Sensor and model were tested under process conditions for different fermentations and laboratory reference analyses were applied to determine the concentration deviations.

The results confirmed that particularly in case of pressure variations the ultrasonic velocity deviations due to the dissolved carbon dioxide have to be compensated. As well, strong concentration deviations appear in case of rapid process changes which among other things are attributed to delayed diffusion processes, which are not considered by the applied compensation. Generally, however, good agreements with the laboratory results are obtained in particular for the main fermentation.

2.2 Paper copies

2.2.1 Ultrasound-based density determination via buffer rod techniques: a review

Ultrasound-based density determination via buffer rod techniques: a review

S. Hoche, M. A. Hussein, and T. Becker

Chair of Brewing and Beverage, Bio-PAT (Bio-Process Analysis Technology), Freising, Germany

Correspondence to: S. Hoche (s hoche@wzw.tum.de)

Received: 18 March 2013 – Revised: 18 June 2013 – Accepted: 8 July 2013 – Published: 31 July 2013

Abstract. The review presents the fundamental ideas, assumptions and methods of non-invasive density measurements via ultrasound at solid–liquid interface. Since the first investigations in the 1970s there has been steady progress with regard to both the technological and methodical aspects. In particular, the technology in electronics has reached such a high level that industrial applications come within reach. In contrast, the accuracies have increased slowly from 1–2 % to 0.15 % for constant temperatures and to 0.4 % for dynamic temperature changes. The actual work reviews all methodical aspects, and highlights the lack of clarity in major parts of the measurement principle: simplifications in the physical basics, signal generation and signal processing. With respect to process application the accuracy of the temperature measurement and the presence of temperature gradients have been identified as a major source of uncertainty. In terms of analytics the main source of uncertainty is the reflection coefficient, and as a consequence of this, the amplitude accuracy in time or frequency domain.

1 Introduction

The medium density is a key parameter for most known processes in chemical, petrochemical, pharmaceutical, food and beverage, biotechnology, water and waste-water industries. The potential to determine online the quantity and quality of the process medium by means of density enables new options of process control and management. There are methods based on direct physical relations or based on the determination of parameters that can be correlated to the density for a specific chemical reaction or a characteristic process course. But most established methods, like coriolis mass flow or vibrating U-tube, have system-inherent limitations that often result in application restrictions in sensor implementation (limits in pipe diameter, limited to bypass application, limited to a certain flow range). Based on the specifications of the process, additional limitations might be sensitivity to bubbles, particles or fouling. In the case of food processing, hygienic design is a dominant constraint. The actual paper reviews ultrasound-based techniques as alternative methods which may be used where standard methods are not applicable.

The easiest way to determine the real-time density is to monitor the ultrasound velocity. According to the Newton–Laplace equation

$$\kappa_S = \frac{1}{\rho_l c_l^2}, \tag{1}$$

the density ρ_l of a liquid medium can be determined knowing the isentropic (adiabatic) compressibility κ_S and the sound velocity c_l. Unfortunately, the adiabatic compressibility is usually determined from sound velocity and density measurements at atmospheric pressure (Kaatze et al., 2008). In 1967 Davis and Gordon (Davis and Gordon, 1967) developed an exact method to measure the adiabatic compressibility by determining volume and sound velocity changes under varying pressure and temperature. Davis and Gordon's research work was followed by extensive investigations to determine thermophysical properties of different materials (Bolotnikov et al., 2005; Daridon et al., 1998a, b; Esperança et al., 2006; Kell, 1975; Żak et al., 2000). Since all three parameters – density, sound velocity and compressibility – are highly temperature dependent, and since the compressibility measurement is limited to laborious methods, the application of sonic velocimetry at constant frequencies is limited to

density determination of binary systems (Asher, 1987; Van Sint Jan et al., 2008). The velocimetric approach is based on temperature and, in some cases, pressure-dependent calibration measurements of sufficiently pure and well-defined liquids (Rychagov et al., 2002) and results in applications such as electrolyte measurements in accumulators or density determination of pure liquids (Swoboda et al., 1983; Vray et al., 1992; Wang et al., 2011; Kuo, 1971; Marks, 1976; Wang and Nur, 1991). The accuracy of such methods generally depends on the type of liquid and its purity (Rychagov et al., 2002; Matson et al., 2002; Wang and Nur, 1991).

Further methods to determine the density via ultrasound are waveguide and interferometric approaches. The waveguide approach generally uses propagation time variations of torsional ultrasonic waves in a transmission line immersed in the sample liquid. Besides torsional waves, the use of flexural or Rayleigh waves is also possible. Even though waveguide sensors have been used by several research groups over the last decades (Kim and Bau, 1989), it is reported (Lynnworth, 1994) that the method suffers from viscosity effects and has to be specifically designed to fulfil certain wavelength aspects.

The interferometric approaches use the effects of overlapping waves. While Pope et al. (1992, 1994) used peak FFT values of the resonance response spectrum over a certain frequency range, Sinha and Kaduchak (Sinha and Kaduchak, 2001; Kaduchak and Sinha, 2001; Sinha, 1998) used swept-frequency acoustic interferometry (SFAI) based on characteristics of standing-wave patterns. Pope's method relies on calibration measurements, and therefore is limited in the same way as the velocimetric methods. The method presented by Sinha and Kaduchak was not developed for highly accurate acoustic measurements. They reported a relative uncertainty of 0.5 % for sound speed and 5 % for the density measurement.

In conclusion to the text above, one can allege that the enormous calibration effort of most ultrasound-based methods may be the reason that, in the past decades, several research groups have focused on reflection-coefficient-based density determination methods via buffer rod systems. The plane wave propagation across one or more interface is the basis of buffer rod techniques. The history of single pulses is described with respect to the excitation amplitude considering reflection, transmission and attenuation terms. Calculating the ratios of feasible pulses results in amplitude-based representation of the reflection coefficient. Further parameters like attenuation and density can be calculated based on the knowledge of the buffer material's properties.

Sachse (1974) and Hale (1988) first reported on this method and presented validation results. Sachse analysed the amplitudes of pulses, scattered by a fluid-filled inclusion in an aluminium block to determine the reflection coefficient (RC), r of the pulse incident on the inclusion. Finally, the measured RC and the known impedance of the matrix material were used to calculate the density of the inclusion fluid. In contrast, Hale used a transmitter–receiver configuration. From the amplitude changes of received signals, he determined the sample density with a bias of less than 2 %.

McClements and Fairly (1991, 1992) first paid attention to attenuation and temperature effects for their validation trials. The developed ultrasonic pulse echo reflectometer consists of a perspex buffer rod and an aluminium reflector plate. The reflectometer has been immersed in a water bath to stabilize the temperature to $\pm 0.1\,^{\circ}\mathrm{C}$. According to Eq. (2) the RC, $r_{\text{buffer-sample}}$ of the interface perspex buffer–sample-fluid was calculated by the use of reference signals, for which the reference medium was air. Assuming total reflection ($Z_{\text{air}} \ll Z_{\text{perspex}}$; $r \approx 1$) and constant incident pulse amplitudes A_{i} the ratio of the first echo's amplitudes leads to an attenuation independent term:

$$r_{\text{buffer-sample}} = A_{1\text{sample}}/A_{1\text{air}}, \tag{2}$$

where $A_{1\text{sample}}$ is the pulse amplitude of the first pulse that is reflected from buffer–sample-fluid interface and $A_{1\text{air}}$ is the pulse amplitude of the first pulse that is reflected from buffer-air interface of the reference measurement. Knowing the RC $r_{\text{buffer-sample}}$, the specific acoustic impedance of the actual sample can be determined. McClements and Fairly achieved remarkable accuracy of $\pm 0.01 \times 10^6\,\mathrm{kg\,m^{-2}\,s^{-1}}$ for the impedance determination. A precision of approximately $\pm 0.5\,\mathrm{m\,s^{-1}}$ was reported for the speed-of-sound measurements. Using both to calculate densities for a series of sodium chloride solutions, an accuracy of $\pm 6\,\mathrm{kg\,m^{-3}}$ (0.5 %) could be achieved.

In general, all subsequent investigations are based upon the same basic relations, only varying in sensor design, methodology adaptions and signal analysis. The review focuses on ultrasound-based density determination via buffer rod techniques (BRT). In Sect. 2 the physical fundamentals and basic assumptions will be discussed as well as the four basic methods that have been identified. In Sect. 3 relevant design considerations will be presented. Finally, in Sect. 4, all major analytical aspects will be discussed with respect to density accuracy, uncertainties and real process application.

2 Physical fundamentals and method classification

The basis of all BRTs is the determination of the RC, which in general is based upon the physical description of plane wave propagation across an interface (see Fig. 1). Every medium is characterized by certain sound velocity c, density ρ and sound attenuation α. Any loss of energy that appears while sound wave propagates through homogeneous medium is summarized in the attenuation term. As soon as the wave arrives at an interface, the wave will be partly transmitted and partly reflected.

The relation of transmission and reflection is governed by the specific acoustic impedance Z of the medium defined as

$$Z = \frac{\omega}{k}\rho = \frac{\omega}{\omega/c - j\alpha}\rho = \frac{c}{1 - j\alpha^c/\omega}\rho, \tag{3}$$

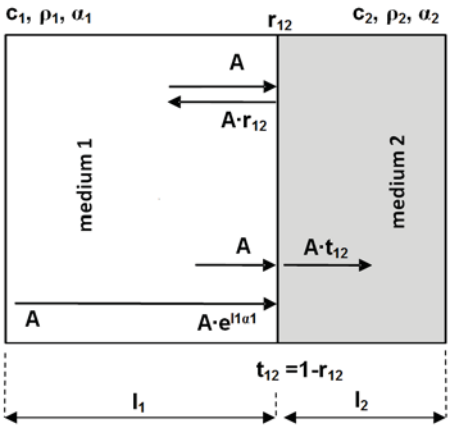

Figure 1. Schema showing the basic principles of sound propagation across an interface at normal incidence.

where k is the complex wave number and ω the angular frequency ($= 2\pi f$). For materials of sufficiently small attenuation ($\alpha \ll \omega/c$ or $\alpha c/\omega \ll 1$), Eq. (3) simplifies to

$$Z = \rho \cdot c. \tag{4}$$

The amount of a wave reflected at a plane interface is often characterized by the RC which is the ratio of the reflected (subscript r) to the incident (subscript i) wave. The RC can be expressed in terms of amplitudes A or intensities I. The intensity is proportional to the square of amplitude, which leads to the following expressions for a wave that passes from medium 1 (subscript 1) to medium 2 (subscript 2):

$$r_A = \frac{A_r}{A_i} = \frac{Z_2 - Z_1}{Z_2 + Z_1}, \tag{5}$$

$$r_I = \frac{I_r}{I_i} = \left(\frac{Z_2 - Z_1}{Z_2 + Z_1}\right)^2. \tag{6}$$

In the same way the transmission coefficient t is given as the ratio of transmitted wave (subscript t) to incident wave:

$$t_A = 1 - r_A = \frac{A_t}{A_i} = \frac{2Z_1}{Z_2 + Z_1}. \tag{7}$$

If one thinks in terms of buffer rod techniques (BRTs), medium 1 might be the buffer rod and medium 2 the sample liquid. Measuring at constant temperatures, the material properties (c and ρ) of the buffer remains constant, and any change in the RC is clearly related to a change of the specific acoustic impedance of the sample liquid. This means according to Eqs. (4)–(6), the density of the sample liquid ρ_2 can be determined via the reflection coefficient if the temperature-dependent properties of the buffer rod (ρ_1, c_1) and the sound velocity of the sample liquid (c_2) are known:

$$\rho_2 = \frac{\rho_1 c_1}{c_2}\frac{(1 + r_A)}{(1 - r_A)} = \frac{\rho_1 c_1}{c_2}\frac{(1 + r_I^2)}{(1 - r_I^2)}. \tag{8}$$

The wave propagation in its basic form is a mechanical oscillation and depends on the physical properties of the material (Saggin and Coupland, 2001; McClements, 1997; Povey and McClements, 1988):

$$\left(\frac{k}{\omega}\right)^2 = \frac{\rho}{\text{modulus of elasticity}}. \tag{9}$$

In the case of pressure waves, the appropriate modulus of elasticity is the longitudinal modulus M, which is equal to the sum of bulk modulus K and 4/3 shear modulus G. For Newtonian fluids the shear modulus can be neglected and the modulus of elasticity is assumed to be equal to the bulk modulus K ($= \kappa^{-1}$; see Eq. 1). If one considers that the wave number is complex and the attenuation in liquids is not negligible, the acoustic impedance becomes complex, expressed as the complex sum of the resistive (real) part, R_a, and the reactive (imaginary) part, X_a:

$$Z_a = \frac{P}{\xi} = R_a + jX_a, \tag{10}$$

where P is the acoustic pressure and ξ the particle displacement. Applying a BRT, the attenuation in the buffer is generally low and the simplification of Eq. (5) is valid. This may change in the case of a fluid as second phase. For high attenuation, a complex form of the RC is introduced which includes a loss angle, θ (O'Neil, 1949; Mason et al., 1949; Moore and McSkimin, 1970):

$$re^{-j\theta} = \frac{Z_2 - Z_1}{Z_2 + Z_1}, \tag{11}$$

leading to a complex acoustic impedance for the sample fluid:

$$Z_2 = R_2 + jX_2 = Z_1\frac{1 - r^2 - j2r\sin\theta}{1 + r^2 - 2r\cos\theta}. \tag{12}$$

The resistive (real) part then becomes

$$R_2 = Z_1\frac{(1 - r^2)}{1 + r^2 - 2r\cos\theta}, \tag{13}$$

and can be approximated as

$$R_2 \approx Z_1\frac{1 + r}{1 - r}\left[1 - \frac{r\theta^2}{(1 - r)^2}\right] = Z_1\frac{1 + r}{1 - r} + O(\theta^2). \tag{14}$$

Typically the acoustic impedance of liquids is less than 0.1 $(1 + j)$ of the buffer impedance, and therefore the loss angle was found not to exceed 5° (Mason et al., 1949). The loss angle dependent remainder can be neglected and the approximation can be used to specify the resistive component of the liquid's acoustic impedance for most buffer-liquid interfaces.

The buffer rod techniques published so far differ mainly in the way that the RC is determined, but not in the calculation of the density. Consequently, the accuracy of all BRT-density measurements basically depends on both the accuracy of the RC and the sound velocity measurement. Based upon the applied RC determination method the BRTs can be classified into multiple reflection methods (MRM), reference reflection methods (RRM), transmission methods (TM) and angular reflection methods (ARM).

2.1 Multiple reflection method (MRM)

The MRM (also known as the ABC method) was first devised by Papadakis (1968). He determined the ultrasonic attenuation in a sample and the RC at the buffer–sample interface over a frequency range of 27–45 MHz. In 1972 Papadakis et al. (1973), together with Fowler and Lynnworth, presented further results in the range 0–15 MHz and introduced a diffraction correction. Based upon the work of Mason and Moore and McSkimin, Sachse (1974) applied the same method to determine the density in a range up to 10 MHz. Adamowski et al. (1998, 1995), Higuti and Adamowski (2002a) and Bjørndal et al. (2008) used identical principles, but enhanced some methodical aspects to overcome several error influences.

The core idea of the MRM is the use of pulse ratios. If the correct pulses are related to each other, the unwanted attenuation, reflection and transmission terms can be neglected, leaving a term that is only dependent on the RC of interest. Principally the remaining term is even independent of the initially generated pulse amplitude. In general, a probe design as shown in Fig. 2 is used for the MRM, in which medium 1 resembles the buffer (subscript 1); medium 2, the sample liquid (subscript 2); and medium 3, the reflector (subscript 3) – all of them characterized by a certain κ, ρ and α. The reflection or transmission coefficients of the different interfaces are indicated in terms of propagation direction and involved mediums; for example,

RC for propagation from medium 1 to medium 2 : $r_{12} = \dfrac{Z_2 - Z_1}{Z_2 + Z_1}$;

transmission coefficient for propagation from medium 2 to medium 1 : $t_{21} = \dfrac{2Z_2}{Z_1 + Z_2}$.

Using the principles of plane wave propagation at normal incidence, one obtains the following for A_{r1}, A_{e11} and A_{e21}:

$$A_{r1} = A_T \cdot r_{12} \cdot \exp(2l_1\alpha_1), \tag{15}$$

$$A_{e11} = A_T \cdot t_{12} r_{23} t_{21} \cdot \exp(2l_1\alpha_1) \cdot \exp(2l_2\alpha_2), \tag{16}$$

$$A_{e21} = A_T \cdot t_{12} r_{23}^2 r_{21} t_{21} \cdot \exp(2l_1\alpha_1) \cdot \exp(4l_2\alpha_2). \tag{17}$$

The subscript r defines the captured pulse as buffer reflection (BR) and the subscript e as an echo pulse. Furthermore in A_{rk} and A_{ejk}, subscript k defines the pulse order (1st BR, A_{r1}; 2nd BR, A_{r2}; etc.) and subscript j the echo order (e.g. pulses of 1st echo, A_{e1k}; pulses of 2nd echo, A_{e2k}). For the ratios A_{r1}/A_{e11} and A_{e11}/A_{e21} one obtains

$$\frac{A_{r1}}{A_{e11}} = \frac{r_{12}}{t_{12} r_{23} t_{21} \cdot \exp(2l_2\alpha_2)}; \quad \frac{A_{e11}}{A_{e21}} = \frac{1}{r_{23} r_{21} \cdot \exp(2l_2\alpha_2)}. \tag{18}$$

The terms of attenuation in medium 1 and the initial transmitted amplitude A_T are cancelled out. Additionally, it becomes clear that disregarding the first interface at the coupled sound source is a valid simplification. Every additional term of the interface 0–1 (e.g.: $A_T = A_0 t_{01} t_{10}$)) would be added to each of the pulses (Eqs. 15, 16 and 17) and therefore also disappear in the ratios of (18).

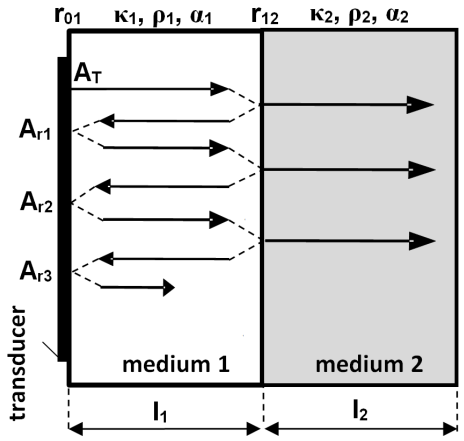

Figure 2. Schematic showing the basic principles and relevant pulses for the MRM: buffer, medium 1; sample, medium 2; reflector, medium 3.

Dividing now one ratio by the other, one reaches an attenuation-independent equation, and the amplitudes A_1, A_2 and A_3 can be used to calculate the RC of interface 1–2, r_{12}:

$$r_{12} = \sqrt{\frac{x}{x-1}}\, x = \frac{A_{r1} A_{e21}}{A_{e11}^2}. \tag{19}$$

The resulting equation is now independent of the attenuation in medium 2. Papadakis (1968) first investigated a glass buffer rod on a fused-silica sample. Later, in Papadakis et al. (1973), a water buffer combined with a nickel sample was investigated; a RC of $r_{12} = 0.9435 \pm 0.0045$ was calculated, which was in good agreement with the theoretical value of 0.945. Furthermore, he introduced the so-called A'AB method, which is more or less the first mention of the RRM, and may be used if attenuation in medium 2 is too high and amplitude A3 is very low. Further details about the RRM will follow in the next section.

Instead of the normal buffer–reflector configuration, Adamowski et al. (1995, 1998) used a double-element transducer (DET) including the buffer, a sample liquid (medium 2) and a high-acoustic-impedance reflector (medium 3: stainless steel). The DET has a piezoceramic emitter and a large-aperture receiver (PVDF membrane) separated by a solid buffer rod (medium 1: PMMA) of length l_0. Another buffer rod (medium 1: PMMA) of length l_1 is placed between receiver and sample medium. The great advantage of Adamowski's approach is the employment of the large-aperture receiver in the DET. The large aperture minimizes the uncertainties if diffraction effects and the transmitted pulse A_T can be gathered for every single excitation. That enables calibrations due to varying excitation amplitudes as they may occur during long-term operations. Nevertheless

applying the MRM, the use of A_T is not necessary. In Adamowski et al. (1995) a comparison of MRM and RRM is presented, and for MRM a bias of 10 kg m^{-3} is reported. The main limitation of Adamowski's DET is the PVDF's limited temperature range of application. At temperatures above 60–70 °C the piezoelectric PVDF slowly loses its imposed polarized structure. A successful application of high-temperature piezoelectric materials (PEM) in a DET has not been reported so far.

Bjørndal et al. (2008) used the MRM to verify a newly developed TM, which will be discussed later. They investigated liquids with a wide range of shear viscosities at a temperature of 27.44 ± 0.04 °C. It was reported that the systematic deviation from reference values of a calibrated pycnometer was smaller for the MRM than for the TM, and reached an error of ±0.15 %.

A special version of the MRM is the approach of Deventer and Delsing (1997). Although this method does not follow the typical ABC approach of Papadakis, it is classified as MRM since some specific reflections are used to calculate the RC without additional calibration measurements. Delsing and Deventer used a double buffer of two different materials. Keeping the terminology of Fig. 2, medium 2 is now the second buffer and medium 3 is the sample liquid. Eliminating A_T in Eq. (17) with the use of Eq. (16) one achieves for r_{23}

$$r_{23} = \frac{A_{e11} \cdot r_{12}}{A_{r1} \cdot t_{12} t_{21} \cdot \exp(2 l_2 \alpha_2)}, \tag{20}$$

and for ρ_3

$$\rho_3 = \frac{Z_2}{c_3} \cdot \frac{4 A_{r1} Z_1 Z_2 \exp(2 l_2 \alpha_2) - A_{e11}(Z_1^2 - Z_2^2)}{4 A_{r1} Z_1 Z_2 \exp(2 l_2 \alpha_2) + A_{e11}(Z_1^2 - Z_2^2)}. \tag{21}$$

Since the properties of medium 1 and 2 are known, the unknown parameters that have to be measured are c_3, A_{e11} and A_{r1}. So basically no echo pulse from a reflector is necessary to calculate the RC, which is a great advantage in the case of highly absorptive liquids. The disadvantage is that not only is the exact knowledge of temperature-dependent density and sound velocity of one medium required, but that of two mediums. Additionally, the attenuation in medium 2 has to be known to calculate the RC. And the sound velocity of the sample liquid is still necessary to calculate the density. Therefore transmission or pulse-echo measurements through the liquid are still a requirement to determine the density.

Deventer and Delsing (1997) used 32-times-averaged digitized signals in order to determine the densities of water at 2, 20 and 40 °C. The measured densities have been compared with tabulated data, and a mean bias of 1 kg m^{-3} was reported. In fact, the presented graph shows standard deviations from ±5 kg m^{-3} at 40 °C up to ±10 kg m^{-3} at 2 °C, and it was not mentioned as to how many densities have been averaged to reach the reported results. In Deventer and Delsing (2001a) the densities of glycerin, water and alcohol were determined in a temperature range from 0 to 40 °C. A mean of 100 measurements and tabulated reference data was used for the validation. Even though a clear separation between the results of the different sample liquids is possible, the results still show varying bias and standard deviation for varying temperatures. It was stated that sound velocity inaccuracies generated an error of approximately 1 % and that a density error of 0.4 % should be reachable.

2.2 Reference reflection method (RRM)

A first version of the RRM was presented by Papadakis et al. (1973). As with all RRM the core idea is the use of plane wave propagation principles at normal incidence in combination with a reference medium. For the so-called A'AB method, Papadakis uses the 1st buffer reflection of a reference medium A' and the same 1st buffer reflection of the sample medium A to calculate the RC. The pulse amplitude B is only used to calculate the attenuation. A similar approach was used later by Adamowski et al. (1998), McClements and Fairly (1991), Saggin and Coupland (2001) and Kulmyrzaev et al. (2000).

Similar to the MRM approach of Deventer and Delsing (1997), the RC determination via RRM does not rely on the presence of a reflector. Of course, calculating the final density via Eq. (8) still requires the sound velocity of the sample medium, and therefore needs either transmission or pulse-echo measurements through the liquid, but the schematic representation of the basic principles to determine the RC can be simplified to medium 1 and 2 (see Fig. 3). For moderate attenuation and thickness of medium 1, one can obtain the amplitudes of the multiple buffer reflections A_{rk} as follows:

$$A_{r1} = A_T \cdot r_{12} \cdot \exp(2 l_1 \alpha_1);\ A_{r2} = A_T \cdot r_{10} \cdot r_{12}^2 \cdot \exp(4 l_1 \alpha_1);$$
$$A_{rk} = A_T \cdot r_{10}^{k-1} \cdot r_{12}^k \cdot \exp(2 k l_1 \alpha_1). \tag{22}$$

The RRM based on one pulse, as applied in McClements and Fairly (1991), Papadakis et al. (1973), Püttmer and Hauptmann (1998), Püttmer et al. (1998, 2000) and Saggin and Coupland (2001), uses the ratio of any detectable buffer reflection of a sample medium and the corresponding buffer reflection of a reference medium, e.g. A_{r1}(sample) and A_{r1}(reference):

$$\frac{A_{r1}(\text{sample})}{A_{r1}(\text{reference})} = \frac{A_T \cdot r_{12}(\text{sample}) \cdot \exp(2 l_1 \alpha_1)}{A_T \cdot r_{12}(\text{reference}) \cdot \exp(2 l_1 \alpha_1)}. \tag{23}$$

Assuming a constant excitation pulse A_T and a similar attenuation α_1 for sample and reference signal one obtains

$$r_{12}(\text{sample}) = r_{12}(\text{reference}) \frac{A_{r1}(\text{sample})}{A_{r1}(\text{reference})}. \tag{24}$$

The RRM based on two pulses as applied in Adamowski et al. (1998) uses the ratio of any detectable buffer reflection and its following reflection, e.g. A_T and A_{r1} or A_{r1} and A_{r1}:

$$\frac{A_{r1}(\text{sample})/A_{r2}(\text{sample})}{A_{r1}(\text{reference})/A_{r2}(\text{reference})} = \frac{r_{12}(\text{reference})}{r_{12}(\text{sample})}. \tag{25}$$

Since successive ratio buffer pulses are used, the excitation pulse A_T does not have to be assumed constant anymore. But

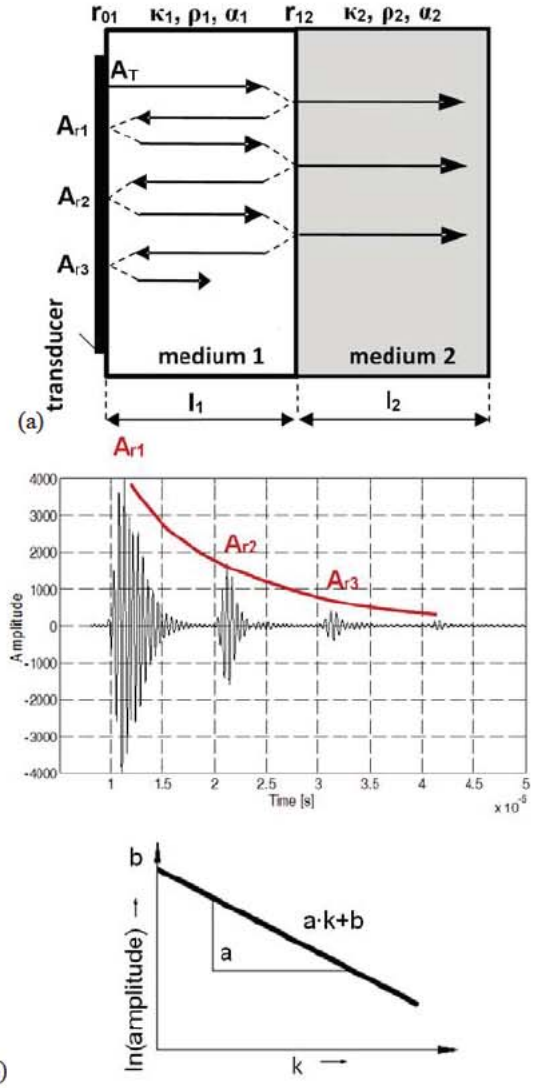

Figure 3. Basic principles and relevant pulses of the RRM: **(a)** schematic of multiple buffer reflections, **(b)** multiple buffer reflection pulses in the time domain and logarithmic decay of pulse amplitudes.

still a similar attenuation α_1 and a similar RC r_{10} have to be assumed if sample and reference measurement are compared:

$$r_{12}(\text{sample}) = r_{12}(\text{reference}) \frac{A_{r1}(\text{reference})/A_{r2}(\text{reference})}{A_{r1}(\text{sample})/A_{r2}(\text{sample})}. \quad (26)$$

Since successive ratio buffer pulses are used, the excitation pulse A_T does not have to be assumed constant anymore. But still a similar attenuation α_1 and a similar RC r_{10} have to be assumed if sample and reference measurement are compared:

$$r_{12}(\text{sample}) = r_{12}(\text{reference}) \frac{A_{r1}(\text{reference})/A_{r2}(\text{reference})}{A_{r1}(\text{sample})/A_{r2}(\text{sample})}. \quad (27)$$

And finally, as applied by Bamberger and Greenwood (2004a, b), the ratio of decays of multiple buffer reflections can be used to obtain the RC via RRM. Describing the amplitude decay logarithmically:

$$\ln A_{rk} = [\ln(r_{10}) + \ln(r_{12}) \cdot 2l_1\alpha_1] \cdot k + [\ln A_T - \ln(r_{10})] = a \cdot k + b, \quad (28)$$

and calculating the ratio exp[a(sample)]/exp[a(reference)], one obtains the RC under the assumption of similar attenuation α_1 and a similar RC r_{10} for reference and sample signals:

$$r_{12}(\text{sample}) = r_{12}(\text{reference}) \cdot e^{[a_{\text{sample}} - a_{\text{reference}}]}. \quad (29)$$

McClements and Fairly (1991, 1992) applied the one-pulse RRM with air as the reference medium. They used a 2.1 MHz transducer of 10 mm diameter driven by a tone burst of 5–10 cycles. Distilled water, castor oil, olive oil, *n*-hexadecane and silicone fluid have been investigated at a constant temperature of 20.2 °C. For a vibrating U-tube as the reference measurement (DMA 40, Anton Paar) an error of 0.5 % is reported, which corresponds to a bias of ±8 kg m^{-3}.

Kushibiki et al. (1995) applied a one-pulse RRM to investigate the acoustic properties of biological tissue and liquid specimen. Instead of air, water was used as the reference medium. Kushibiki et al. used a transmission line to measure velocity dispersion and attenuation. Basically the methodological assembly is comparable to Bjørndal's MRM approach. It was not mentioned why an RRM instead of an MRM was applied. Several broadband transducers (1.5 mm diameter) in combination with different gap distances have been used to cover the frequency range from 70 to 500 MHz. Different oils have been investigated and a maximum bias of 8 kg m^{-3} is reported. The temperature was reasonably constant around 23 °C, and the density validation values have been gathered via pycnometer. The investigations of Kushibiki et al. particularly show the feasibility of the method to investigate properties of very thin specimen.

Adamowski et al. (1998) applied the two-pulse RRM. Due to the special DET design it was possible to monitor the incident pulse. An unfocused 1.6 MHz broadband transducer was used, driven by a sinusoidal burst of one cycle. Distilled water, castor oil and ethanol have been investigated in a temperature range from 19 to 40 °C. The presented results have been calculated at a frequency of 1.4 MHz, and a bias of ±10 kg m^{-3} for reference values from the literature was reported. Furthermore, the apparatus was tested under varying flow conditions and a stable, negative bias of −3 to −6 kg m^{-3} compared to pycnometer reference measurement was reported. In Adamowski et al. (1995) similar equipment was used and results (average of 15 measurements) of RRM and MRM have been compared for constant temperatures (25 ± 0.5 °C). In the limited temperature range a bias of 1–2.5 kg m^{-3} could be reached.

Bamberger and Greenwood (2004a, b) and Greenwood and Bamberger (2004) applied the multiple-pulse RRM and used a 5 MHz transducer of 25 mm diameter. They investigated sodium compound solutions, kaolin slurries and sugar-water solutions. No information about the temperature i

Table 1. Expectable reflection coefficient difference for a defined density and sound velocity range, different buffer materials and different angles of incidence.

Material	Start value of sample medium		End value of sample medium		Longitudinal RC difference		
	ρ [kg m^{-3}]	c [m s^{-1}]	ρ [kg m^{-3}]	c [m s^{-1}]	angular incidence (45°)	angular incidence (25°)	normal incidence
PMMA	1.055	1510	1.010	1535	0.0095	0.0111	0.0120
quartz glass					0.0026	0.0037	0.0044
aluminium					0.0031	0.0038	0.0042
stainless steel					0.0013	0.0016	0.0018

given, and in terms of validation this does not matter since reference densities have been determined by weighting a known quantity. It would matter, however, if someone wants to consider applicational aspects, e.g. dynamic temperature changes. A bias of ±10 kg m^{-3} is reported for the sodium compound solutions and ±25 kg m^{-3} for the kaolin slurries. In Greenwood and Bamberger (2004) only the error for the acoustic impedance is given, which ranges from 1.8 % to −1.9 % for a 6.3 mm pipe wall and from −0.9 % to 8.7 % for a 3.8 mm pipe wall. The acoustic velocities have been measured by an independent system. Both the accuracy and the velocity values are not presented. In fact Bamberger and Greenwood presented a validation of the acoustic impedance and not the density. And since the velocity values are missing, an estimation of the density accuracy from the impedance validation data is not possible. There are two quite astonishing facts that are not cleared up in the publication. Table 1 in Greenwood and Bamberger (2004) indicates that only a few certain echo amplitudes are used to analyse the amplitude slope, but it is not stated why not all echoes or why exactly the presented echoes have been chosen. Furthermore, it is stated that the echo slope is a self-calibrating feature to overcome the influence of variations in the excitation voltages. But to prove the stability only the pulse width has been changed, although the published information indicates that the pulser voltage can be varied.

In summary, the following facts can be stated:

- Using the RRM to determine the RC, only buffer reflections are necessary. However, to calculate the density of the sample, the sound velocity in the medium is still necessary. Thus, aside from the angular approach (ARM), at least one echo from a reflector or some additional transmission measurements are required to determine the density.
- The RC of the used reference medium r_{12}(reference) either has to be known or, like in the case of air, can assumed to be equal to 1.
- The RRM is based on two separate measurements – of the sample and of the reference medium. The assumption of similar attenuation α_1 and RC r_{10} is only valid if a similar temperature distribution across the buffer can be guaranteed for reference and sample measurement.
- The one-pulse RRM is most susceptible to errors. The assumption of constant excitation pulses is not always valid, and has a great impact on the accuracy of the method. The excitation pulse is practically never exactly the same, and considering ageing of piezoelectric materials, the practical application would need periodic calibrations.

Besides the MRM, dual and multiple pulse RRM which are independent of the excitation amplitude, several alternative strategies have been developed to overcome the problem of varying excitation amplitudes. In Lynnworth and Pedersen (1972), Rychagov et al. (2002) and Jensen (1981) and Deventer (2004) a reference path approach is applied to monitor the excitation variations. The part of the signal that is reflected from a reference interface of constant properties can be used to standardize the received signal and negate excitation variations. Another option is the combination of reference and sample measurement as proposed by Greenwood et al. (1999, 2000) and Guilbert and Sanderson (1996). In this way the same pulse excitation can be sent to reference and sample measurement transducer. Comparable temperature distribution in both buffers can be assumed as well. But using two different transducers probably generates other systematic errors due to misalignment or differing transducer properties. A special case of this method is presented by Püttmer and Hauptmann (1998) and Püttmer et al. (1998, 2000), who used an additional delay line that is connected to the reverse side of the piezoceramic to determine signals from a reference interface. In this way a similar excitation pulse can be guaranteed for reference and sample measurement by using one transducer only. However, the advantage of similar temperature distributions is lost. A clear separation of each pulse is obtained by choosing a different length for the reference buffer and correcting the resulting difference by a calibration factor. In Fisher et al. (1995) a double buffer similar to Deventers MRM was used. However, instead of using the echo of the first buffer to calculate the RC directly, the additional

reference echo was used to compensate effects such as ageing or depolarization of the piezoceramic.

2.3 Transmission methods (TM)

The TM contains all methods that use sender and receiver separately in a parallel assembly to determine the RC. Generally the TM can be classified into two approaches: the first approach is based on the work of Hale (1988), who uses only receiver signals (TMOR); the second approach as presented by Bjørndal et al. (2008) uses the signals of both transducers (TMSR).

Even though Hale's approach is not a true buffer rod technique, it is worth mentioning since it is the basis for further developments. Hale used a transmitter–receiver configuration without any additional delay line. The used configuration and terminology is given in Fig. 4, for which in Hale's approach medium 1 is the sender and medium 3 is the receiver.

Hale assumed that the attenuation does not change significantly for fluids of quite similar composition (like tap water and salty water) and that the sender impedance equals the receiver impedance ($Z_1 = Z_3$). Therefore, it was possible to state that any change in acoustic impedance of the sample liquid Z_2 is directly proportional to the measured change of amplitude A_4:

$$A_1 = \frac{(Z_1 + Z_2)^2}{4e^{-\alpha_2 l_2} Z_1 Z_2} A_4. \tag{30}$$

Considering calibration measurement for two liquids (indices c1 and c2) of known acoustic impedances Z_{c1} and Z_{c2} and constant excitation amplitude A_1, one reaches

$$\frac{(Z_1 + Z_{c1})^2}{4\exp(-\alpha_{c1} l_2) Z_1 Z_{c1}} A_{4c1} = \frac{(Z_1 + Z_{c2})^2}{4\exp(-\alpha_{c2} l_2) Z_1 Z_{c2}} A_{4c2}. \tag{31}$$

Under the assumption of similar internal losses ($\alpha_{c1} = \alpha_{c2}$) the attenuation term can be neglected, and the impedance Z_1 can be calculated:

$$Z_1 = \frac{Z_{c1} - kZ_{c2}}{1-k} + \sqrt{\left(-\frac{Z_{c1} - kZ_{c2}}{1-k}\right)^2 - \frac{Z_{c1}^2 - kZ_{c2}^2}{1-k}}, \tag{32}$$

where

$$k = \frac{\exp(-\alpha_{c1} l_2) Z_{c1} A_{4c2}}{\exp(-\alpha_{c2} l_2) Z_{c2} A_{4c1}}.$$

The density results showed less than 2 % variation from the true values which have been determined via weight measurements of known volumes. McGregor (1989) discussed several possible methods to measure the density by using the same probe arrangement like Hale. He stated that a continuous wave system, with and without interference, would provide the most accurate means of determining the velocity and the characteristic impedance of the fluid under test.

Henning et al. (2000) mounted the transducers on a glass tube wall of half-wave thickness. Furthermore, the setup was

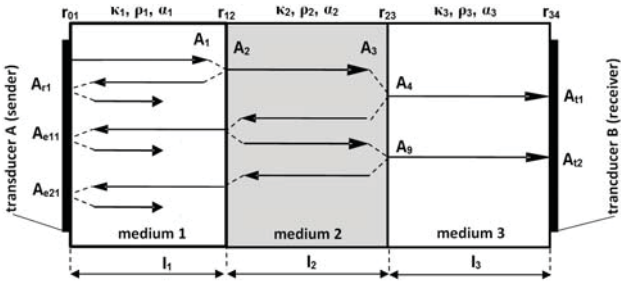

Figure 4. Schema showing the basic principles and relevant pulses for the TM and giving the terminology for Hale's, Henning's and Bjørndal's approach.

calibrated for two liquids of known acoustic impedance to determine Z_1. But in the case of Henning's setup, Z_1 is only the apparent transducer impedance. Indeed, this fictive impedance describes the combined impedance of glass wall and transducer as a result of the sound propagation through the glass wall of half-wave thickness. Furthermore the basic TMOR approach was expanded for the amplitude A_9:

$$\frac{A_9}{A_4} = \left(\frac{Z_1 - Z_2}{Z_1 + Z_2}\right)^2 \exp(-2\alpha_2 l_2). \tag{33}$$

Still the attenuation is neglected in order to calculate the transducer impedance. But now two equations can be used to calibrate the transducer impedance. Using both Eqs. (32) and (33) a mismatch between the transducer impedances was reported. In the end both impedances have been used to determine the acoustic impedance of the sample liquid. Even though the glass tube wall is of half-wave thickness, it is quite clear from theory that the amplitudes A_4 and A_9 as described by the equations are not equal to the amplitudes received by the transducer. From the physical point of view the received pulses are also influenced by the wall material and contain also information from superpositioned reflections inside the tube wall. Nevertheless, in Henning et al. (2000) both the basic and the expanded TMOR have been compared for several liquids using an aerometer measurement as reference. While the basic TMOR showed a bias of 3 to $-40\,\mathrm{kg\,m^{-3}}$, the expanded TMOR resulted in a bias of -16 to $10\,\mathrm{kg\,m^{-3}}$. Furthermore, it was reported that the absolute error increases to a few percent in the case of increasing sound absorption corresponding to the liquid properties or diffuse scattering at particles.

Additionally to the signals of the receiver (transducer B), Bjørndal et al. (2008) employs pulses received by transducer A. Comparable with the MRM, one achieves an equation that cancels the influence of the attenuation, the transducer and the electronics sensitivity. Bjørndal employs two pulses of transducer A and two pulses of transducer B (R_echo12_12 method, terminology given in Fig. 4):

$$r_{12} = \pm\left(1 - \frac{A_{e11} A_{t1}}{A_{r1} A_{t2}}\right)^{-0.5}. \tag{34}$$

It is reported that the systematic deviation from reference values was slightly higher for the TMSR compared with MRM, and it is stated that using information of both transducers, non-identical sound fields and a misalignment in the transducer configuration might be the reason for the higher deviation. In Bjørndal and Frøysa (2008) all possible pulse combinations besides Eq. (34) are discussed, even some further methods that employ transmitted pulses from both sides in which transducer A and B are used alternately as senders. After a detailed uncertainty analysis with respect to bit resolution and noise, it was outlined that the R_echo12_12 method (Eq. 34) possesses a relative uncertainty close to the optimal and case-dependent R_echo123_123 (which uses 3 pulses of receiver and transducer; details in Bjørndal and Frøysa (2008) and may be the best choice of all TMSR to be compared with the MRM).

2.4 Angular reflection method (ARM)

The ARM was presented first by Greenwood and Bamberger (2002) and Greenwood et al. (1999). Concerning the determination of the RC, the ARM is a simple one-pulse RRM (Eq. 24). But to determine the sound velocity and the density of the medium (see Eq. 5) the ARM uses measurements at two different angles.

The RC of the longitudinal wave, r_{LL} at a given angle of incidence (see Fig. 5) depends on the angle β_L, the density ρ, the longitudinal velocity c of the sample liquid and the longitudinal velocity c_L, the shear velocity c_T and the density ρ_S of the buffer material (Greenwood et al., 1999; Krautkramer and Krautkramer, 1983). The equations are generally given as

$$r_{LL} = \frac{G - H + J}{G + H + J}, \tag{35}$$

where

$$G = \left(\frac{c_T}{c_L}\right)^2 \sin 2\beta_L \sin 2\beta_T, \tag{36}$$

$$H = \cos^2 2\beta_T, \tag{37}$$

$$J = \frac{\rho c \cos\beta_L}{\rho_S c_L \cos\beta} = \frac{Z_2 \cos\beta_L}{Z_1 \cos\beta}, \tag{38}$$

and from Snell's law,

$$\sin\beta = \frac{c \sin\beta_L}{c_L}, \quad \sin\beta_T = \frac{c_T \sin\beta_L}{c_L}. \tag{39}$$

Instead of measuring the sound velocity c, the RC is determined using an RRM approach (Eq. 24) to calculate the parameter J via Eq. 35). Now Eqs. (38) and (39) can substitute the unknown angle β in

$$\sin^2\beta + \cos^2\beta = 1. \tag{40}$$

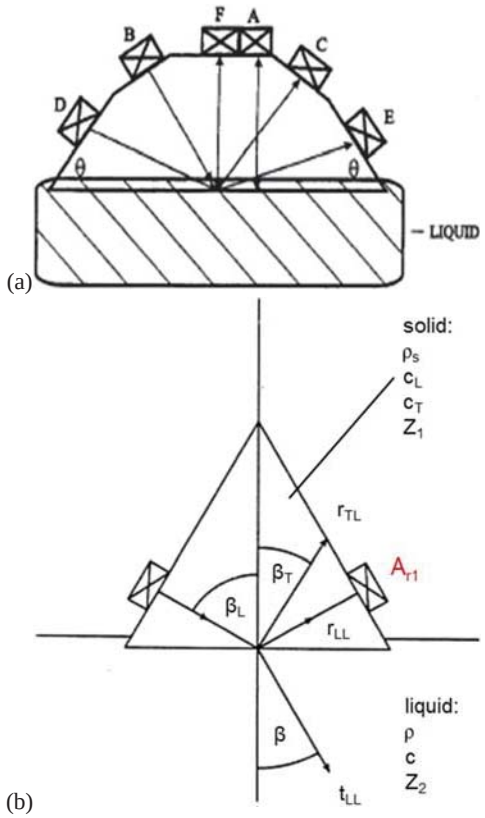

Figure 5. Schematic showing **(a)** the wedge design of Greenwood and Bamberger, **(b)** the design given by Krautkramer and the definitions of terminology.

Doing so for two different angles, equalizing both and writing the resulting equation in terms of ρ gives a term which is independent from the sound velocity in the liquid:

$$\rho = \rho_S \left(\frac{\sin^2\beta_{L1} - \sin^2\beta_{L2}}{\cos^2\beta_{L1}/J_1^2 - \cos^2\beta_{L2}/J_2^2} \right)^{0.5}. \tag{41}$$

Finally, the sound velocity in the liquid can be calculated with

$$c = \left(\frac{\sin^2\beta_L}{c_L^2} + \frac{\rho^2 \cos^2\beta_L}{J^2 Z_1^2} \right)^{-0.5} \tag{42}$$

In summary the following facts can be stated:

- The great advantage of the ARM is the determination of the sound velocity on the basis of reflection coefficient measurements at two angles. Only signal information from the interface is required, and therefore no sound propagates through the sample medium.
- The basics of the ARM reflection coefficient determination are comparable to the RRM. Consequently, all facts stated for the RRM also count for the ARM. Only the sound velocity determination is different.

– The ARM also provides the opportunity to measure the sound velocity via pulse-echo or transmission approach. Instead of measurements at two angles, one would be sufficient. The missing angle β in Eq. (38) could be calculated via Eq. (39).

– The angle and the temperature-dependent parameters – density, longitudinal and transversal sound velocity – of the buffer material have to be known precisely. The slightest deviation from the real value can generate a significant error in the density.

The ARM was validated for sugar-water solutions and surrogate slurries via weighting of known volumes. For the analysis of the sugar-water samples the wedge was submerged to reach a uniform wedge temperature. An error of 0.1–1.3 % was reported, which is a bias of 1–14 $\mathrm{kg\,m^{-3}}$. The experiments for the surrogate slurries have been accomplished at a test loop for varying slurry flow rates, aeration flow rates and two constant temperatures (25 and 50 °C). Each density was calculated by averaging 45 signals. The validation was accomplished by comparing the average of 40 sensor densities with reference densities. The bias varied between 13 and 260 $\mathrm{kg\,m^{-3}}$. Neglecting some extreme deviations, an overall bias of 20 $\mathrm{kg\,m^{-3}}$ could be accomplished.

3 Probe design considerations

The design of ultrasonic density probes as presented by the aforementioned authors is a complex process. In most publications, the probe's dimensions and material are simply mentioned as a given fact, not as a required necessity. In fact, an unequivocal identification of clearly unaffected pulses is one of the basic requirements for all presented methods. As soon as one of the required pulses is superpositioned by any other pulse or effect, which is not considered by the plane wave propagation theory, the resulting values will be affected by a systematic error.

3.1 Pulse excitation and separation

The best way to exemplify all interrelations clearly is to follow the design process of a buffer which might be used for an RRM approach. In its simplest version, we want to see the first reflected pulse, only affected by the reflection at the interface and the buffer material's attenuation. Neglecting all application-based boundary conditions, the only real limiting conditions are the choice of the ultrasound source and the frequency of and the type of excitation pulse. By making the right choice one can affect the pulse duration. Choosing a transducer which generates a low-damped narrowband pulse of low frequency, one achieves a relatively long pulse. Choosing a high frequency, highly damped broadband pulse, one achieves a short pulse. If a burst excitation of several cycles is used, one can specify the frequency quite accurately, but this generates a long-lasting sound pulse. Using a pulse excitation, one can generate a shorter sound pulse, but the pulse frequency generally relies on the system's resonance frequency. In any case, often the most convenient way to investigate the resulting sound pulse duration is to test and measure the pulse length t_p of a chosen ultrasound source for varying excitation pulse amplitudes, cycles and frequencies. Knowing t_p and the temperature-dependent sound velocity c_1 of the buffer material, it is possible to calculate the minimum buffer thickness for a given temperature range to prevent superposition phenomena for the multiple buffer reflections A_rn.

When a reflector is used to determine the sound velocity or to adopt the MRM, further parameters besides the temporal determination of the pulse position are relevant to prevent superposition of buffer reflections and echoes. If so, the pulse amplitude and the amount of buffer reflections also have to be considered. For constant excitation amplitude those parameters only depend on the buffer materials absorption and the RC at the interphase. Combined with the pulse length t_p those parameters define the buffer reflections duration t_br. In order to prevent superposition between the buffer reflections A_rn and the echo pulses $A_{\mathrm{e}jk}$, the following condition has to be fulfilled:

$$\frac{l_2}{c_2} = \mathrm{TOF}_2 > t_\mathrm{br}, \tag{43}$$

where TOF_2 is the signal's time of flight in the sample medium. Alternatively, dimensions and materials can be designed in a way that the echo pulses arrive in a time gap between two buffer reflections. This target is hard to achieve since the echo position depends on the sample mediums sound velocity, and thus such special designs are often usable only for a defined sample medium and temperature range (Bjørndal et al., 2008; Bjørndal and Frøysa, 2008). In the case of the MRM as introduced by Papadakis the superposition between the 1st pulses of the 1st and 2nd echo (A_e11 and A_e21) and the reflections of those pulses inside the reflector have to be eliminated, and then the condition $l_3/c_3 = \mathrm{TOF}_3 > t_\mathrm{p}$ is satisfied. Bjørndal et al. (2008) presents most of those dimensional considerations. Additionally, Bjørndal and Püttmer (1998) introduce conditions for edge wave contributions with and without mode conversion. The edge wave distributions mainly depend on the buffer diameter and the ratio of transducer radius to buffer thickness and therefore also represent the near-field phenomena. The mode conversion depends on the shear wave velocity and therefore on the elastic properties of the buffer material.

3.2 The choice of material

As indicated in the previous section, most design considerations depend on the material's properties. Thus, besides the option to change the dimension of buffer or reflector, one can simply change the material to achieve a desired signal pattern. The choice of material also defines the resolution that

has to be reached for a given process of defined density range. The following table shows start and end values (density and sound velocity) of a typical yeast fermentation and the resulting RC difference that can be expected for different buffer materials.

Indeed, it becomes apparent that according to Eq. (9) any buffer material can be used to determine the density using the reflection coefficient. But, as shown in Table 1, only materials of acoustic impedance comparable to the impedance of the sample medium possess an acceptable sensitivity for small density variations (Püttmer and Hauptmann, 1998; Püttmer et al., 2000; Bjørndal et al., 2008; Greenwood et al., 1999). The same holds true for the ARM; increasing angular difference to the normal incidence even decreases the RC difference.

Additional requirements for the buffer materials are good chemical resistance, reasonable temperature stability and a low sound attenuation (Püttmer and Hauptmann, 1998; Püttmer et al., 2000). If special liquids are analysed, e.g. suspensions containing abrasive materials, further criteria such as mechanical resistivity may be of importance. Concerning the mode conversion in the case of angular incidence – for example, if the ARM is applied or in the case of edge waves – the elastic properties of the buffer material may also be of interest. Materials of a high Poisson's ratio generally possess a higher conversion to shear waves.

Besides deploying the choice of material to guarantee a clear pulse separation, the pulse amplitude can be affected. Choosing a buffer material of acoustic impedance, comparable with the sample mediums impedance, results in a low reflection coefficient. The buffer reflections A_{rn} are less in quantity and lower in amplitude. Most of the energy is transferred into the sample medium. However, if an echo comes back (A_{e11}), most of the energy is transferred back into the buffer. Thus probably too little energy remains for a second detectable echo (A_{e21}). The same holds true for the reflector. Choosing a reflector material of high acoustic impedance results in high echo amplitudes. However, materials of high acoustic impedance generally possess high sound velocity, low sound attenuation and a high reflection coefficient. Therefore, resulting from extensive reflector dimensions and a considerable amount of reflections inside the reflector, this may interfere with the second echo (A_{e21}). In such cases a special reflector shape often is the most feasible alternative (Carlson et al., 2003a; Deventer and Delsing, 2001b). A reflector of low acoustic impedance may simplify the task to achieve the maximum signal purity, but also results in lower echo amplitudes.

3.3 Temperature variation, sound field and signal-to-noise ratio considerations

Regardless of the method applied or material chosen, if the temperature changes, everything changes concerning sound propagation. This fact also counts for design considerations. Every single boundary condition mentioned above has to be valid for the entire temperature range. If the temperature changes, so does the speed of sound, density, sound absorption and dimensions of all materials involved. Therefore, not only does the pulse's position change but also the pulse amplitudes. In the best-case scenario, the amplitude slightly decreases; in the worst case, whole pulses are no longer detectable, which might hamper the analysis of RC or ultrasound velocity (USV). Mak (1991) compared several MRMs concerning the influence of systematic (beam diffraction) and random errors (noise). He showed that varying attenuation and signal-to-noise ratio (SNR) affect the method's error. The higher the SNR and the less influence of diffraction, the smaller the errors in the RC. Therefore, the reference methods (ARM, RRM) might show better results, since they are independent from beam diffraction, while the accuracy of the MRM depends on the accuracy of the diffraction correction. Mak used a 50 MHz broadband transducer. Both the reference methods and the MRM showed quite low RCs at low frequencies, and both methods converged for higher frequencies near the transducer's centre frequency and showed comparable results. Adamowski et al. (1995, 1998) used a constructive solution to eliminate diffraction issues. The so-called DET technique employs a receiver of an aperture larger than the emitter that generates the sound field. As long as the beam spreading does not reach the dimensions of the receiver diameter, the principles of MRM for plane wave propagation are valid without correction.

While the correction of diffraction in the far field is discussed by several authors (Papadakis, 1959; Papadakis et al., 1973; Bjørndal et al., 2008; Kushibiki et al., 2003), the near-field problem is often not mentioned at all. Although the beam is assumed to be parallel in the near field (Povey and McClements), it is recommended to avoid it totally. The intensity varies greatly with distance, the surface's amplitudes are not constant and the whole wave front cannot be expected to be normal to the phase velocity vector. Essentially the plane wave propagation is not valid within the near field. Consequently, besides all dimensional considerations mentioned in Sects. 3.1 and 3.2, the first condition that has to be kept is the near-field distance N between the sender and first interface:

$$N = \frac{a^2}{\lambda}, \tag{44}$$

with a being the transducer radius. Table 2 shows methodic details as applied by different authors and the resulting near-field length in comparison to the chosen buffer length. Besides Greenwood, who applied the ARM, and Papadakis, who applied the MRM for attenuation measurements, the researchers used the path length of dimensions (double buffer rod length) greater than or at least in the range of the near-field distance.

Diffraction effects are generally corrected via Williams' expression (Williams, 1951; Williams and Labaw, 1945). Although Williams stated that his expression is only accurate

Table 2. Near-field relevant, methodic details of relevant publications.

Source	Transducer diameter d [mm]	Centre frequency f [MHz]	Material	Buffer rod length [mm]	Near-field distance N [mm]
Adamowski et al. (1995, 1998)	19.0	1.6	PMMA	30.0 42.0	53.48
Bjørndal et al. (2008)	12.5	5.0	aluminium	80.0	30.90
Deventer and Delsing (1997)	10.0	3.7	PEEK/PMMA	26.0 20.0	34.26
Greenwood et al. (1999)	12.5	2.25	Rexolite	6.3	37.56
McClements and Fairly (1991, 1992)	10.0	2.1	PMMA	40.0	19.44
Papadakis (1968)	12.7	10.0	fused quartz	25.4/62.2	67.66
			aluminium	25.4	63.20
			steel	18.9	68.34
Püttmer and Hauptmann (1998)	20.0	2.0	quartz glass	31.0	33.67

for $k \cdot a > 100$ and distances $z_W \geq (k \cdot a^4)^{1/3}$, the exact expression without approximations (see Williams, 1951, Eq. 17) might be usable in an extended domain. Nevertheless, so far it has not been reported whether corrections in the near field or for sound fields across an interphase within the near field can be applied successfully to reach a reflection coefficient accuracy of 1E-4 or less (see Table 5).

Knowing all these facts it becomes clear that if spatial limitations for the sensor application exist and a buffer miniaturization becomes necessary, only increasing the pulse frequency to achieve pure signals is not enough. Often the dimensions of the transducer with respect to the buffer mediums sound velocity have to be adapted.

3.4 Constructional uncertainties

The main constructional uncertainty which is occasionally discussed is the parallelism of surfaces. In ARMs, of course, the accuracy of the angles will be of similar importance. In Carlson et al. (2003b) it is reported that the misalignment of the transducer to buffer material is the main source of error causing an overestimation of attenuation and acoustic impedance. In Bjørndal et al. (2008) it is stated that effects of nonparallelism can be neglected for surfaces that are parallel within 0.01 mm. In Adamowski et al. (1995) a maximum parallelism of 0.0004 mm mm^{-1} and a change of 0.7 % in the reflection coefficient for an intentionally caused misalignment of 0.0024 mm m^{-1} was reported.

4 Discussion

While reviewing critically all published methods and validation results with regard to validation complexity, error analysis and real process relevance, several gaps and questions appeared which will be discussed in the following sections. The first point will be the analysis of relevant pulses. Further points will include the equipment used for ultrasound generation and detection, reference density and temperature measurement, the sound velocity determination and extended uncertainty considerations.

4.1 Signal processing

Signal processing is a wide field with many fundamental details. The applied methods range from simple time domain (Greenwood and Bamberger, 2002; Greenwood et al., 1999) to extensive frequency domain methods (Bjørndal et al., 2008). The equations presented so far represent the time domain approach and refer to the signal amplitude, but do not state which pulse amplitude is used in the end. In Greenwood and Bamberger (2002), Greenwood et al. (1999), Püttmer and Hauptmann, (1998) and Püttmer et al. (1998, 2000), the maximum peak-to-peak amplitude within a certain time window has been examined:

$$A_{\text{pulse}} = \text{maximum}\,[A(t_{w1} : t_{w2})] - \text{minimum}\,[A(t_{w1} : t_{w2})], \quad (45)$$

where A_{pulse} represents the value that is inserted in the respective equation of reflection coefficient calculation and t_{w1} and t_{w2} the time boundaries of the analysed pulse. In the following sections, $A(t)$ will represent the pulse in the time domain and $a(f)$ in the frequency domain.

Papadakis (1968) had started analysing amplitudes in the time domain for attenuation analysis, but later he changed to spectrum analysis (Papadakis et al., 1973). After correcting the frequency dependent diffraction, Papadakis et al. analysed the frequency-dependent reflection coefficient and attenuation (Papadakis et al., 1973; Sachse, 1974):

$$A_{\text{pulse}}(f) = a(f). \quad (46)$$

It was found (Sachse, 1974) that the reflection coefficient and density are nearly constant over a frequency range around the centre frequency of the transducer's maximum response. That might be the reason for obtaining the amplitudes from the spectra at a particular frequency (f_1) (Adamowski et al., 1995). Higuti (Higuti and Adamowski, 2002b; Higuti et al., 2001), who followed the DET approach of Adamowski, introduced the energy method, in which the energy spectral

density of each pulse is used for the reflection coefficient analysis:

$$A_{\text{pulse}} = \int_{-\infty}^{+\infty} |a(f)|\,\mathrm{d}f. \tag{47}$$

It is stated that the deployment of the energy method results in smaller variations when compared to the single-frequency method, because it averages the noise over frequency. For added Gaussian white noise of varying amplitude to simulation results, Higuti found that the energy method improves the results with smaller SNRs. By calculating the spectral density only for a small frequency band, the performance could be enhanced due to the rejection of frequencies outside the band of the transducer. Experimental results showed an error of less than 0.2 % and proved the enhanced performance of the presented new signal processing method.

In Bjørndal et al. (2008) a more detailed analysis of signal-processing methods in the time and frequency domain is presented. In the time domain the amplitude value was not determined simply as the main peak-to-peak difference per pulse; instead the peak-to-peak value was determined per period:

$$A_{\text{pulse}} = \text{maximum}\left[A(t)_{\text{pn}}\right] - \text{minimum}\left[A(t)_{\text{pn}}\right], \tag{48}$$

where $A(t)_{\text{pn}}$ represents the n-th period of the analysed time domain pulse. Depending on the amount of analysed periods (e.g. from P_1 to P_2) one can calculate a mean reflection coefficient R_{m} for each signal (Bjørndal et al., 2008):

$$R_{\text{m}} = \frac{1}{P_2 - P_1 + 1} \sum_{n=P_1}^{P_2} R_n. \tag{49}$$

It is reported (Bjørndal et al., 2008) that if the first period of the waveforms is included, there may be large errors, particularly when the amplitudes are analysed in the time domain, but also in the case of the frequency domain analysis. In the frequency domain the analysis followed the spectral density approach (Eq. 47), but the so-called l2 norm was introduced based on the mathematic basics of L^{p} spaces:

$$A_{\text{pulse}} = \sqrt{\int_{f_1}^{f_2} |a(f)|^2\,\mathrm{d}f}. \tag{50}$$

It is stated (Bjørndal et al., 2008) that the frequency domain integration introduces a spectral-averaging approach, reducing the effect of single-frequency interference in the echo signals. The l2 norm accentuates the dominant part of the frequency spectrum, making it easier to evaluate the effect of the upper frequency limit. Equally to the periodic peak-to-peak analysis in the time domain, the frequency spectrum was analysed on a half-periodical basis. Additionally, a Hanning window function was applied to reduce the spectral leakage. The windows have been centred at the local extreme values of each analysed peak (Bjørndal et al., 2008). The accuracy improvement compared to a frequency domain approach without window function was not reported.

Applying the different signal-processing methods to PSPICE simulation results, it was found (Bjørndal et al., 2008) that the frequency domain approach gives significantly less density deviation than the time domain analysis. The experimental results could not confirm the theoretical evaluation; in some cases the time domain analysis indicates more accurate results and less deviation. Furthermore, Bjørndal suggested a time domain integration method following Raum et al. (1998), but it was also adverted to the high sensitivity of the time integration approach to DC offsets and waveform disturbance effects:

$$A_{\text{pulse}} = \int_{t_1}^{t_2} |\text{env}(A(t))|\,\mathrm{d}t. \tag{51}$$

Besides the different signal analysis methods, the signal-processing parameters and the applied preprocessing steps are of high relevance to reach the reported accuracies. Concerning the preprocessing, most authors mentioned that a certain amount of signals have been averaged before applying the different signal analysis methods. Through signal averaging the SNR can be enhanced and the amplitude resolution can be increased beyond the AD-converter limitations (Bjørndal et al., 2008). The use of a 25 MHz low-pass filter is mentioned in Bjørndal et al. (2008); further references for filter usage have not been found. Furthermore, in Bjørndal et al. (2008) the use of least-squares-sense cubic spline approximation was reported to increase the vertical and temporal resolution.

Relevant signal-processing parameters are the pulse length in time, the amount of data points with respect to the sampling rate, the amplitude resolution and the usage of any additional processing steps to improve the frequency or magnitude accuracy, such as filtering, signal averaging, zero padding or application of window functions. Table 3 overviews the signal-processing details of several relevant authors with regard to the reached accuracies.

4.2 Signal generation and detection

Most authors used highly advanced equipment for their investigations. Generally pulse or function generators provide the electrical pulse which is converted to sound pulses by commercially available transducers. After amplification, the signal is recorded by an oscilloscope and conveyed to a personal computer for further signal analysis. Standard signal generators are generally limited to 20 V peak excitation, which is sufficient for most of the investigations. Custom signal generators for higher excitation voltages and amplifiers are available but require special circuits since the input voltage of commercial oscilloscope is often limited. To avoid noisy interferences and overloading of the oscilloscope, the

Table 3. Processing details from different literature sources with regard to density accuracies.

Source	Window size	Sampling rate (MHz)	Averaged signals	Applied method	Used domain	Density accuracy
Adamowski et al. (1995, 1998)	500 (1024, zero padding)	100	64	MRM	time/frequency	1.50 %
Bjørndal et al. (2008)	1000 (32 768, zero padding)	59	256	MRM, TRM	time/frequency	0.15 %
Deventer and Delsing (1997)	512	200	32	MRM	frequency	< 1 %
Greenwood et al. (1999)	4096	40	45	ARM	time	< 1 %
Bamberger and Greenwood (2004a, b)	–	–	–	RRM	frequency	< 1 %
McClements and Fairly (1991, 1992)	–	100	≈ 2000	RRM	time/frequency	0.50 %
Papadakis et al. (1973), Papadakis (1968)	–	–	–	MRM	time/frequency	–
Püttmer and Hauptmann (1998), Püttmer et al. (2000)	–	–	–	RRM	time	0.20 %

excitation and receiving circuit should be decoupled. Results concerning the influence of excitation voltage and voltage variations on the methods accuracy are not reported. While in Greenwood and Bamberger (2004) it is stated that the decay RRM approach is independent of changes in the pulser voltage, and although it can be assumed that the MRM is independent from the excitation voltage, it is quite doubtful that the density error is totally independent. A change of the excitation voltage or signal amplification might change the degree of interference between subsequent pulses, the SNR and the pulse appearance. The independency has definitely not been proven experimentally so far. The same counts for the excitation and transducer type. Results are reported for different excitation types (Table 4 shows an overview) ranging from peak, rectangular and sinusoidal pulses to bursts of several cycles, but a decent comparative evaluation is missing so far. Indeed, in Bjørndal et al. (2008) simulation results are reported for varying cycles, but a comparison to peak excitation and an experimental evaluation were not shown. Moreover, investigations regarding the transducers type or piezoelectric materials (PEM) have not been found so far. It is known that the very different properties of the PEM result in completely different probe types (Lach et al., 1996). Concerning the determination of the reflection coefficient, different transducers constructed with different PEM might show different sensitivities and variance.

Concerning measurements in real process environments, the use of general purpose equipment, such as oscilloscopes or function generators, is a double-edged sword. Indeed it is commercially available technology of proven accuracy, but it is often both immoderate and unfeasible for specific tasks such as reflection coefficient determination. Using the typical sampling frequency of 250 MHz to characterize a 2 MHz signal in the frequency domain is clearly oversampling – no additional information is extracted, but it might be necessary to reach high time of flight or amplitude accuracy in the time domain. In the end, the effort for signal-processing increases dramatically with increasing sampling frequency. Indeed, standard oscilloscopes can monitor the voltage-time course with a high sampling frequency but provide only a moderate vertical resolution of 8 bit. Based on simulation results it was shown (Püttmer et al., 2000; Bjørndal and Frøysa, 2008; Bjørndal et al., 2008) that a 12-bit resolution is the best choice to reach reasonable errors. Since the price of an oscilloscope is not negligible, the vertical resolution is quite low and no further usable features like amplification or variable programmable signal processing steps are provided, an oscilloscope often is replaceable. As shown in Greenwood et al. (1999, 2006), a time-to-digital converter with reasonable sampling frequency and an analogue-to-digital converter with reasonable vertical resolution also serve the purpose. Similar considerations apply to signal generation and processing. An arbitrary function generator and a personal computer might not be the best choice for measurements in real process environments, but as long as it is not clear which excitation function is the best choice for a certain method, reports about compact units that incorporate all main tasks, signal generation, signal detection and signal processing will take a while in coming.

4.3 Reference analytics, validation and uncertainty considerations

The following section reviews and discusses the measurement uncertainties in terms of density determination via BRT of all significantly involved variables: density, reflection coefficient, ultrasound velocity and temperature.

Besides the uncertainties of the simplification in Eq. (14) the reflection coefficient mainly depends on the amplitude error. According to the propagation of uncertainty the degree of dependency is defined by the equation of each method (Eqs. 19, 24, 27, 29 and 34). The amplitude error basically depends upon three main factors: the amplitude resolution, the time resolution and the SNR. The amplitude resolution dependency was discussed in Bjørndal and Frøysa (2008), Bjørndal et al. (2008) and Püttmer et al. (2000); both research groups arrived at the conclusion that a resolution of 12 bit or better is required to reach accuracies below 0.5 % error.

Table 4. Details of sound generation equipment as published by different authors.

Author/Source	Equipment		Excitation		Transducer
Adamowski et al. (1995, 1998)	function generator	oscilloscope (8 bit)	pulse/ burst	2–3 cycles	KB-Aerotech (1.6 MHz)
Bjørndal et al. (2008)	function generator	oscilloscope (8 bit)	sinusoidal burst		Panametrics (5 MHz)
Deventer and Delsing (1997)	pulse generator	oscilloscope (8 bit)	pulse	–	Panametrics (5 & 10 MHz)
Greenwood et al. (1999)	function generator	data acquisition card (PC)/digitizer (12 bit)	burst	10 cycles	–
Bamberger and Greenwood (2004a, b)	ultrasonic pulser	oscilloscope (–)	–		–
McClements and Fairly (1991, 1992)	function generator	oscilloscope (–)	burst	5–10 cycles	Karl Deutsch (0.3–1 MHz), Sonatest (1–6 MHz)
Papadakis et al. (1973); Papadakis (1968)	pulse generator	oscilloscope (–)	pulse		Y-cut quartz (30 MHz)
Püttmer and Hauptmann (1998), Püttmer et al. (2000)	analogue signal generator	time-to-digital converter (12 bit)	burst	1 cycle	lead metaniobate disk (2 MHz)

The SNR dependency was discussed in Mak (1991), Higuti et al. (2001), Bjørndal and Frøysa (2008) and Bjørndal et al. (2008). Based on theoretical uncertainty considerations it was shown that the MRM is highly sensitive to noise. The more pulses included in the reflection coefficient calculation and the lower the SNR for each included pulse, the higher the uncertainty. Particularly in the case of the MRM, the SNR of A_{e11} and A_{e21} decreases dramatically when attenuation increases. Also, the SNR of A_{e21} becomes quite low in the case of a low r_{23}. Additionally, in Mak (1991) the influence of diffraction correction uncertainties is discussed as a systematic error. Based on the fact that the RRM is independent of diffraction it was stated that the MRM is the least accurate method for calculating the reflection coefficient. Experimentally this general statement could not be proved so far; results of both MRM and RRM converged for the centre frequency of the transducer. Also the experimental results of Adamowski et al. (1995) showed similar errors for both methods. The comparison of MRM and TMSR in Bjørndal et al. (2008) showed a smaller systematic deviation from reference values for the MRM method. In Higuti et al. (2001) the statements are rested upon simulated signals with artificially added Gaussian white noise. In contrast to Bjørndal et al. (2008), who reported for a SNR of 50 an uncertainty of 25 kg m^{-3}, in Higuti et al. (2001) for a similar SNR an error of only 1–5 kg m^{-3} was presented.

So far, Bjørndal (Bjørndal et al., 2008) is one of the few to have limited the sampling frequency and investigated the time resolution uncertainty by applying cubic spline approximation to synthetic 6 MHz signals. Hence, the time resolution was increased from approximately 17 ns to 1 ns via mathematical approximation. In particular, the time domain results could be improved, and it can be assumed that the effect for signals of lower time resolution is even higher.

Unfortunately, none of the authors discussed the effect of systematic errors due to interference of subsequent pulses. Indeed, most authors state that clearly unaffected pulses are required for an accurate analysis, and cite several probe design considerations based upon a defined pulse length, but the truth is that the pulses are never diminished totally (see Püttmer et al., 1998, Figs. 7 and 8). As a basic rule, a pulse is regarded as terminated when the amplitude is below the noise level. But the subsequent signal is nothing more than a systematic oscillation hidden behind noise. Analysing those effects could help in separating such systematic errors from the signal.

The USV as a source of uncertainty often seems to be ignored. Most authors do not state how the speed of sound is determined and which accuracies could be reached (see Table 6). Generally the time of flight in the sample medium is determined and related to the propagation path. But often, particularly for small distances, the propagation path cannot be determined with adequate precision. The most chosen solutions to reach a higher precision are calibration measurements with standards (Marczak, 1997; Bjørndal et al., 2008; Higuti et al., 2001; Higuti and Adamowski, 2002b; Adamowski et al., 1998), which might become quite laborious if thermal expansion of the propagation path is

considered. Alternatively a material of low thermal expansion such as ZERODUR® (Bjørndal et al., 2008; Hoppe et al., 2003) could be used. In a range of ±25 K the thermal expansion can be neglected within an USV error of 0.2 m s^{-1}. Standard for the time-of-flight determination is the cross correlation which can be applied in the time domain (Adamowski et al., 1995, 1998) or frequency domain (Deventer and Delsing, 1997). The great advantage of BRTs is the provision of a stable reference pulse that can be compared to echo pulses. Therefore the time-of-flight determination in pulse echo mode is independent of electronics time jitter. The only problematic parameter is the time resolution. When a simple cross correlation is applied, the time-of-flight resolution is still dependent on the sampling rate. For example, providing sampled data of 100 MHz sampling rate leads to a 1 m s^{-1} velocity resolution for a 23 mm propagation path (Adamowski et al., 1995). That might be the reason why most researchers oversample the data. In fact, mathematical approximation is a feasible solution to achieve higher accuracies with less time resolution (Hoche et al., 2011; Hoppe et al., 2001). Apart from that, when echo detection in pulse echo mode becomes problematic (e.g. highly absorptive liquids, superposition of buffer reflections and echo pulses) often transmission measurements are necessary, which increases the uncertainties and the effort in technical equipment and analysis.

In fact, an accuracy of 0.1 m s^{-1} is reachable applying state-of-the-art technologies and methods, and the sound velocity is not actually the most critical source of uncertainty. Analysing the partial derivatives of Eq. (8) according to the propagation of uncertainties, one reaches the following: for c_1,

$$\frac{\partial \rho_2}{\partial c_1}\Delta c_1 = \frac{\rho_1(1+r_A)}{c_2(1-r_A)}\Delta c_1; \tag{52}$$

for c_2,

$$\frac{\partial \rho_2}{\partial c_2}\Delta c_2 = -\frac{\rho_1 c_1(1+r_A)}{c_2^2(1-r_A)}\Delta c_2; \tag{53}$$

for ρ_1,

$$\frac{\partial \rho_2}{\partial \rho_1}\Delta \rho_1 = \frac{c_1(1+r_A)}{c_2(1-r_A)}\Delta \rho_1; \tag{54}$$

and for r_A,

$$\frac{\partial \rho_2}{\partial r_A}\Delta r_A = \frac{2c_1\rho_1}{c_2(1-r_A)^2}\Delta r_A. \tag{55}$$

The calculated proportions of uncertainties for different assumed errors are shown in Table 5. In the first row of uncertainties a constant error of 0.1 % is assumed for all variables. The uncertainty examination shows that the contribution of reference values and measured sound velocity are comparable, while the contribution from the reflection coefficient is comparably small. Unfortunately the reachable reflection coefficient accuracies have not been reported so far. In the second row of uncertainties, realistic errors are assumed. The reflection coefficient of error was estimated from theoretical considerations and uncertainties. The error contribution of sound velocity and density is still small, and the reported accuracies are sufficient to reach acceptable density uncertainties. But the contribution of a realistic reflection coefficient error to the density uncertainty is comparatively high, particularly considering that the reflection coefficient can result from several amplitude errors. For the coupled PMMA–water a density uncertainty of 0.25 kg m^{-3} can be expected overall. This uncertainty is still high compared to existing reference analytics such as the vibrating U-tube (see Table 6), but seems sufficient to use the BRTs as a monitoring tool in bioprocesses of small density change (see Table 1).

Table 5. Contributed uncertainties of the relevant variables: buffer density, buffer sound velocity, sample medium sound velocity and reflection coefficient, with PMMA being the buffer and water being the sample medium.

	ρ_1 [kg m^{-3}]	c_1 [m s^{-1}]	c_2 [m s^{-1}]	r_A
value	1181.77	2764.92	1482.38	−0.3766
error 1	±0.1 %	±0.1 %	±0.1 %	±0.1 %
uncertainty 1 [kg m^{-3}]	±0.998	±0.998	±0.998	±0.438
error 2	±1 kg m^{-3}	±0.2 m s^{-1}	±0.2 m s^{-1}	±1E-04
uncertainty 2 [kg m^{-3}]	±0.085	±0.007	±0.013	±0.116

The most important uncertainty contribution which controls every influencing factor discussed so far is the temperature. The temperature accuracy affects the calibration measurements of the propagation path and buffer material's properties. Moreover, the temperature error affects uncertainties of temperature-dependent reference models as provided by the literature or certified reference standards. Using, for example, Marzcak's (Marczak, 1997) model to calculate the speed of sound of water at 20 °C, a 0.1 K temperature bias results in a 0.3 m s^{-1} USV bias, but only 0.03 m s^{-1} bias for a 0.01 K temperature bias. Due to the high impact of temperature on all relevant parameters, a temperature accuracy of at least ±0.01 K is recommended. Most non-invasive temperature measurement techniques are too inaccurate and expensive (Childs et al., 2000). The standard for invasive temperature measurement is still the electrical resistance thermometry. In general, accuracies below 0.1 K can be achieved only through individual calibration regardless of the material. For highly accurate measurements, 4-wire systems, voltage reversal and low resistances are recommended.

The temperature also influences the dimensions and properties of the used materials, the characteristics of the sound field and even the properties of the PEM. So it is quite understandable that most authors have restricted their investigations to a constant temperature. In turn, the results of these works have to be evaluated with respect to the reported temperature stability. While in Bjørndal et al. (2008) a stability

Table 6. Accuracies of involved measurement principles as published by different authors.

Reference	Density reference	Reference accuracy ($kg\,m^{-3}$)	Measurement points/temperature accuracy	USV accuracy ($m\,s^{-1}$)
Adamowski et al. (1995, 1998)	pycnometer	$\pm 0.3\,kg\,m^{-3}$	–/±0.5 K (varying)	1.0
Bjørndal et al. (2008)	literature/ standards	$\pm 0.10\,kg\,m^{-3}$	–/± 0.01 K (constant)	–
Deventer and Delsing (1997)	literature	–	2 points/± 0.01 K (varying)	–
Greenwood et al. (1999)	volume weighting	–	3 points/– (varying)	–
Bamberger and Greenwood (2004a, b)	volume weighting	–	– /–	–
McClements and Fairly (1991, 1992)	vibrating U-tube	$\pm 0.10\,kg\,m^{-3}$	–/0.1 (constant)	0.5
Papadakis et al. (1973); Papadakis (1968)	–	–	–/–	–
Püttmer and Hauptmann (1998), Püttmer et al. (2000)	vibrating U-tube	$\pm 0.10\,kg\,m^{-3}$	1 point/ – (constant)	–

of ±0.04 K was reached, Adamowski et al. (1995) reported only ±0.5 K.

Additionally, temperature gradients have to be considered. Most researchers try to avoid gradients and control not only the temperature of the sample medium but also the environmental temperature (Bjørndal et al., 2008; Higuti et al., 2007). The procedure is acceptable for highly accurate validations but of low relevance for any practical application. In real process application often the sample medium or the environmental medium temperature varies, in the worst case even both. While the temperature of the sample medium is often controlled or behaves in a predictable way, the environmental temperature does not. Depending on the time of the year, the daytime, the local weather and the location and construction of the facility, the environmental temperature can vary in a range of ±5 to ±20 K. The point is that, in reality, there will be temperature gradients which are generally not constant, so the gradients have to be considered. Furthermore, the temperature control of the buffer is only a solution when the sample medium is also of constant temperature.

The methods that are affected most by temperature gradients are the ARM and RRM. When reference and calibration measurements are executed at different temperatures or gradients, the error can increase enormously. As stated before, temperature control is often not an acceptable solution and often not stable enough; therefore two options remain – either the calibration for all relevant temperatures and gradients, which is extremely laborious, or an additional probe that determines parallel, under identical conditions to the reference values (Greenwood, 2000; Greenwood et al., 1999). Indeed, the parallel reference measurement minimizes the uncertainty caused by temperature gradients, but introduces new uncertainty sources due to the use of two excitation electronics, sender, receiver, and coupling systems that might be not identical. In the case of an MRM as proposed by Deventer and Delsing (2001b), temperature differences between sample medium and buffer rod interface temperature have to be considered. Therefore both should be monitored continuously. Similar effects have to be considered for propagation path calibrations (Higuti et al., 2007) and varying dynamic behaviour due to temperature changes of different magnitude which results in hysteresis effects (Deventer and Delsing, 2001a; Higuti et al., 2007).

In fact, there is another temperature gradient that has not been considered so far – the temperature gradient in the sample medium. As long as there is a temperature difference between sample medium and environment, there will be a gradient at the buffer–liquid interface, which implies three major issues:

1. The temperature variation over the sound propagation path influences the accuracy of the sound velocity measurement. In general, the properties vary with propagation path, and so does the sound velocity. In the end, the measured velocity, USV_p represents the average of all variations. For a known temperature dependency of

the velocity, USV(T) and a known temperature gradient $T(x)$ over the propagation path x, the relation can be described as follows:

$$\mathrm{USV_p} = \frac{1}{T(x_2) - T(x_1)} \int_{x1}^{x2} \left[USV(T(x)) \cdot \frac{\partial T(x)}{\partial x} \right] \mathrm{d}x. \quad (56)$$

The main conclusion of this expression is that if one wants to determine the temperature that fits to the measured USV, or vice versa, one has to determine the temperature at the right position or the mean temperature over the propagation path.

2. Equation (56) only introduces the general problem. The basic problem concerning the density determination is the combination of propagation path information and interfacial information. Knowing the temperature gradient means only that the measured sound velocity is not the sound velocity as it is next to the interface which is the relevant sound velocity for the reflection coefficient.

3. Thinking in terms of real process measurements, the temperature gradient cannot be considered to be simply a function of temperature difference. As soon as the sound velocity is measured in flows the gradient becomes dependent on the flow conditions.

To summarize, it can be expected that highly accurate measurements require multiple-point temperature measurements (see Table 6: Deventer and Delsing, 1997 and Greenwood et al., 1999) to gather all relevant temperatures and to estimate the gradients. Relevant temperature-dependent validations of ultrasound-based density determination are published in Adamowski et al. (1998), Greenwood and Bamberger (2002), Higuti et al. (2007), Deventer and Delsing (1997) and Deventer and Delsing (2001a).

The only method that can be assumed to be independent of gradients in the sample medium is the ARM. The density is determined via RRMs at two different angles (Eq. 41). The sound velocity can be calculated as an additional parameter from the determined density, but is not necessary for the density determination. If Eq. (42) is used, the calculated sound velocity can be assumed to be the interfacial sound velocity of the sample medium. On the other hand, the density uncertainties of the ARM can be assumed to be even more complex than presented in Eqs. (52)–(55). And, in case the sound velocity is not determined by the TOF-distance relation but by Eq. (42), the sound velocity uncertainty becomes similar in complexity.

The last point concerning the temperature-related uncertainties will be the temperature dependency of transducers and PEM. Most transducers possess a matching layer or wear plate. The transmission through such layers clearly is temperature dependent and can be described in terms of wavelength and layer thickness. Furthermore, for quartz crystals and piezocermic materials, it is known that the resonance behaviour changes with temperature (Hammond and Benjaminson, 1965; Yang, 2006). This effect can actually be used to measure the temperature. Once an MRM is used or the RRM and ARM are calibrated for different temperatures, those influences can be neglected in terms of attenuation or varying transmission coefficients, but the frequency behaviour might change significantly. Consequently, signal-processing methods in the frequency domain possibly have to be modified to consider temperature-dependent variations, particularly the single-frequency method (see Eq. 46).

4.4 Relevant errors for industrial conditions

This section discusses errors which are especially relevant for industrial applications. First of all, errors due to thin layers, which may represent coupling layers, matching layers or buffer surface deposits, will be discussed. Surface deposits might be applied as a protective layer or might appear as a result of fouling.

In Püttmer et al. (1999), the focus is on investigation of surface deposits by simulations via SPICE. After validation with polystyrene layers of varying thickness, the developed model was applied for materials of varying acoustic impedance and thickness. Scattering effects due to nonplane surfaces have been neglected. The results show that for layers of impedance lower than the buffer material and $\lambda/100(\lambda/50)$ thickness, the error of the sample medium's acoustic impedance can reach up to 0.5 % (2.6 %); the USV error up to 0.05 % (0.1 %). For layers of impedance higher than the buffer material, the error increases rapidly. It is stated that deposits of low acoustic impedance such as polymers can be tolerated with a thickness up to $\lambda/50$.

In Deventer (2003) also the influence of fouling deposits is investigated via a PSPICE model. Commensurate with a different probe design, the effects of deposits are simulated for a PMMA buffer instead of quartz glass (Püttmer et al., 1999). For the deposit material a density of 1500 kg m^{-3} and a sound velocity of 3000 m s^{-1} was assumed and thicknesses of 0.5, 1 and 2 µm have been investigated. It was stated that, compared to a clean surface, the amplitude difference is quite high, but changing the layer thickness results only in small changes. While comparing the results with those of Püttmer et al. (1999), it was assumed that the model might be inconsistent. But comparing the details of both publications explains the difference: (1) in Püttmer et al. (1999) layer thicknesses relative to wavelength in the deposit material are investigated, which would correspond more likely to 8 and 17 µm layer thicknesses in the case of Deventer (2003). (2) In Püttmer et al. (1999) no results of amplitude changes but errors in the determination of acoustic impedance and sound velocity are presented. (3) Checking the presented results of Püttmer et al. (1999) for impedances higher than the buffer materials, as investigated in Deventer (2003), one can assume that the amplitude difference is quite high compared to clean

surface. Thus, based on the information given in Deventer (2003), no inconsistency is noticeable.

In Higuti et al. (2006) a model of acoustic or electroacoustic transmission lines was developed. The model was validated experimentally with signals from the true measurement cell, but without deposits. Metallization layers on the PVDF-receiver surface, varying thicknesses of the PVDF receiver, varying coupling layers and deposits on the buffer surface have been investigated. The thickness of the metallization layers was reported to be around 500 Å. In contrast to Deventer (2003) it was stated that layer thicknesses up to 1 µm do not introduce significant changes in the signals, and their effects can be neglected. In the case of the receiver thickness, the pulse centre frequency changes with temperature, while the bandwidth remains constant. It is shown that layer thickness variations significantly change the frequency domain information, which might result in errors > 2 % when applying the single-frequency approach. The error can be minimized by using the energy method and time delay compensation. The density error was kept within ±0.2 % for receiver thickness variations and within ±0.1 % for coupling layer variations up to 50 µm. Deposit results have been presented for varying thickness and different materials. For all presented materials the density error does not exceed 0.2 % up to 2 µm layer thickness. For higher thicknesses the error quickly reaches 6 % and more.

Actually, neither in Püttmer et al. (1999) nor in Deventer (2003) or Higuti et al. (2006) is the relevance of the assumed fouling properties and layer thicknesses discussed. For milk fouling layers, for example, a layer thickness of 500–700 µm and an impedance of 2.97 MRayl has been reported (Wallhäußer et al., 2009). Hence, concerning the impedance of biological fouling layers, the assumption of lower acoustic impedance seems to be correct for most buffer materials. Whether relevant thicknesses have been investigated so far is questionable. Generally it can be stated that not much is known about the acoustic properties of real fouling layers and that electrical analogous systems can be applied to investigate the influence of thin layer deposits under ideal conditions (Deventer, 2003; Higuti et al., 2006; Püttmer et al., 1999) and to simulate design aspects of probes with a few limitations (Deventer, 2004). In Püttmer et al. (1999) it is shown that the error due to thin layers can be reduced as long as the degree of fouling can be detected. Reference calibrations with air are proposed, while in Deventer (2003) it is recommended to detect fouling at higher frequencies via broadband transducers. Also, in Higuti et al. (2006) it is stated that a periodic calibration with a reference medium might be necessary.

Besides surface deposits, short-term variations of process variables might have an influence on the method's accuracy. The influence of temperature variations and measurement accuracy has already been discussed above. Also, the influence of varying flow condition on temperature gradients has already been indicated, but not the direct signal diversion due to a flow perpendicular to the propagation path. Generally it is assumed that the diversion can be neglected as long as the sound velocity in the medium is considerably higher than the flow velocity. Assuming a moderate flow of 5 m s^{-1} typically results in a diversion angle of 0.2°. In consequence, each molecule is distracted approximately 0.003 mm per mm propagation path while the signal propagates through the sample medium. First of all, the diversion results in an offset diffraction, and furthermore the angular difference from normal incidence causes a difference of approximately 0.1 % in the reflection coefficient. Greenwood et al. (1999) investigated flow velocities up to 2.5 m s^{-1} and found that the varying flow conditions did not significantly affect the average density bias. In Adamowski et al. (1995, 1998) varying flow velocities up to 10 m s^{-1} were investigated. It was found that the experimental results are not affected by the flow rate. Indeed, changes of reflection coefficient, sound velocity and density appeared, but relative to the temperature variation, the observed deviations have been within the precision range of the method. It is reported that cavitation occurred for mean flow velocities above 10 m s^{-1}, and for this reason the results became inconsistent. Further issues might occur in the case of non-homogenous suspensions or bubbly flow. As correctly stated by Schäfer et al. (2006), the measurement effect bases on reflection at interfaces. Non-homogenous distributions of solid or gaseous objects across the interface would lead to a certain error. In Greenwood and Bamberger (2002) the feasibility of the ARM for homogenous suspensions was proven. The influence of bubbly flow was also investigated, and it was reported that three of the six investigated instruments have been significantly affected by the air feed. It can be assumed that generally the bubble dependency depends on the design and placement of the probe. As long as the bubbles do not adhere to the interface, no significant effect on the reflection coefficient should be noticeable. For the ARM also, the sound velocity determination only depends on the interfacial information. In the case of the other methods the situation for the sound velocity is quite different. Depending on the amount of air inside a certain volume, the density and compressibility change:

$$\rho = \frac{(M_1 + M_2)}{(V_1 + V_2)}, \tag{57}$$

$$\kappa = \frac{(\kappa_1 V_1 + \kappa_2 V_2)}{(V_1 + V_2)}, \tag{58}$$

where M and V represent the mass and volume and the indices indicate the particular phase. According to Eq. (1) the sound velocity changes as a result. In Hoppe et al. (2002) it was stated that the bubbles operate like a high-pass filter. It was shown in Hoppe et al. (2001) that the amplitude and the zero crossing times of detected pulses decrease, but the arrival time of the signal does not change. It was further stated that the influence of gas bubbles on the speed-of-sound accuracy can be minimized by adequate signal processing.

Generally the attenuation due to bubbles is frequency dependent. The bubble size governs the resonance frequency of a bubble, and therefore the bubble size distribution with respect to the main frequency defines the degree of attenuation (Carstensen and Foldy, 1947; Silberman, 1957; Fox et al., 1995). According to Eq. (3), also the acoustic impedance could be affected for disadvantageous bubble distributions. Henning et al. noticed only a change of impedance for high bubble intensities (Hoppe et al., 2002).

5 Conclusions

In the last decades, several research groups have investigated varying methods based on BRTs. The reported methods can be classified into four main groups: MRM, TRM, RRM and ARM. Each method holds characteristic advantages and disadvantages. ARM and RRM are perfectly suited for highly sound absorbing liquids but require calibration measurements. The RRM is only suited for moderate sound absorbing liquids, but does not require calibrations. The TRM can be ranked somewhere in between, but as with the ARM, the method requires an additional receiver, which introduces additional sources of uncertainty. Although the RRM was proven theoretically to be more sensitive to SNR-caused inaccuracies than any other method, the experimental results did not confirm the theoretical evaluations. Basically all methods are sensitive to temperature gradients. While for MRM it is sufficient to determine the accurate temperature at the interface in order to determine the correct acoustic impedances, in the case of ARM and RRM it might be necessary to calibrate the probe for all relevant temperature gradients. An appropriate correction seems to be possible, but so far has not been proven to work accurately.

The main design limitations result from intentions to avoid pulse superposition. Pure pulses can be guaranteed by avoidance and suppression of radial mode vibrations and adequate dimensioning with respect to the given pulse duration and material properties. In some cases additional near-field constraints might have influenced the chosen dimension. Although angular reflections within the near field might disturb the sound field in a way that one should prevent the assumption of plane wave propagation, the ARM as well as the RRM can be assumed to be widely unaffected by those phenomena as long as all changes of the sound field are considered in the calibration. In the case of MRM and TRM, diffraction correction often is a major requirement for adequate errors. Alternatively to corrections, large-aperture receivers can be used in some applications to minimize the error.

The published results show minimum achievable density errors of 0.15 % for constant temperature and 0.4 % for varying temperatures, which is sufficient to identify liquids of significant different density. The question if the reported errors are sufficient for a suitable control of a specific process or not in the end depends on the density variation that can be expected. Sensitive biotechnological processes such as yeast fermentation generally show a density variation of $< 60\,\mathrm{kg\,m^{-3}}$, which results in density accuracy requirements of at least $1\,\mathrm{kg\,m^{-3}}$ or 0.1 %. In the case of density-based models for concentration measurements of multicomponent mixtures, an even lower error might be necessary.

The uncertainty analysis shows that errors in the reflection coefficient contribute significantly to the overall density error but has been investigated least so far, whereas the contributions of realistic errors of the sound velocities and buffer material's density are comparably low. Indeed, most authors neither state the accuracies of the sound velocities nor the accuracy of the reflection coefficient measurement. Although the few presented USV errors are $\geq 0.5\,\mathrm{m\,s^{-1}}$, state-of-the-art technologies can provide accuracies $\leq 0.1\,\mathrm{m\,s^{-1}}$ even for low sampling frequencies. Moreover, the buffer material's density can be determined with acceptable accuracies keeping the uncertainties of the sample liquid's density within the required accuracy. Consequently, improvements in the reflection coefficient determination are the right choice to improve the density accuracy. Main improvements are reached by increasing the SNR and improving the amplitude determination. Most authors apply signal averaging, which reduces the Gaussian noise. But averaging of the whole signal is only a feasible method as long as the signal acquisition rate is much higher than changes of process parameters. In the case of fast varying sound velocity, signal averaging can cause systematic errors. We assume that it might be better not to average the whole signal but only the relevant pulses after being centred to a characteristic location. Errors due to systematic changes in the frequency domain can be minimized by applying the integration method to an adequate frequency band. The temperature measurement is identified as another main source of error. Often the temperature at a certain position is required to calculate the buffer material's properties from reference polynomials. In addition, temperature gradients may occur, particularly during dynamic process changes. Thus, for real-time process application and exact validation it is necessary to measure the temperature as accurately as possible ($\leq \pm 0.01\,\mathrm{K}$) and to observe temperature gradients as they may arise. Altogether it seems possible to reach an accuracy of $\leq 1\,\mathrm{kg\,m^{-3}}$ even for dynamic conditions. At present, the remaining uncertainty could be a result of both the assumed simplifications for the reflection coefficient at solid–liquid interfaces or the technological limitations – state of the art is a 12-bit resolution at 1 GHz sampling rate; a higher vertical resolution of 14 bit or more often results in significantly lower sampling rates.

A sensor system for real-time process application will have to be suitable to fulfil all involved task reaching, from generation of the excitation signal and sound signal capturing over temperature measurement and up to signal processing. To date, most of the basics have been investigated, but still final statements about which technology or method suits best a certain case of application are not possible. It is not

known if simple peak excitations are sufficient or if bursts of a certain frequency are the best choice. It is not clear exactly if signals of a specified frequency require a certain sampling frequency in order to reach the desired density accuracy or not. Similar can be stated for the different signal-processing methods. Applying spline interpolation in the time domain might reach comparable results such as integration in the frequency domain. The big question is which one requires less computational effort. From the technological point of view it is clear that a vertical resolution of 12 bit or better is required to reach accurate results. For statements about electronic effort, computation power and the required memory, first the basic aspects of signal generation and signal processing have to be discussed in more detail. Definitely not all methodical options to determine the reflection coefficient via BRT have been investigated so far, but the basic rules are clear: minimization or correction of temperature gradients, and maximization of SNR.

Edited by: M. Jose da Silva
Reviewed by: three anonymous referees

References

Adamowski, J. C., Buiochi, C., Simon, C., Silva, E. C. N., and Sigelmann, R. A.: Ultrasonic measurement of density of liquids, J. Acoust. Soc. Am., 97, 354–361, 1995.

Adamowski, J. C., Buiochi, C., and Sigelmann, R. A.: Ultrasonic Measurement of Density of Liquids Flowing in Tubes, IEEE Transactions on Ultrasonics, Ferroelectrics, and Frequency Control, 45, 48–56, 1998.

Asher, R. C.: Ultrasonics in chemical analysis, Ultrasonics, 25 17–19, 1987.

Bamberger, J. A. and Greenwood, M. S.: Measuring fluid and slurry density and solids concentration non-invasively, Ultrasonics, 42, 563–567, 2004a.

Bamberger, J. A. and Greenwood, M. S.: Non-invasive characterization of fluid foodstuffs based on ultrasonic measurements, Food Res. Int., 37, 621–625, 2004b.

Bjørndal, E. and Frøysa, K. E.: Acoustic Methods for Obtaining the Pressure Reflection Coefficient from a Buffer Rod Based Measurement Cell, IEEE Trans UFFC, 55, 1781–1793, 2008.

Bjørndal, E., Frøysa, K. E., and Engeseth, S. A.: A Novel Approach to Acoustic Liquid Density Measurements Using a Buffer Rod Based Measuring Cell, IEEE Trans UFFC, 55, 1794–1808, 2008.

Bolotnikov, M. F., Neruchev, Y. A., Melikhov, Y. F., Verveyko, V. N., and Verveyko, M. V.: Temperature Dependence of the Speed of Sound, Densities, and Isentropic Compressibilities of Hexane + Hexadecane in the Range of (293.15 to 373.15) K, J. Chem. Eng. Data 50, 1095–1098, 2005.

Carlson, J. E., Deventer, J., and Micella, M.: Accurate temperature estimation in ultrasonic pulse-echo systems, World Congress on Ultrasonics, Paris, 2003a.

Carlson, J. E., Deventer, J., Scolan, A., and Carlander, C.: Frequency and Temperature Dependence of Acoustic Properties of Polymers Used in Pulse-Echo Systems, IEEE ULTRASONICS SYMPOSIUM, 8030032, 885–888, 2003b.

Carstensen, E. L. and Foldy, L. L.: Propagation of Sound Through a Liquid Containing Bubbles, J. Acoust. Soc. Am., 19, 481–501, 1947.

Childs, P. R. N., Greenwood, J. R., and Long, C. A.: Review of temperature measurement, Rev. Sci. Instrum., 71, 2959–2978, doi:10.1063/1.1305516, 2000.

Daridon, J. L., Lagourette, B., Xan, B., and Montel, F.: Petroleum characterization from ultrasonic measurement, J. Petrol. Sci. Eng., 19 281–293, 1998a.

Daridon, J. L., Lagrabette, A., and Lagourette, B.: Speed of sound, density, and compressibilities of heavy synthetic cuts from ultrasonic measurements under pressure, J. Chem. Thermodynam., 30, 607–623, 1998b.

Davis, L. A. and Gordon, R. B.: Compression of Mercury at High Pressure, J. Chem. Phys., 46, 2650–2660, 1967.

Deventer, J.: Detection of, and compensation for error inducing thin layer deposits on an ultrasonic densitometer for liquids, Instrumentation and Measurement Technology Conference 2003, 648–651, 2003.

Deventer, J.: One dimensional modeling of a step-down ultrasonic densitometer for liquids, Ultrasonics, 42, 309–314, 2004.

Deventer, J. and Delsing, J.: An Ultrasonic Density Probe, IEEE ULTRASONICS SYMPOSIUM, 1997.

Deventer, J. and Delsing, J.: Thermostatic and Dynamic Performance of an Ultrasonic Density Probe, IEEE Trans UFFC, 48, 675–682, 2001a.

Deventer, J. and Delsing, J.: Thermostatic and Dynamic Performance of an Ultrasonic Density Probe, IEEE Trans. UFFC, 48, 675–682, 2001b.

Esperança, J. M. S. S., Visak, Z. P., Plechkova, N. V., Seddon, K. R., Guedes, H. J. R., and Rebelo, L. P. N.: Density, Speed of Sound, and Derived Thermodynamic Properties of Ionic Liquids over an Extended Pressure Range. 4. [C3mim][NTf2] and [C5mim][NTf2], J. Chem. Eng. Data, 51, 2009–2015, 2006.

Fisher, B., Magpori, V., and von Jena, A.: Ultraschall (US)-Dichtemesser mm Messen der spezifischen Dichte eines Fluid, EP 0 483 491 81, Europe, 1995.

Fox, F. E., Curley, S. R., and Larson, G. S.: Phase Velocity and Absorption Measurements in Water Containing Air Bubbles, The J. Acoust. Soc. Am., 27, 534–539, 1995.

Greenwood, M. S.: Ultrasonic fluid densitometer having liquid/wedge and gas/wedge interfaces, 6, 082, 181, United States, 2000.

Greenwood, M. S. and Bamberger, J. A.: Ultrasonic sensor to measure the density of a liquid or slurry during pipeline transport, Ultrasonics, 40, 413–417, 2002.

Greenwood, M. S. and Bamberger, J. A.: Self-Calibrating Sensor for Measuring Density Through Stainless Steel Pipeline Wall, J. Fluid. Eng., 126, 189–192, 2004.

Greenwood, M. S., Skorpik, J. R., Bamberger, J. A., and Harris, R. V.: On-line Ultrasonic Density Sensor for Process Control of Liquids and Slurries, Ultrasonics, 37, 159–171, 1999.

Greenwood, M. S., Adamson, J. D., and Bamberger, J. A.: Long-path measurements of ultrasonic attenuation and velocity for very dilute slurries and liquids and detection of contaminates, Ultrasonics, 44, e461–e466, 2006.

Guilbert, A. R. and Sanderson, M. L.: A novel ultrasonic mass flowmeter for liquids, IEE colloquium on: Advances in Sensors for Fluid Flow Measurement, London, 1996.

Hale, J. M.: Ultrasonic density measurement for process control, Ultrasonics, 26, 356–357, 1988.

Hammond, L. D. and Benjaminson, A.: The Linear Quartz Thermometer - a New Tool for Measuring Absolute and Difference Temperatures, Hewlett-Packard Journal, 16, 1965.

Henning, B., Prange, S., Dierks, K., Daur, C., and Hauptmann, P.: In-line concentration measurement in complex liquids using ultrasonic sensors, Ultrasonics, 38, 799–803, 2000.

Higuti, R. T. and Adamowski, J. C.: Ultrasonic Densitometer Using a Multiple Reflection Technique, IEEE Trans UFFC, 49, 1260–1268, 2002a.

Higuti, R. T. and Adamowski, J. C.: Ultrasonic densitometer using a multiple reflection technique, IEEE Trans. Ultrason., Ferroelect., Freq. Contr., 49, 1260–1268, 2002b.

Higuti, R. T., Montero de Espinosa, F. R., and Adamowski, J. C.: Energy method to calculate the density of liquids using ultrasonic reflection techniques, Proc. IEEE Ultrason. Symp., 319–322, 2001.

Higuti, R. T., Buiochi, C., Adamowski, J. C., and Espinosa, F. M.: Ultrasonic density measurement cell design and simulation of non-ideal effects, Ultrasonics, 44, 302–309, 2006.

Higuti, R. T., Galindo, B. S., Kitano, C., Buiochi, C., and Adamowski, J. C.: Thermal Characterization of an Ultrasonic Density-Measurement Cell, IEEE Transactions on Instrumentation and Measurement, 56, 924–930, 2007.

Hoche, S., Hussein, W. B., Hussein, M. A., and Becker, T.: Time-of-f light prediction for fermentation process monitoring, Eng. Life Sci., 11, 1–12, 2011.

Hoppe, N., Schönfelder, G., Püttmer, A., and Hauptmann, P.: Ultrasonic density sensor – Higher accuracy by minimizing error influences, Proc. IEEE Ultrason. Symp., 361–364, 2001.

Hoppe, N., Schönfelder, G., and Hauptmann, P.: Ultraschall-Dichtesensor für Flüssigkeiten – Eigenschaften und Grenzen, Technisches Messen, 3, 131–137, 2002.

Hoppe, N., Püttmer, A., and Hauptmann, P.: Optimization of Buffer Rod Geometry for Ultrasonic Sensors with Reference Path, IEEE Trans UFFC, 50, 170–178, 2003.

Jensen, B. R.: Measuring equipment for acoustic determination of the specific gravity of liquids, 4, 297, 608, United States, 1981.

Kaatze, U., Eggers, F., and Lautscham, K.: Ultrasonic velocity measurements in liquids with high resolution – techniques, selected applications and perspectives, Meas. Sci. Technol., 19, 1–21, doi:10.1088/0957-0233/19/6/062001, 2008.

Kaduchak, G. and Sinha, D. N.: Apparatus and method for remote, noninvasive characterization of structures and fluids inside containers, 8, 186, 004 B1, United States, 2001.

Kell, G. S.: Density, Thermal Expansivity, and Compressibility of Liquid Water from 0° to 150 °C: Correlations and Tables for Atmospheric Pressure and Saturation Reviewed and Expressed on 1968 Temperature Scale, J. Chem. Eng. Data, 20, 97–105, 1975.

Kim, J. O. and Bau, H. H.: Instrument for simultaneous measurement of density and viscosity, Rev. Sci. Instrum., 60, 1111–1115, 1989.

Krautkramer, J. and Krautkramer, H.: Ultrasonic Testing of Materials, 3rd edn. ed., Springer-Verlag, New York, 1983.

Kulmyrzaev, A., Cancelliere, C., and McClements, D. J.: Characterization of aerated foods using ultrasonic reflectance spectroscopy, J. Food Eng., 46, 235–241, 2000.

Kuo, H. L.: Variation of Ultrasonic Velocity and Absorption with Temperature and Frequency in High Viscosity Vegetable Oils, Japanese Journal of Applied Physics, 10, 167–170, 1971.

Kushibiki, J., Akashi, N., Sannomiya, T., Chubachi, N., and Dunn, F.: VHF/UHF range bioultrasonic spectroscopy system and method, IEEE Trans. Ultrason., Ferroelec. Freq. Contr., 42, 1028–1039, 1995.

Kushibiki, J., Okabe, R., and Arakawa, M.: Precise measurements of bulk-wave ultrasonic velocity dispersion and attenuation in solid materials in the VHF range, J. Acoust. Soc. Am., 113, 3171–3178, 2003.

Lach, M., Platte, M., and Ries, A.: Piezoelectric materials for ultrasonic probes, NDTnet, 1, 1996.

Lynnworth, L. C. and Pedersen, N. E.: Ultrasonic mass flowmeter, Proc. IEEE Ultrason. Symp., 87–90, 1972.

Lynnworth, L. C.: Ultrasonic nonresonant sensors, in: Sensors – A Comprehensive Survey, edited by: Göpel, W., Hesse, J., and Zemel, J. N., Mechanical Sensors, VCH Publishers Inc., New York, 311–312, 1994.

Mak, D. K.: Comparison of various methods for the measurment of reflection coefficient and ultrasonic attenuation, British Journal of NDT, 33, 441–449, 1991.

Marczak, W.: Water as standard in the measurements of speed of sound in liquids, J. Acoust. Soc. Am., 102, 2776–2779, 1997.

Marks, G. W.: Acoustic Velocity with Relation to Chemical Constitution in Alcohols, The Journal of the Acoustical Society of America, 41, 103–117, 1976.

Mason, P., Baker, W. O., McSkimin, H. J., and Bepiss, J. H.: Measurement of Shear Elasticity and Viscosity of Liquids at Ultrasonic Frequencies, Phys. Rev., 75, 936–946, 1949.

Matson, J., Mariano, C. F., Khrakovsky, O., and Lynnworth, L. C.: Ultrasonic Mass Flowmeters Using Clamp-On or Wetted Transducers, 5th International Symposium on Fluid Flow Measurement, Arlington, Virginia, 2002,

McClements, D. J.: Ultrasonic Characterization of Foods and Drinks: Principles, Methods, and Applications, Critical Reviews in Food Science and Nutrition, 37, 1–46, 1997.

McClements, D. J. and Fairly, P.: Ultrasonic pulse echo reflectometer, Ultrasonics 29, 58–62, 1991.

McClements, D. J. and Fairly, P.: Frequency scanning ultrasonic pulse echo reflectometer, Ultrasonics, 30, 403–405, 1992.

Mc Gregor, K. W.: Methods of Ultrasonic Density Measurement, Australasian Instrumentation and Measurement Conference, Adelaide, S. Aust., 1989.

Moore, R. S. and McSkimin, H. J.: Physical Acoustics, Academic Press, New York, 167–242, 1970.

O'Neil, H. T.: Reflection and Refraction of Plane Shear Waves in Viscoelastic Media, Phys. Rev., 75, 928–935, 1949.

Papadakis, E. P.: Correction for Diffraction Losses in the Ultasonic Field of a Piston Source, J. Acoust. Soc. Am., 31, 150–152, 1959.

Papadakis, E. P.: Buffer-Rod System for Ultrasonic Attenuation Measurements, J. Acoust. Soc. Am., 44, 1437–1441, 1968.

Papadakis, E. P., Fowler, K. A., and Lynnworth, L. C.: Ultrasonic attenuation by spectrum analysis of pulses in buffer rods: Method and diffraction corrections, J. Acoust. Soc. Am., 53, 1336–1343, 1973.

Pope, N. G., Veirs, D. K., and Claytor, T. N.: Fluid Density and Concentration Measurment using noninvasive in situ ultrasound

resonance interferometry, Ultrasonics Symposium, 1992, 855–858, 1992.

Pope, N. G., Veirs, D. K., and Claytor, T. N.: Fluid density and concentration measurment using noninvasive in situ ultrasonic resonance interferometry, 5, 359, 541, United States, 1994.

Povey, M. J. W. and McClements, D. J.: Ultrasonics in Food Engineering. Part I: Introduction and Experimental Methods, J. Food Eng., 8, 217–245, 1988.

Püttmer, A. and Hauptmann, P.: Ultrasonic density sensor for liquids, Proc. IEEE Ultrason. Symp., 497–500, 1998.

Püttmer, A., Lucklum, R., Henning, B., and Hauptmann, P.: Improved ultrasonic density sensor with reduced diffraction influence, Sensors Actuators A, 67, 8–12, 1998.

Püttmer, A., Hoppe, N., Henning, B., and Hauptmann, P.: Ultrasonic density sensor–analysis of errors due to thin layers of deposits on the sensor surface, Sensor. Actuator., 76, 122–126, 1999.

Püttmer, A., Hauptmann, P., and Henning, B.: Ultrasonic density sensor for liquids, IEEE Trans. Ultrason., Ferroelec. Freq. Contr., 47, 85–92, 2000.

Raum, K., Ozguler, A., Morris, S. A., and O'Brien, W. D. J.: Channel Defect Detection in Food Packages Using Integrated Backscatter ultrasound Imaging, IEEE Trans UFFC, 45, 30–40, 1998.

Rychagov, M. N., Tereshchenko, S., Masloboev, Y., Simon, M., and Lynnworth, L. C.: Mass Flowmeters for Fluids with Density Gradient, IEEE Ultrasonics Symposium, 465–470, 2002.

Sachse, W.: Density determination of a fluid inclusion in an elastic solid from ultrasonic spectroscopy measurements, Proc. IEEE Ultrason. Symp., 716–719, 1974.

Saggin, R. and Coupland, J. N.: Concentration Measurement by Acoustic Reflectance, J. Food Sci., 66, 681–685, 2001.

Schäfer, R., Carlson, J. E., and Hauptmann, P.: Ultrasonic concentration measurement of aqueous solutions using PLS regression, Ultrasonics, 44, e947–e950, 2006.

Silberman, E.: Sound Velocity and Attenuation in Bubbly Mixtures Measured in Standing Wave Tubes, J. Acoust. Soc. Am., 29, 925–933, 1957.

Sinha, D. N.: Noninvasive identification of fluids by swept frequency acoustic interferometry, 5, 767, 407, United States, 1998.

Sinha, D. N. and Kaduchak, G.: Chapter 8: Noninvasive determination of sound speed and attenuation in liquids, in: Experimental Methods in the Physical Sciences, Academic Press, 307–333, 2001.

Swoboda, C. A., Frederickson, D. R., Gabelnick, S. D., Cannon, P. H., Hornestra, F., Yao, N. P., Phan, K. A., and Singleterry, M. K.: Development of an Ultrasonic Technique to Measure Specific Gravity in Lead-Acid Battery Electrolyte, IEEE Transactions on Sonics and Ultrasonics, 30, 69–77, 1983.

Van Sint Jan, M., Guarini, M., Guesalaga, A., Ricardo Perez-Correa, J., and Vargas, Y.: Ultrasound based measurements of sugar and ethanol concentrations in hydroalcoholic solutions, Food Control, 19, 31–35, 2008.

Vray, D., Berchoux, D., Delachartre, P., and Gimenez, G.: Speed of Sound in Sulfuric Acid Solution: Application to Density Measurement, Ultrasonics Symposium, 465–470, 1992.

Wallhäußer, E., Hussein, M. A., Hinrichs, J., and Becker, T.: The acoustic impedance – an indicator for concentration in alcoholic fermentation and cleaning progress of fouled tube heat exchangers, 5th International Technical Symposium on Food Processing, Monitoring Technology in Bioprocesses and Food Quality Management, Potsdam, Germany, 1 September, 2009.

Wang, H., Cao, Y., Zhang, Y., and Chen, Z.: The design of The ultrasonic liquid density measuring instrument, Third International Conference on Measuring Technology and Mechatronics Automation, 2011.

Wang, Z. and Nur, A.: Ultrasonic velocities in pure hydrocarbons and mixtures, J. Acoust. Soc. Am., 89, 2725–2730, 1991.

Williams, A. O. J. and Labaw, L. W.: Acoustic Intensity Distribution from a "Piston" Source, J. Acoust. Soc. Am., 16, 231–236, 1945.

Williams, A. O. J.: The Piston Source at High Frequencies, J. Acoust. Soc. Am., 23, 1–6, 1951.

Yang, J.: Chapter 10: Temperature Sensors, in: Analysis of Piezoelectric Devices, World Scientific Publishing Co. Pte. Ltd., Singapore, 371–386, 2006.

Żak, A., Dzida, M., Zorbęski, M., and Ernst, S.: A high pressure device for measurements of the speed of sound in liquids, Rev. Sci. Instrum., 71, 1756–1765, 2000.

2.2.2 Critical process parameter of alcoholic yeast fermentation: speed of sound and density in the temperature range 5–30 °C.

Critical process parameter of alcoholic yeast fermentation: speed of sound and density in the temperature range 5–30 °C

Sven Hoche,[1] Mohamed A. Hussein[1]* & Thomas Becker[2]

1 Technische Universitat Munchen, Bio PAT (Bio Process Analysis Technology), Weihenstephaner Steig 20, Freising 85354, Germany
2 Technische Universitat Munchen, Chair of Brewing and Beverage Technology, Weihenstephaner Steig 20, Freising 85354, Germany

(Received 15 January 2014; Accepted in revised form 1 April 2014)

Summary To implement process analytical technology in beer manufacturing, a systematic study of the ternary system water maltose ethanol with respect to the critical process parameters, density, speed of sound and temperature was performed. The results are presented in the form of temperature and mass-fraction-dependent polynomial expressions. On average, a variation of 1% mass fraction maltose results in variations of 3.548 m s^{-1} ultrasound velocity and 0.0041 g cm^{-3} density, whereas in the case of ethanol, the variations are 8.060 m s^{-1} and −0.0018 g cm^{-3}. Indeed, the relations are strictly nonlinear. Nevertheless, the determined data show the feasibility to predict online, concentrations of multicomponent mixtures of polar liquids by determining density and ultrasound velocity. With <0.1% error, the measured data show excellent agreement with reference data of binary mixtures as given in literature.

Keywords Alcoholic beverages, beer and the brewing process, chemical composition, fermentation, physicochemical properties, quality control, thermal analysis, yeast.

Introduction

The implementation of process analytical technology (PAT) in the food and beverage industries has drawn more and more interest. PAT includes the evaluation of critical process parameters (CPPs) and the application of in-line and online analytical instruments to measure the CPPs aiming to reach consistent product quality and to reduce waste and overall costs. Concerning beverages like juices, wine or beer, the sugar and ethanol concentrations are the critical quality attributes (CQA).

The actual research project investigates the options to apply PAT to beer manufacturing using ultrasound-based analytical instruments. Temperature, density and ultrasound velocity are the evaluated CPPs to quantify uniquely the CQAs. While binary mixtures, like water–ethanol or water–sugar mixtures, were investigated quite intensively (Parke & Birch, 1999; Petong *et al*., 2000; Vatandas *et al*., 2007; Schöck & Becker, 2010), data of the ternary mixtures are rarely found. The binary systems can be characterised uniquely by only two physical variables, for example, temperature and sound velocity. However, the concentration determination of the ternary system requires at least the speed of sound at two different temperatures (Schöck & Becker, 2010) or a significant third variable (e.g. density). In (Contreras *et al*., 1992; Gepert & Moskaluk, 2007) the binary system of water with the sugar species sucrose, fructose and glucose were studied with respect to temperature, density, speed of sound and refractive index. It is stated that the density and the refractive index are virtually insensitive to the sugar type and could be used as an estimator of the sugar content, without regard to the type of sugar. In contrast, the speed of sound was more sensitive to the sugar species. It was shown that the sensitivity depends on the compressibility and therefore on the stereochemistry of the sugar species (Contreras *et al*., 1992). Finally, the presented model was applied to predict the sugar contents within 0.2% weight per volume. Although the work of Contreras *et al*. (1992) is only valid for the binary system water–sugar, it indicates that taking data of the wrong sugar type might introduce enormous errors. Depending on sugar type, temperature and mass fraction, speed of sound differences up to 10 m s^{-1} can appear. Investigations of the temperature-dependent speed of sound exist for the ternary system water–sucrose–ethanol (Schöck & Becker, 2010). Furthermore, published density and sound velocity data for the ternary system water–sucrose–ethanol are limited to 30 °C (Resa *et al*., 2004, 2005).

*Correspondent: Fax: +49/8161/71 3883;
e mail: hussein@wzw.tum.de.

Clearly, there is a lack of information concerning the temperature-dependent sound velocity and density data of sugar–ethanol solutions, particularly for the equally relevant sugar species glucose, fructose, maltose and maltotriose. The actual study presents the CPP determination within a relevant range of process parameters for anaerobic yeast fermentation of malt-based sugar solutions. The data are required to develop mathematical models to determine online the CQAs and to validate suitable measurement principles (Hoche *et al*., 2013).

Materials, methods and experimental set-up

Solutions of ethanol, maltose and demineralised water were prepared by weighting the components mass fractions within a precision of 0.1 g for a total weight 1000 g. The exact mass fraction was determined by laboratory analysis. The ethanol mass fraction E (ROTIPURAN®, ≥99.8%; Carl Roth GmbH & Co. KG; Karlsruhe, Germany; http://www.carlroth.com) was varied from 0 to 6% in 1% steps, the maltose mass fraction M (SUNMALT-S, maltose: ≥92%, glucose: ≤3%; Hayashibara Shoji Inc., Okayama, Japan; http://www.hayashibara.co.jp/contact_en.php) from 0 to 12% in 2% steps and the temperature T from 10 to 30 °C in 5 K steps. In pretrials, 16% solutions of SUNMALT and a HPLC grade maltose (D(+)-Maltose Monohydrat, ≥95%; Carl Roth GmbH & Co. KG) were compared, and no significant difference in density or speed of sound was found. Additionally, for reasons of model extension and improvement, the mixtures 14%M–0%E, 16%M–0%E, 14%M–6%E and 16%M–6%E were measured at T: 10,15,20,25,30 °C, and the following mixtures 0%M–6%E, 2%M–0%E, 4%M–4%E, 6%M–3%E, 12%M–0%E, 12%M–6%E at T:5 °C. All samples were prepared with demineralised water at 20 °C. All experiments were executed at normal pressure.

Density measurement

A vibrating U-tube density meter (L-Dens 313, Anton Paar DMA-40; Anton Paar GmbH, Graz, Austria; http://www.anton-paar.com) was used to determine the density. The density accuracy is indicated with 1E-3 g cm $^{-3}$.

Speed of sound measurement

The speed of sound is determined via the pulse-echo method. Ultrasonic signals were generated and captured via a multichannel signal transformer (MCST, 14 bit amplitude resolution, 50 MHz time resolution). A MB2S transducer (General Electrics, 2 MHz centre frequency) and a rectangular excitation pulse of a half period duration were applied to generate the ultrasound signal. The time of flight (TOF) was analysed via cross-correlation and root approximation as presented in (Hoche *et al*., 2011). Relativising the covered distance, l to the passed time, TOF determines the speed of sound, USV:

$$\mathrm{USV} = \frac{l}{\mathrm{TOF}} \tag{1}$$

Uncertainty considerations showed that USV accuracies ≤0.1 m s $^{-1}$ require a distance accuracy in the range of a few μm, which can hardly be achieved by manual measurements. The solution often is a calibration with a liquid of which the speed of sound and temperature is known. In contrast to the investigations of (Contreras *et al*., 1992) who used the (Del Grosso & Mader, 1972) calibration reference, it is recommended to apply (Marczak, 1997). Further uncertainty considerations concerning the calibration procedure showed that to achieve the required distance accuracy, a temperature accuracy ≤10 mK ought to be aimed at. Once the temperature is known, the reference's USV can be calculated. Analysing the TOF from the signals and rearranging equation 1, the exact sound propagation path can be calculated. Besides the temperature accuracy, the temperature uniformity across the propagation path is of immense importance for the accuracy of the USV (see paragraph 3).

Experimental set-up

The experimental set-up consists of two main circuits, the water and the sample circuit. The sample liquid circuit contains the speed of sound measurement cell [ultrasound velocity measurement cell (USVMC)], the density meter, the storage container, silicone pipes, spiral chiller and the centrifugal micropump (see Fig. 1). The water circuit contains two separate circuits to provide a homogenous, temperature-controlled environment for the chiller and the USVMC. The whole experimental set-up was assembled in a temperature-controlled chamber (controlled to 20 °C) to provide reproducible conditions.

The submerged storage container and the immersed spiral chiller are employed to ensure the temperature stability across the sound propagation path. Temperature differences had to be expected at measurement temperatures that differ from the environmental temperature due to sample circulation through pump and density meter (both not submergible). The sample liquid circulation is required due to the density meter measurement principle and the avoidance of bubbles from de-aeration. The voltage supply of the centrifugal micro pump (M400-S, RS Components GmbH) was kept constant at 6 V. Trials with water at 20 °C showed a flow rate of approximately 3 L h $^{-1}$.

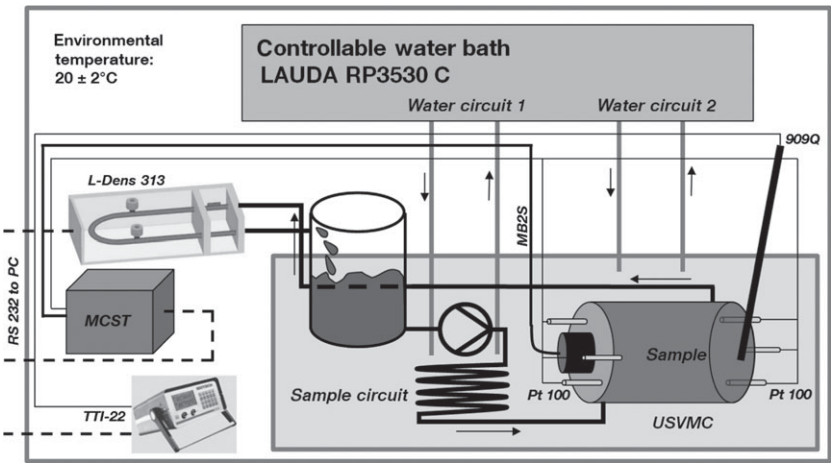

Figure 1 Scheme of the experimental set up for the online measurement of ultrasound signals in the ultrasound velocity measurement cell (US VMC) via multichannel signal transformer (MCST) and transducer (MB2S), the temperature (TTI 22 and 909Q) and the density (L Dens 313).

The temperature control was provided by a Lauda RP3530 C cooling thermostat, which gives a temperature stability of ±0.02 K according to the technical specifications. Generally, the 909Q thermometer showed variations of ±5 mK. The USVMC consists of two Poly (methyl methacrylate) (PMMA) cylinders (diameter: 100 mm, length: 20 mm) flanged to a PMMA tube (diameter: 80 mm, length: 100 mm) and three Pt100 at each side of the tube, immersible in varying depths. The transducer was pressed waterproofed to the PMMA cylinder by an additional flange. The PMMA was chosen as USVMC material due to its good acoustic and processing properties and moreover its transparency, which allows monitoring of the transducer's coupling and the appearance of bubbles.

Temperature measurement

Speed of sound and density are measured at two different locations, and equality of temperature could not be guaranteed. Consequently, the temperature had to be determined at both locations. The temperature accuracy of the density meter is indicated with 0.1 °C. To characterise the temperature of the USVMC, a measurement chain consisting of TTI-22 (Isothermal Technology Ltd, Merseyside, England; http://www.isotech.co.uk) and a standard platinum resistance thermometer (SPRT 909Q, 25.5 Ω; Isothermal Technology Ltd.) was used, resulting in a certified accuracy of ≤5 mK.

Trial procedure

At each series of measurements, the temperature and the maltose mass fraction was kept constant, while the ethanol mass fraction was increased stepwise. Prior to each series, demineralised water was circulated overnight at a similar temperature to calibrate the propagation path. Cleaning, disassembling and drying to guarantee the sample's purity could not be carried out within time. Instead, 50 mL was sampled twice to analyse the mass fraction offline, the first sample prior and the second after the measurement. Between sample filling and measurement start, a 30-min down time was maintained to ensure temperature and concentration equilibrium. Furthermore, the sample liquid was pre-temperature-stabilised in the water circuit. The measurement duration was a minimum of 1 h to ensure a sufficient amount of data. Both sample discharge and leak tightness were ensured by pressurised gas. Summarising, all the procedures were designed to eliminate the need for disassembly. Cleaning cycles were executed periodically, in particular to avoid fouling layers in the density meter.

Laboratory measurement

The samples token was analysed offline via Alcolyzer Beer Analyzing System (DMA 4500 M; Anton Paar). The system provides an accuracy of 0.01% g g ^{1} sugar content, 0.01% mL mL ^{1} ethanol content and 1E-5 g cm ^{3}. All given laboratory results are valid for 20 °C.

Data analysis

In the end, each analysis point of the main trials is characterised by temperature and component mass fraction. From each unique parameter combination, 100 values of USV, density and temperature were extracted from the data pool. Overall the standard deviations were <0.02 m s ^{1} (USV), <1.5 mK (temperature) and <0.055 kg m ^{3} (density). The bias of the laboratory analysis of the component mass fraction was generally <0.05%. The parameter average of each analysis point

was calculated and used for modelling. As discussed already by Resa *et al.*, 2004 (2005), prediction theories based on additivity of single component properties are incorrect in case of mixtures of polar liquids. Consequently, linear regression of the monitored properties as applied successfully by several authors might be the best choice. First, all values were scaled and a stepwise linear regression was applied to identify significant predictors. Terms from multilinear model of defined order are added and removed systematically based on their statistical significance. At each step, the significance of the model (F-statistics) and the probability value are calculated according to the analysis of variance to decide whether the term is added or removed.

Finally, a linear regression is executed and the relevant regression coefficients are calculated. The coefficients b and the variables V of the regression model according to following equation:

$$\text{value} = \sum_{i=0}^{n} b_i V_i \qquad (2)$$

are presented in tabular form in Tables 1 and 2, whereby M is the maltose mass fraction, E the ethanol mass fraction and T the temperature in °C.

Results

Thermal characterisation of the USVMC

The temperature variation of 10–30 °C results in a thermal expansion of ±0.16 mm for PMMA, which would generate an USV error in the range of ± 2.5 m s $^{-1}$ if not considered. Consequently, the calibration procedure of the sound propagation path (RD) and the influence of temperature gradients on the method's accuracy ought to be evaluated. The description of the temperature dependency of the RD is based on the material's thermal expansion coefficient (PMMA: 70E-6 K $^{-1}$) and the exact length of the tube at 20 °C. Therewith, following points were investigated: sensitivity to gradients, occurrence of gradients under ideal conditions and reproducibility. The sensitivity was investigated by comparing the thermal behaviour of a 150 mm PMMA tube with and without control of the environmental temperature. The used Pt100s were calibrated individually by comparing with the 909Q, which resulted in RMSE ≤10 mK. Without temperature-controlled environment, temperature gradients up to ±3 K ($T_{\text{interphase}}$-T_{liquid}) could be determined, which resulted in RD errors up to ±0.1 mm compared with the theoretical values and USV errors up to ±1 m s $^{-1}$. The temperature was increased in 5 K steps from 10 to 30 °C and decreased subsequent in similar manner. Each temperature level was maintained for at least 2 h. Submerging the USVMC into the temperature-controlled environment decreased the gradients to <0.1 K, the RD deviations to ±0.01 mm and USV errors to ±0.1 m s $^{-1}$. Nevertheless, while evaluating the reproducibility, a steady increase in the RD values combined with repeatable hysteresis characteristics was noticed. Examining all possible sources of error, the hygroscopicity of PMMA (Drotning & Roth, 1989; Balakrishnan *et al.*, 2009) was identified to be the origin of the observed cyclic changes. The technical information provided by Evonik shows that a mass uptake up to 2.1% is possible, resulting in one-dimensional changes of up to 0.5% (Drotning & Roth, 1989). Furthermore, it is known that the water uptake kinetic is a time-dependent process, which can be described by a logarithmic dependency. Nevertheless, the parameter that describes the time-dependent behaviour and the maximum water uptake is not constant but depends on the environmental humidity, the material's thickness and the temperature.

Table 1 Coefficients b and variables V of the USV model [m s $^{-1}$]; validity: T: 5 30 °C, M: 0 16% maltose, E: 0 6% ethanol; R^2: 0.99964

Coefficients		Variables	
b0	1401.49050E+00	V0	1
b1	5.24909E+00	V1	T
b2	6.96326E 02	V2	T^2
b3	4.77420E 04	V3	T^3
b4	11.09431E+00	V4	E
b5	2.28510E 01	V5	$E{\cdot}T$
b6	2.13121E 03	V6	$E{\cdot}T^2$
b7	1.15929E 01	V7	E^2
b8	3.63321E 03	V8	$E^2{\cdot}T$
b9	3.07545E+00	V9	M
b10	2.26556E 02	V10	$M{\cdot}T$
b11	1.12740E 01	V11	$M{\cdot}E$
b12	1.31515E 03	V12	$M{\cdot}E{\cdot}T$
b13	8.53391E 03	V13	$M{\cdot}E^2$
b14	9.70835E 02	V14	M^2
b15	6.40807E 04	V15	$M^2{\cdot}T$
b16	2.23096E 03	V16	M^3

Table 2 Coefficients b and the variables V of the density model [g cm $^{-3}$]; validity: T: 5 30 °C, M: 0 16% maltose, E: 0 6% ethanol; R^2: 0.99995

Coefficient		Variables	
b0	9.99876E 01	V0	1
b1	4.57170E 06	V1	T^2
b2	1.90160E 03	V2	E
b3	3.51203E 05	V3	E^2
b4	4.62559E 07	V4	$E^2{\cdot}T$
b5	4.06726E 03	V5	M
b6	8.98799E 08	V6	$M{\cdot}T^2$
b7	1.63279E 05	V7	$M{\cdot}E$
b8	1.54108E 06	V8	$M{\cdot}E^2$
b9	1.47828E 07	V9	$M^2{\cdot}T$
b10	4.45923E 07	V10	M^3

By reviewing relevant publications, a report of similar phenomena was found in Koc and Vatandas (2006). As the measurement cell in (Koc & Vatandas, 2006) was also made of PMMA, the observed USV hysteresis might not be the property of the liquid but a result of the PMMA's dimension change combined with time-delayed thermal conduction and expansion phenomena.

Concluding, it was decided to change the path length to 100 mm. All relevant PMMA parts were conditioned for 12 days at 100% humidity and 80 °C to achieve an equilibrium-like status. The final set-up showed reproducible temperature gradients of <0.05 K, RD deviations of ±5 µm and provided an USV error of ±0.05 m s ^{1} over the whole temperature range. After a sufficiently long period (>2 weeks), RD changes and significant concentration drifts were still noticed in the case of long-time sample liquid circulation and thermal cycles. Consequently, the trial procedure was chosen as presented in paragraph 2: constant temperatures instead of step functions and cyclic recalibrations. In consequence, the USV accuracies reached <±0.02 m s ^{1}. Due to the higher reliability, not the Pt100 but the 909Q temperature sensor was applied as reference sensor in the main trials.

Temperature and mass-fraction-dependent USV and density of the ternary system water maltose ethanol

The stepwise regression concerning the USV resulted in 17 significant predictors. Both predictors and coefficients are presented in Table 1. The model statistics showed a RMSE of 0.4350 m s ^{1} and a coefficient of determination of 0.99964. Figure S1 shows the residual analysis at a glance and proves the adequacy of the model to represent the measurement. The remaining main residues that differ from the normal distribution are caused by variations of the reference mass fraction measurement and model deviations at the boundaries (e.g. binary mixtures and pure water). As visible in Fig. 2, the USV rises steadily with mass fraction and temperature. At 30 °C, both water-6% ethanol and water-12% maltose reach approximately similar USVs (see Fig. 2a,b). Basically, the USV rises faster with ethanol than with maltose mass fractions (see Fig. 3).

Temperature and mass-fraction-dependent density of the ternary system water maltose ethanol

The stepwise regression concerning the density resulted in 11 significant predictors (see Table 2). The model statistics showed a RMSE of 0.11 kg m ^{3} and a coefficient of determination of 0.99995. Figure S2 presents the results of the residual analysis and proves the adequacy of the measurement results and the model.

As in case of the USV model, the majority of the residues are normal distributed, which proves the adequacy of the model to represent the measurement results. The remaining residues are caused by variations of the reference mass fraction measurement and model deviations at the boundaries. As Figs 4 and 5 show, the density rises steadily with increasing maltose mass fraction, but decreases with increasing ethanol mass fraction and temperature.

Discussion

The applied measurement methods provide the actual state of the art accuracy for online measurements. Furthermore, additional systematic errors such as temperature gradients, thermal expansion, and material-based hysteresis effects, dilution or accumulation effects were avoided as good as possible. Nevertheless, a comparison of the binary mixtures with reference data to check the data accuracy seems to be reasonable.

The temperature and mass-fraction-dependent densities of the water–ethanol model were compared with data of D'Arrigo and Paparelli (1988) and Liley *et al.* (1997). Compared with the data of Liley *et al.* (1997), the model shows an RMSE of only 2.9249E-4 g cm ^{3}; compared with D'Arrigo and Paparelli (1988), the RMSE is 0.0115 g cm ^{3}. While in case of the comparison with Liley *et al.* (1997), the deviations are only small and nonsystematic, and the deviations are nonconstant and systematic in case of the comparison with D'Arrigo and Paparelli (1988) (see Fig. 6a). For the temperature

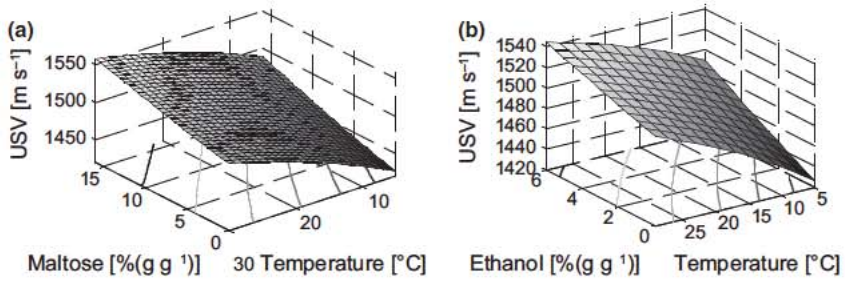

Figure 2 Surface and contour plot of the temperature and mass fraction dependent USVs of the binary mixtures water maltose (a) and water ethanol (b).

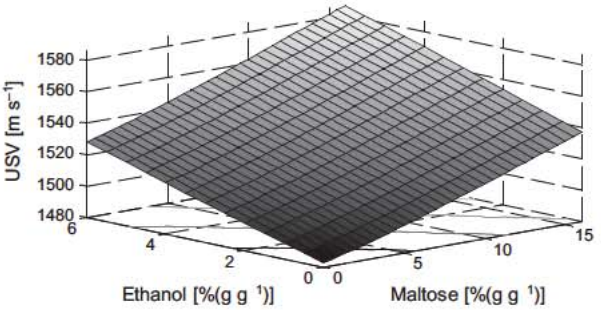

Figure 3 Mass fraction dependent surface and contour plot of the USV of ternary mixtures of water, maltose and ethanol at 20 °C according to the presented model.

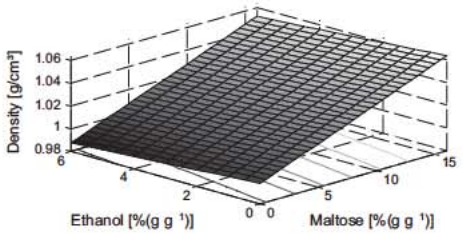

Figure 5 Mass fraction dependent surface and contour plot of the density of ternary mixtures of water, maltose and ethanol at 20 °C according to the presented model.

and mass-fraction-dependent densities of maltose, no reference data could be found. However, it was possible to draw comparisons with the densities of other sugar types (Contreras *et al.*, 1992). The units were converted via the given densities assuming that the given concentrations are generated or measured at 20 °C. As stated in (Contreras *et al.*, 1992), the densities do not vary much within the fructose, glucose and sucrose. But as shown in Fig. 6b–d, the measured maltose densities differ significantly. The deviations increase steadily with mass fraction from almost 0 to 5 kg m ^{3}.

The temperature and mass-fraction-dependent USVs of the water–ethanol model were compared with data of Brunn *et al.*, 1974; D'Arrigo and Paparelli, 1988; and Vatandas *et al.*, 2007). If necessary, units were converted via the given density model assuming that the presented mass fractions are valid for 20 °C. While the results of D'Arrigo and Paparelli, 1988 and Brunn *et al.*, 1974 agree with the results of the presented model within the investigated range, the values calculated with the model given by Vatandas *et al.* (2007) deviate enormously (see Fig. 7a and Table 3).

No reference USVs could be found in case of the water–maltose mixtures. Indeed, in Matsuoka *et al.* (2002), velocity dispersion results are presented, but no model or USV data within the actual investigated mass fraction range. Nevertheless, the differences to binary mixtures of other saccharides (Contreras *et al.*, 1992) are illustrated in Fig. 7b–d. In Contreras *et al.* (1992), it is reported that in contrast to the density, the USV is sensitive to the type of sugar. The sensitivity is explained in terms of differences in the stereochemistry and differing structural interactions with solvent molecules. The actual investigations basically confirm Contreras's statement. At similar mass fraction, both monosaccharaides show a higher USV, but the glucose shows lower USVs than the fructose. As sucrose consists of one glucose and one fructose molecule and maltose of two glucose molecules, one could expect the maltose's USV to be lower than the sucrose's USV. Nevertheless, in Lerbret *et al.* (2005), it is reported that the maltose–water systems are less homogeneous owing to the tendency of maltose molecules to form clusters and thus reducing their possibility to destructure the water hydrogen bond network. In case of sucrose, the higher probability from intramolecular hydrogen bonds strongly reduces their interaction with both, water or other sugar molecules. So, considering the density differences (see Fig. 6b–d), structural and molecular phenomena, the higher USV of the maltose might be reasonable. On the other hand, systematic differences caused by different calibration references or measurement methods cannot be excluded completely.

Concerning the measurement of the CPPs, a review of suitable methods to determine both density and USV noninvasively online is given in (Hoche *et al.*, 2013).

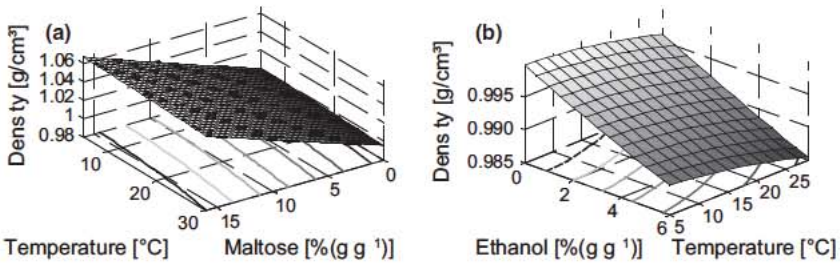

Figure 4 Surface and contour plot of the temperature and mass fraction dependent density of the binary mixtures water maltose (a) and water ethanol (b).

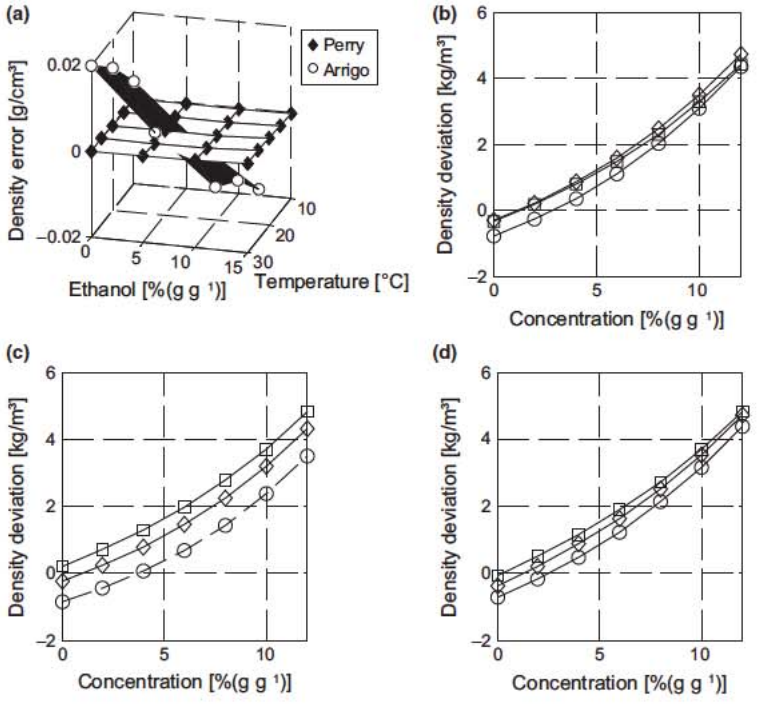

Figure 6 Density deviations (model value reference values) of the presented model to reference data of (a) ethanol (D'Arrigo & Paparelli, 1988; Liley *et al.*, 1997), (b) glu cose (Contreras *et al.*, 1992), (c) fructose (Contreras *et al.*, 1992), (d) sucrose (Contre ras *et al.*, 1992); ○: 10 °C, ◊: 20 °C, □: 30 °C.

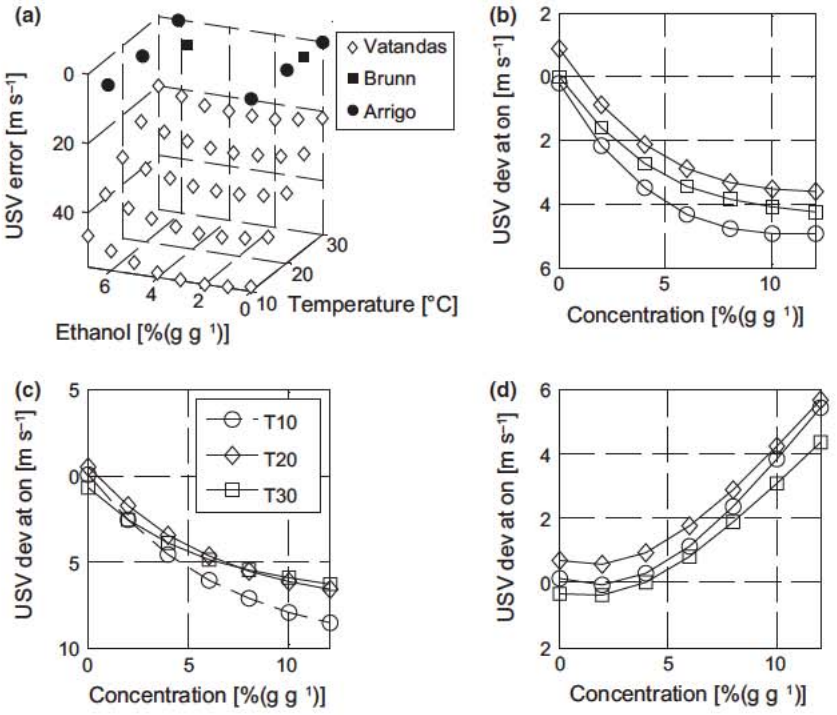

Figure 7 USV deviations (model value reference values) of the presented model to reference data of (a) ethanol (D'Arrigo & Paparelli, 1988; Vatandas *et al.*, 2007) (Brunn *et al.*, 1974), (b) glucose (Contreras *et al.*, 1992), (c) fructose (Contreras *et al.*, 1992), (d) sucrose (Contreras *et al.*, 1992); ○: 10 °C, ◊: 20 °C, □: 30 °C.

Conclusions

The temperature and mass-fraction-dependent USVs and densities were identified as CPPs to estimate significant CQAs of beverages. Consequently, a systematic study was executed within relevant process conditions of anaerobic yeast fermentation to establish the CQA estimation in beer manufacturing. The introduced experimental method and set-up provided the required reproducibility and accuracy. Nevertheless, materials

Table 3 RMSE and R^2 of different reference data compared with the presented USV model

Reference source	RMSE [m s ^{1}]	R^2
Arrigo	1.30	0.99840
Brunn	1.56	0.99248
Vatandas	38.93	0.00000

that change significantly their dimensions caused by time-dependent phenomena, like water absorption due to hygroscopicity, ought to be avoided if possible.

Furthermore, the developed models were found to be adequate to represent the data. In the following step, the models were applied to validate the measured data by comparing with reference data. Concerning the appearance of other sugar types in minor concentrations, significant differences in USV and density have to be considered, which might be a relevant source of error for the CQA estimation. Further investigations are still required, particularly considering the fact that no adequate data exist for maltotriose.

Closing, the novel data of the actual study provide an adequate basis to investigate different models to estimate the CQAs of alcoholic yeast fermentation of malt-based sugar solutions and to validate suitable process instrumentation to measure the CPPs. The feasibility of the varying models with respect to the required CPP accuracy is to be discussed in following publications.

Funding

This research project was supported by the German Ministry of Economics and Technology (via AiF) and the WiFö (Wissenschaftsförderung der Deutschen Brauwirtschaft e.V., Berlin). Project AiF 16536 N.

Conflict of interest

The authors declare no competing financial interest.

References

Balakrishnan, J., Fischer, B.M. & Abbott, D. (2009). Sensing the hygroscopicity of polymer and copolymer materials using terahertz time domain spectroscopy. *Applied Optics*, **48**, 2262 2266.

Brunn, S.G., Sørensen, P.G. & Hvidt, A. (1974). Ultrasonic properties of ethanol water mixtures. *Acta Chemica Scandinavica. Series A: Physical and Inorganic Chemistry*, **28**, 1047 1054.

Contreras, N.I., Fairly, P., McClements, D.J. & Povey, M.J.W. (1992). Analysis of the sugar content of fruit juices and drinks using ultrasonic velocity measurements. *International Journal of Food Science and Technology*, **21**, 515 529.

D'Arrigo, G. & Paparelli, A. (1988). Sound propagation in water ethanol mixtures at low temperatures. I. Ultrasonic velocity. *Journal of Chemical Physics*, **88**, 405 415.

Del Grosso, V.A. & Mader, C.W. (1972). Speed of sound in pure water. *Journal of the Acoustical Society of America*, **52**, 1442 1446.

Drotning, W.D. & Roth, E.P. (1989). Effects of moisture on the thermal expansion of poly(methylmethacryIate). *Journal of Material Science*, **24**, 3137 3140.

Gepert, M. & Moskaluk, A. (2007). Acoustic and thermodynamic investigations of aqueous solutions of some carbohydrates. *Molecular and Quantum Acoustics*, **28**, 95 100.

Hoche, S., Hussein, W.B., Hussein, M.A. & Becker, T. (2011). Time of f light prediction for fermentation process monitoring. *Engineering in Life Sciences*, **11**, 1 12.

Hoche, S., Hussein, M.A. & Becker, T. (2013). Ultrasound based density determination via buffer rod techniques: a review. *Journal of Sensors and Sensor Systems*, **2**, 103 125.

Koc, A.B. & Vatandas, M. (2006). Ultrasonic velocity measurements on some liquids under thermal cycle: Ultrasonic velocity hysteresis. *Food Research International*, **39**, 1076 1083.

Lerbret, A., Bordat, P., Affouard, F., Descamps, M. & Migliardo, F. (2005). How homogeneous are the trehalose, maltose, and sucrose water solutions? An insight from molecular dynamics simulations. *Journal of Physical Chemistry B*, **109**, 11046 11057.

Liley, P.E., Thomson, G.H., Friend, D.G., Daubert, T.E. & Buck, E. (1997). Physical and chemical data. In: *Perry's Chemical Engineers' Handbook* (edited by R.H. Perry, D.W. Green & J.O. Maloneay). Pp. 204. New York: McGraw Hill.

Marczak, W. (1997). Water as standard in the measurements of speed of sound in liquids. *Journal of the Acoustical Society of America*, **102**, 2776 2779.

Matsuoka, T., Okada, T., Murai, K., Koda, S. & Nomura, H. (2002). Dynamics and hydration of trehalose and maltose in concentrated solutions. *Journal of Molecular Liquids*, **98 99**, 317 327.

Parke, S.A. & Birch, G.G. (1999). Solution properties of ethanol in water. *Food Chemistry*, **67**, 241 246.

Petong, P., Pottel, R. & Kaatze, U. (2000). Water ethanol mixtures at different compositions and temperatures. A dieletric relaxation study. *Journal of Physical Chemistry A*, **104**, 7420 7428.

Resa, P., Elvira, L. & Montero de Espinosa, F. (2004). Concentration control in alcoholic fermentation processes from ultrasonic velocity measurements. *Food Research International*, **37**, 587 594.

Resa, P., Elvira, L., Montero de Espinosa, F. & Gomez Ullate, Y. (2005). Ultrasonic velocity in water ethanol sucrose mixtures during alcoholic fermentation. *Ultrasonics*, **43**, 247 252.

Schock, T. & Becker, T. (2010). Sensor array for the combined analysis of water sugar ethanol mixtures in yeast fermentations by ultrasound. *Food Control*, **21**, 362 369.

Vatandas, M., Koc, A.B. & Koc, C. (2007). Ultrasonic velocity measurements in ethanol water and methanol water mixtures. *European Food Research and Technology*, **225**, 525 532.

Supporting Information

Additional Supporting Information may be found in the online version of this article:

Figure S1. Residual analysis results of the USV model in m s ^{1}, showing the residual distributions (top left: regular, bottom left: cumulative) and the parity plots (top right: normalized probability, bottom right: regular).

Figure S2. Residual analysis results of the density model in kg m-^{3}, showing the residual distributions (top left: regular, bottom left: cumulative) and the parity plots (top right: normalized probability, bottom right: regular).

2.2.3 Density, ultrasound velocity, acoustic impedance, reflection and absorption coefficient determination of liquids via multiple reflection method.

Density, ultrasound velocity, acoustic impedance, reflection and absorption coefficient determination of liquids via multiple reflection method

S. Hoche, M.A. Hussein *, T. Becker

Technische Universität München, Bio-PAT (Bio-Process Analysis Technology), Freising 85354, Germany

ARTICLE INFO

Article history:
Received 23 May 2014
Received in revised form 17 October 2014
Accepted 21 October 2014
Available online 30 October 2014

Keywords:
Liquid properties
Density
Absorption
Reflection coefficient
Multiple reflection method

ABSTRACT

The accuracy of density, reflection coefficient, and acoustic impedance determination via multiple reflection method was validated experimentally. The ternary system water maltose ethanol was used to execute a systematic, temperature dependent study over a wide range of densities and viscosities aiming an application as inline sensor in beverage industries.

The validation results of the presented method and setup show root mean square errors of: 1.201E 3 g cm ^{3} (±0.12%) density, 0.515E 3 (0.15%) reflection coefficient and 1.851E + 3 kg s ^{1} m ^{2} (0.12%) specific acoustic impedance. The results of the diffraction corrected absorption showed an average standard deviation of only 0.12%. It was found that the absorption change shows a good correlation to concentration variations and may be useful for laboratory analysis of sufficiently pure liquids.

The main part of the observed errors can be explained by the observed noise, temperature variation and the low signal resolution of 50 MHz. In particular, the poor signal to noise ratio of the second reflector echo was found to be a main accuracy limitation. Concerning the investigation of liquids the unstable properties of the reference material PMMA, due to hygroscopicity, were identified to be an additional, unpredictable source of uncertainty. While dimensional changes can be considered by adequate methodology, the impact of the time and temperature dependent water absorption on relevant reference properties like the buffer's sound velocity and density could not be considered and may explain part of the observed deviations.

1. Introduction

In the past, several methods to investigate the density via ultrasonic were investigated [1 8]. In particular the non invasive characteristic suits the buffer rod techniques (BRTs) to be applied as process analytical technology (PAT) in food and beverage industries, to determine the density and the ultrasonic velocity of multicomponent mixtures [9]. The basis of the BRTs is the plane wave propagation across one or more interface and the knowledge of the reference's (buffer) material properties. Four BRT sub groups could be identified: the multiple reflection method (MRM), the transmission methods (TM), the reference reflection methods (RRM) and the angular reflection methods (ARM). In case of a process application in beverage industries, moderate attenuation, inconstant process conditions, and temperature gradients have to be considered. It was found that the MRM is the best choice, particularly considering the minor calibration effort, the sensor design and the analytical output.

To calculate the reflection coefficient (RC), the density, the absorption and the specific acoustic impedance (SAI) via MRM, the time of flight (TOF) and the amplitudes of three echo pulses have to be evaluated. We may specify them as: A_{r1} the 1st of the multiple echo signal which are reflected at the buffer liquid interphase, A_{e11} the 1st echo signal which was transmitted into the sample liquid and reflected by the reflector, and A_{e21} the 1st echo signal which was transmitted into the sample liquid and passed the liquid volume twice before being received (compare Fig. 3). Further details concerning the method including the series expansion of the echo description will be found in [8,10 15]. The details concerning the amplitude and TOF evaluation will follow in next paragraph. Knowing the relevant amplitudes, the reflection coefficient of a plane wave passing the interface from medium 1 (buffer) to medium 2 (fluid), r_{12} can be calculated via:

$$r_{12} \quad \sqrt{\frac{x}{x \quad 1}} \quad \text{and} \quad x \quad \frac{A_{r1} \cdot A_{e21}}{A_{e11}^2}, \tag{1}$$

* Corresponding author.

whereby the indices of the amplitude values define only the position within the complete signal (see Fig. 3). The indices of the other parameters define the corresponding medium: 1 – buffer material, 2 – sample liquid, 3 – reflector material; or medium combination at the interphase. From the TOF in the sample liquid and the known distance, l_2 between buffer and reflector, the sample liquid's ultrasonic velocity (c_2) can be calculated:

$$c_2 = \frac{2l_2}{TOF_2}. \tag{2}$$

Knowing both variables, the buffer's sound velocity and density at the actual temperature, the liquid's density can be calculated:

$$\rho_2 = \frac{\rho_1 c_1}{c_2}\frac{(1+r_{12})}{(1-r_{12})}. \tag{3}$$

The acoustic impedance, Z is the product of density and sound velocity:

$$Z_2 = c_2\rho_2 = \rho_1 c_1 \frac{(1+r_{12})}{(1-r_{12})}. \tag{4}$$

And, in case that reflector and buffer are made of similar material and assuming that both the sample liquid's composition and temperature is similar at both interfaces, the sample liquid's attenuation, α can be calculated by:

$$\alpha_2 = ln\left(\frac{B}{C\cdot r_{12}^2}\right)\cdot\frac{1}{2l_2}. \tag{5}$$

The investigated liquids are solutions and can be considered as a homogeneous medium. As well reflection and transmission losses are considered and diffraction effects will be corrected. Accordingly, the calculated loss coefficient corresponds to the absorption coefficient which is mainly caused by viscous energy absorption and thermal conduction.

2. Materials, methods and experimental setup

According to the methods requirements an experimental setup was designed that provides all parameters to characterize ternary component mixtures and to validate the methods accuracy (see Fig. 1). A vibrating U-tube density meter (L-Dens 313, Anton Paar, accuracy: 1E−3 g/cm^3, 0.1 °C) was used to determine the density. The temperature is provided by a measurement chain of TTI-22 (Isothermal Technology Ltd.) and a standard platinum resistance thermometer (SPRT 909Q, 25 Ω, Isothermal Technology Ltd.) resulting in an certified accuracy of ⩽5 mK (resolution: 0.1 mK). The time-of-flight (TOF) in the liquid is determined between the echoes A_{r1} and A_{e11} via pulse-echo method, cross correlation and zero crossing approximation [16]. The ultrasonic velocity is calculated from periodical reflector distance (RD) calibrations with demineralized water [17]. And the temperature controlled environment is provided by a cooling thermostat (Lauda RP3530 C). The applied trial procedure provided following reproducible conditions at each concentration combination: average temperature variation: ±5 mK, temperature gradients across the sound propagation path: ⩽0.05 K, and sound velocity errors ⩽0.05 m/s over the investigated temperature range of 10–30 °C. To monitor the temperature uniformity across the propagation path and to ensure a sufficient stability for the measurements six waterproofed Pt100 were immersed in different depth. The complete methodical details are presented in [9].

2.1. The ultrasonic measurement cell (USVMC)

The USVMC was especially designed to allow extensive temperature supervision, the investigation of varying liquids, a simultaneous reference density measurement of acceptable accuracy and to offer the investigation of varying reflector distances, buffer materials, and buffer dimension. For the sake of completeness and reproducibility, all MRM relevant details of the USVMC are provided in the following section. The USVMC consists of two Poly(methyl methacrylate) (PMMA)-cylinders flanged at each side of a PMMA tube. As visualized in Fig. 2, the transducer was pressed waterproofed to the PMMA cylinder by an additional flange. Materials, dimensions, and specifications were chosen according to the design considerations as stated in [8]. Dimension changes of the propagation path due to thermal expansion and hygroscopicity of PMMA [18,19] were considered by cyclic calibrations with demineralized water at each temperature [9]. The mean values of the USVMC at 20 °C are given Table 1.

The temperature dependent sound velocity of PMMA was evaluated preliminary to the main trial (validity: 10–30 °C):

$$USV_{PMMA}(T) = 2811.107\frac{m}{s} - 2.074\cdot 10^{-3}\frac{m}{°C\cdot s}\cdot T - 2.544\cdot 10^{-5}\frac{m}{°C^2\cdot s}\cdot T^2, \tag{6}$$

whereby T represents the temperature in °C. The sound velocity of PMMA at 20 °C results in 2759.43 m/s which is in good agreement with values found in literature. The temperature dependent density

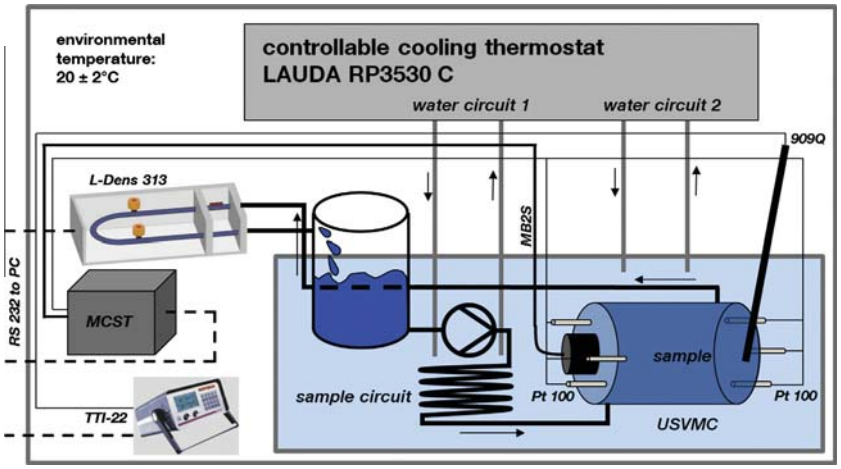

Fig. 1. Scheme of the experimental setup to measure on-line measurement the ultrasonic signals, the temperature and the density (MCST: Multi-Channel-Signal-Transformer, USVMC: Ultrasound Velocity Measurement–Measurement-Cell).

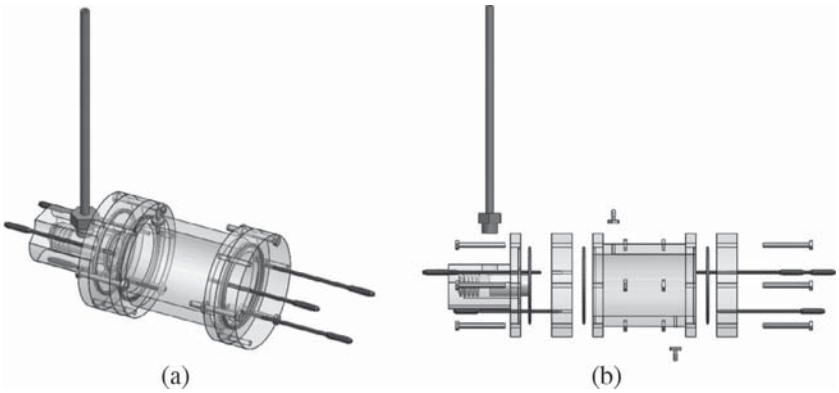

Fig. 2. 3-D assembly drawing (a) and exploded view (b) of the USVMC showing the main parts: PMMA tube (measurement volume), the flanged PMMA cylinders at each side and the additional flange to ensure a waterproofed mounting of the transducer.

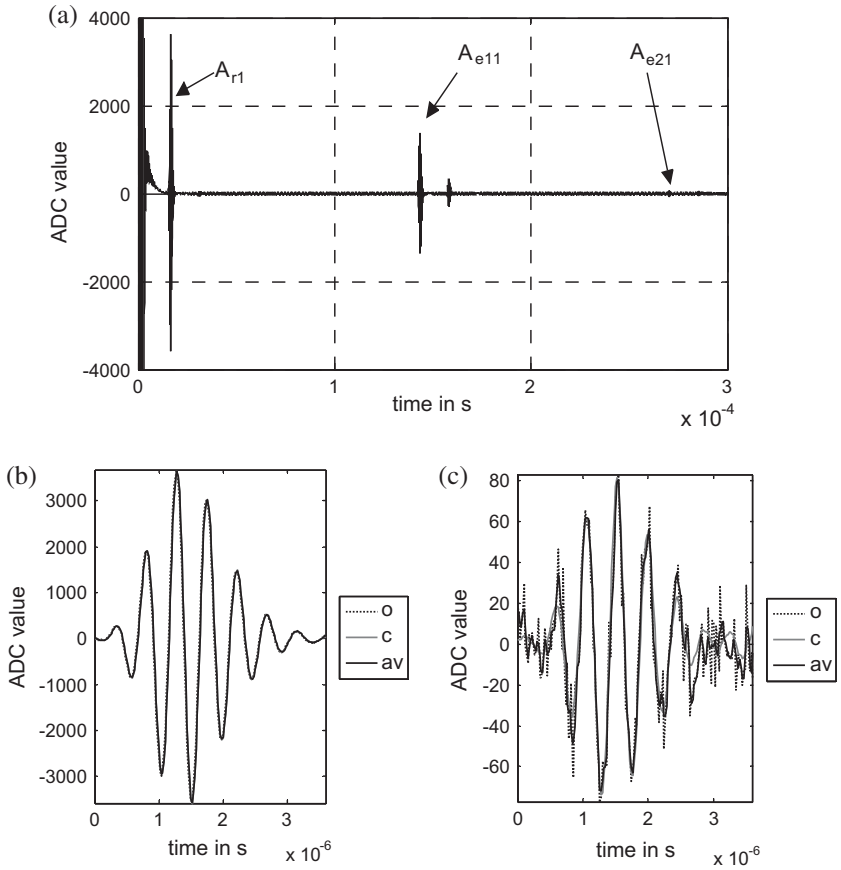

Fig. 3. Typical signal as recorded by the described system in the USVMC (a) showing A_{r1} – the 1st of the multiple echo signals which are reflected at the buffer- liquid interphase, A_{e11} – the 1st echo signal which was transmitted into the sample liquid and reflected by the reflector, and A_{e21} – the 1st echo signal which was transmitted into the sample liquid and passed the liquid volume twice before being received. And the extracted echo signals: A_{r1} (b) and A_{e21} (c) exemplifying the different processing steps: o – original echo; c – centered via polynomial approximation; av – averaged echo.

Table 1
Dimensions of the USVMC at 20 °C; mean length and thicknesses were determined by calibration with demineralized, deaerated water.

PMMA cylinder	Mean thickness	l_1 in mm	20.081
PMMA cylinder	Diameter	d_1 in mm	ca.100
PMMA tube	Mean length	l_2 in mm	100.388
PMMA tube	Diameter	d_2 in mm	ca.80

of the PMMA was calculated via the density at 20 °C and the volumetric thermal expansion provided by manufacturer: $\rho_{1,20°C} = 1.17\ g/cm^3$, $\alpha_L = 70E\ 6\ m^{\ 1}$, whereby α_L is the one dimensional, linear, thermal expansion coefficient.

2.2. Signal generation, recording, and processing

Eqs. (3) and (4) illustrate clearly that the accuracy of the density, the specific acoustic impedance, and the loss coefficient depend in large part on the accuracy of the reflection coefficient. On the other hand, the reflection coefficient accuracy depends on the amplitude determination (see. Eq. (1)), which can be influenced

by a multitude of varying error sources. The investigated methods to determine the characteristic amplitude of a signal echo are the peak-to-peak Amplitude in time domain (A_{TPP}) and the spectral density (FDL2) according to the l2-norm in the frequency domain:

$$r_{TPP}: \quad A_{TPP} = maximum[A(t_{w1}:t_{w2})] - minimum[A(t_{w1}:t_{w2})], \tag{7}$$

$$r_{FDL2} \quad A_{echo} = \sqrt{\int_{f_1}^{f_2} |a(f)|^2 df}, \quad \text{with } f_1 = 1.5\ \text{MHz}, \ f_2 = 2.7\ \text{MHz}, \tag{8}$$

whereby t_{w1} and t_{w2} represent the start and the end time of the truncated echo signal. The main methodical errors which may cause deviations of the determined amplitudes are signal superposition of echo signals or with radial mode vibrations. Both can be avoided by choosing a feasible piezo material and the correct setup dimensions with respect to the signal frequency, the echo duration, and the material properties (see [8]). Geometric diffraction losses may be considered by applying a feasible correction [20]. The remaining error sources are more or less hardware and system dependent: random and systematic noise in relation to the echo amplitudes, and the limited amplitude and time resolution, which may be combined by the term quantization error. The details of the hardware as it was applied in the presented investigations is described in the following passage.

The signals are recorded by an analogue–digital converter with variable gain amplifier (AD8330), 14 bit vertical resolution and 50 MHz time resolution. The variable gain amplifier (VGA) includes a 0.1 MHz high pass filter and provides a maximal gain of 50 dB. Although it can be assumed that the MRM is excitation independent, both excitation and amplification were remained constant to avoid additional uncertainties. The variable gain was used only to adjust the amplification to reach the maximum signal amplitude within the ADC range. The optimum settings were found by tests at maximum reflection coefficient. Since buffer and reflector are made of PMMA, the first buffer reflection provides the maximum amplitude. The optimum ratio of voltage and amplification was found by maximizing the signal to noise ratio (SNR). Finally, the transducer (General Electrics, center frequency: ca. 2 MHz, effective diameter: 10 mm) was excited by a rectangular 100 V excitation of 250 ns and the gain was set to 15.5 dB.

Due to theory, averaging and resolution limitations can cause significant amplitude errors. On the other hand the individual SNR of each analyzed echo signal also contributes to the overall error. Due to the chosen material combination particularly the second echo (A_{e21}, see Fig. 3) is of low amplitude and contributes a high SNR error (see Table 2). Initial evaluations showed that in case of the stated experimental details non-averaged echo signals cause a higher error than the averaged. Therefore, the experimental conditions are rated to be sufficiently constant to justify averaging for the used setup and hardware. In consequence, it was decided to investigate two averaging strategies: the averaging of relevant echo signals after centering via polynomial approximation (PAC) and the result averaging (RA), meaning that the reflection coefficient resulting from non-averaged signals was averaged before calculating all other variables. In case of the PAC each relevant echo signal is processed by individual moving average buffers. Small time differences between the individual echo signals within a moving average buffer might still cause significant amplitude deviations in the resulting, averaged echo. The lower the signal resolution with respect to the signal frequency and the time difference, the higher may be the deviations. The time difference is calculated between the characteristic zero crossing and the nearest discrete data point and the whole echo signal is shifted by the determined difference. Therefor the echo signal was piece wise approximated by a polynomial and recalculated point by point. Further details of the amplitude analysis are presented in the following passage.

Table 2
Typical SNR (A_{echo}/A_{noise}) and SNR_{dB} ($20\log_{10}(A_{echo}/A_{noise})$) of the relevant echo signals before (O) and after processing (PAC + averaging).

	A_{r1}	A_{e11}	A_{e21}
SNR_O	84.4	32.3	2.1
SNR_{dBO} in dB	38.5	30.2	6.4
SNR_{PAC}	471.3	179.8	10.7
SNR_{dBPAC} in dB	53.5	45.1	10.6

The first buffer reflection (A_{r1}) can be identified and truncated by its characteristics – the maximum, the rising time, and the damping time – resulting in a 3.6 μs (181 points) long lasting echo signal (see Fig. 3). The truncation of the first and second echo signal is realized by the predefined echo characteristics, cross correlation, and the determined TOF within the liquid sample. After extraction and centring, the echo signals are transferred to a 50 echoes covering moving average buffer.

The amplitude analysis is applied to the averaged, centered echo signals. In time domain the peak-to-peak amplitude (TPP, Eq. (7)) is analyzed and polynomial approximation is applied to overcome time resolution limitations. The order of the polynomial approximation and the amount of points used for the approximation with respect to the signal's frequency, time resolution and the SNR is of immense importance for the final accuracy. If not stated different a 3rd order polynomial approximation across 5 points is applied for the amplitude analysis in time domain and a 4th order polynomial across 9 points to center the echo signals. In frequency domain the spectral density (FDL2) is calculated for the bandwidth 1.5–2.7 MHz according to the l2-norm. To reach an acceptable frequency resolution for a minimal integration error (numerical integration via Simpson's rule) symmetric zero padding is applied resulting in a 2^{13} points echo signal and a frequency resolution of approximately 6.1 kHz.

Finally, the determined amplitudes are diffraction corrected via the echo distance normalized to the near field length according to [20,21].

2.3. Validation

The design schematic (see Fig. 1) illustrates the main disadvantage of the experimental setup. As soon as the sample liquid leaves the cooling thermostat controlled environment, it is affected by the environmental temperature. Due to the temperature difference, the density provided by the L-dens 313 might differ from the density at the buffer-sample-interface. But, since temperature and component concentrations are known, the 'true' density can be calculated from the model presented in [9]. The sample liquid's sound velocity is measured. The buffer material's sound velocity and density were calculated from the known temperature dependent characteristics. Therefore, all variables are present to calculate the 'true' reflection coefficient and specific acoustic impedance. Only the sound absorption misses accurate reference data. Since there is a large amount of data, the validation is limited to the temperature dependent data of pure water and mixtures of 12%g/g maltose and varying ethanol mass fractions. For each combination of temperature and concentrations 100 values were analyzed to calculate the presented average value and standard deviation (STD). The overall root mean square error (RMSE) is calculated from the errors of the measured average values to the average of the 'true' values.

3. Results

The reflection coefficient is the basis for all following parameter calculations (see Eqs. (1), (3)-(5)). Consequently any

deviation or fluctuation will affect directly the accuracy of all other variables. So first, a slight impression of the influence of varying signal processing strategies on the reflection coefficient might be given. In addition to the introduced PAC signal pre-processing, SP_{PAC}, the moving average post-processing of the reflection coefficient from unprocessed signals, SP_{RA} was evaluated. And for both methods the results of the amplitude analysis methods TPP and FDL2 were analyzed. As expected from the poor SNR of the unprocessed signals (see Table 2) the SP_{RA} doesn't reach the accuracies of the SP_{PAC}. On the other hand the SP_{RA} results show lower STDs. The best accuracies resulted from FDL2 + PAC processing. Consequently, the finally presented MRM-resulting validation results of acoustic impedance, density and absorption are given for the FDL2 + PAC reflection coefficient. The results across the investigated field of temperatures and concentrations with respect to the reference values are presented in Figs. 4 and 5and Tables 3 and 4.

Table 3
Absolute RMSEs and STDs of the reflection coefficients for signal amplitudes analyzed in time domain, r_{TPP} and frequency domain, r_{FDL2} from unprocessed echo signals, SP_{RA} and echo signals that were centered and averaged, SP_{PAC}.

	r_{TPP}		r_{FDL2}	
	RMSE	STD	RMSE	STD
SP_{RA}	1.706E−3	5.730E−4	1.183E−3	2.599E−4
SP_{PAC}	1.099E−3	8.588E−4	0.515E−3	4.073E−4

Table 4
Mean of the observed values, absolute RMSEs, and STDs of all variables; reflection coefficient r, specific acoustic impedance Z, density ρ and acoustic absorption α; calculated via FDL2 and PAC.

	Mean	RMSE	STD
r_{FDL2}	−0.3396	0.515E−3	4.073E−4
Z_{FDL2} (kg s^{-1} m^{-2})	1.5912e + 006	1.851E + 3	1.467E + 3
ρ_{FDL2} (g/cm^3)	1.0355	1.201E−3	9.526E−4
α_{FDL2} (Np/cm)	0.2195	–	2.564E−4

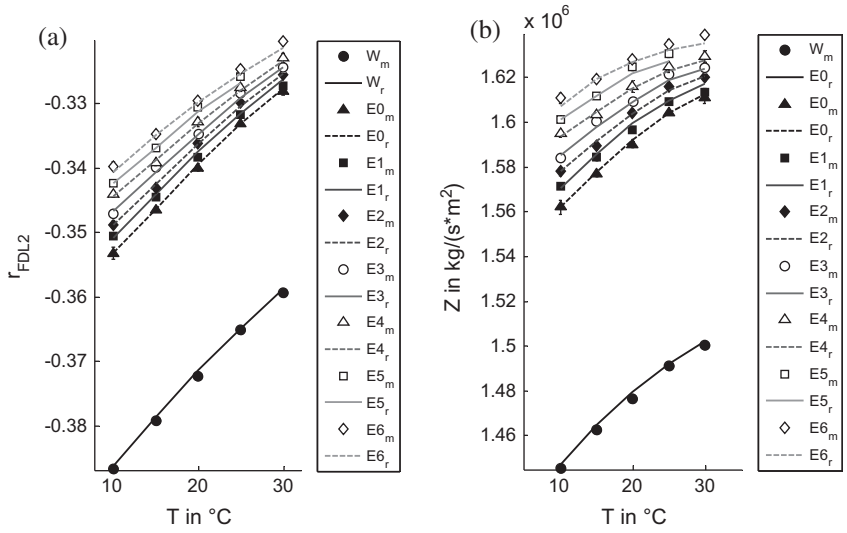

Fig. 4. Reflection coefficient (a) and specific acoustic impedance (b) of the investigated liquids: W – demineralized water; E – water–maltose–ethanol mixtures; whereby the maltose mass fraction is constant (12%g/g), the numeration defines the varying ethanol mass fraction in %g/g; indices: m – measured via the MRM, r – calculated reference ('true' values).

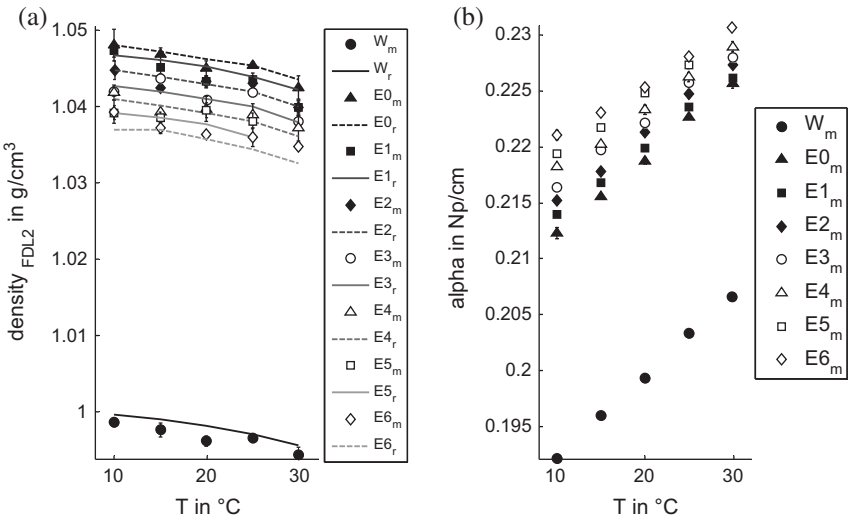

Fig. 5. Density (a) and absorption (b) of the investigated liquids: W – demineralized water; E – water–maltose–ethanol mixtures; whereby the maltose mass fraction is constant (12%g/g), the numeration defines the varying ethanol mass fraction in %g/g; indices: m – measured via the MRM, r – calculated reference ('true') values.

4. Discussion

The validation results show that for the presented setup and methods mean errors within ±1.201E−3 g cm^{-3} (±0.12%) density, 0.515E−3 (0.15%) reflection coefficient and 1.851E + 3 kg s^{-1} m^{-2} (0.12%) specific acoustic impedance (SAI) can be expected. While the RC and SAI accuracy is mainly affected by the accuracy of the amplitude evaluation, the diffraction correction and the applied numerical methods, the density accuracy is additionally affected by the sound velocity error.

Significant accuracy improvements can be expected at higher time resolutions and from SNR improvements, particularly for the A_{e21} echo. Theoretical verifications at mathematical generated, ideal signals based on the Berlage wavelet showed that 60% of the observed error is explainable by the three considered parameters: signal resolution, temperature variation and noise. On the one hand, noise can be reduced by improvements of the electronic circuits, signal averaging or filtering. But, aiming an application as inline process sensor and considering non-constant process conditions or low signal acquisition rates, echo averaging might cause unacceptable amplitude errors. The most promising alternative is the simultaneous recording of the identical signal by different channels and subsequent averaging. Alternatively, each signal echo may be recorded with individual gain to improve the SNR but this approach requires exact knowledge or calibration of the gain factors to avoid systematic amplitude errors. On the other hand, the SNR can be improved by improving the distribution of echo amplitudes across the signal. For example, using an acoustical hard material as reflector generates higher echo amplitudes and therefore a much better SNR.

In contrast, to be able to observe small changes of the liquid's density, the buffer material ought to provide a sufficiently good sensitivity and therefor ought to possess only a moderate density and sound velocity [4,5,8,22]. PMMA, which was applied as reference material in several works [6,11,22–24], is basically such an acoustical soft material and suited to fulfill this requirement. But, as discussed in [9], PMMA also tends to be hygroscopic. Depending on temperature and environmental humidity more or less water is absorbed. In literature it is reported that dimensions and mechanical properties change. Exact information about significant density or sound velocity variations due to water absorption are missing, but can be expected. To give an impression of expectable errors for the presented method and sensor: density errors of 1 kg/m^3 can already be caused by reference density deviations of 1 kg/m^3 or reference sound velocity deviations of 3 m/s. So, materials with low water absorption like PEEK or Rexolite® are recommended when analyzing aqueous solutions. Besides unstable material properties temperature, gradients across the signal path might be an additional, application relevant issue. If not considered or corrected, the temperature deviations can cause inaccurate sound velocities or miss-estimation of the diffraction correction factor and the reflection coefficient. For the presented method and sensor, density errors of 1 kg/m^3 can already be caused by sound velocity deviations of 1.5 m/s or reflection coefficient deviations of 4.5E−4. So, materials with low water absorption like PEEK or Rexolite® are recommended when analyzing aqueous solutions.

Due to missing reference data a validation of the diffraction corrected absorption was not possible. But the average standard deviation was only 0.12%. Furthermore, the results show that the absorption rises with temperature, ethanol and maltose concentration. The results for binary mixtures presented by [25–27] support this general statement for low ethanol concentrations. It is reported that strong absorption peaks were found at intermediate alcoholic concentrations [25–27]. The magnitude of the absorption peak increases with increasing molecular volume of the organic constituent, and there is a simultaneous shift of the position of the maximum towards lower alcohol concentrations.

In the actual study only low ethanol concentrations below the absorption peak were investigated. Instead the temperature was varied and a higher sensitivity of absorption to concentration variations at low temperatures was found. The change of the loss coefficient is due to the change of viscosity, caused by the variation of component concentration. Since the diffraction was considered and corrected, we consider the loss coefficient to correspond in large part to the classical absorption. Indeed there may be additional effects, e.g. scattering from the small amount of ash of the investigated maltose reference or relaxation processes.

Anyway, as reported in [9] the sound velocity increases with rising ethanol and maltose concentration, while density increases with maltose, but decreases with ethanol concentration. Together with the knowledge of the temperature dependency both relations can be used to determine the composition of the sample liquid. Basically, the validation results show the feasibility of the method to be applied as noninvasive, inline sensor to determine component concentration based on a sound velocity – density – temperature relation as it is required in food and beverage industries. The finally reachable concentration accuracy depends not only on the variable accuracy but also on the expected variable variance of the process, the model characteristics (coefficients, model order), and the impurities in the process compared to the model liquid.

Acknowledgements

This research project was supported by the German Ministry of Economics and Technology (via AiF) and the WiFö (Wissenschaftsförderung der Deutschen Brauwirtschaft e.V., Berlin). Project AiF 16536 N.

References

[1] H. Wang et al., The design of The ultrasonic liquid density measuring instrument, in: Third International Conference on Measuring Technology and Mechatronics Automation, 2011.
[2] R.C. Asher, Ultrasonics in chemical analysis, Ultrasonics 25 (1987) 17–19.
[3] J.M. Hale, Ultrasonic density measurement for process control, Ultrasonics 26 (6) (1988) 356–357.
[4] A. Püttmer, P. Hauptmann, B. Henning, Ultrasonic density sensor for liquids, IEEE Trans. Ultrason., Ferroelectr. Freq. Contr. 47 (1) (2000) 85–92.
[5] R.T. Higuti, J.C. Adamowski, Ultrasonic densitometer using a multiple reflection technique, IEEE Trans. UFFC 49 (9) (2002) 1260–1268.
[6] D.J. McClements, P. Fairly, Ultrasonic pulse echo reflectometer, Ultrasonics 29 (1991) 58–62.
[7] M.S. Greenwood, Ultrasonic fluid densitometer having liquid/wedge and gas/wedge interfaces, United States, 2000.
[8] S. Hoche, M.A. Hussein, T. Becker, Ultrasound-based density determination via buffer rod techniques: a review, J. Sens. Sens. Syst. 2 (2013) 103–125.
[9] S. Hoche, M.A. Hussein, T. Becker, Critical process parameter of alcoholic yeast fermentation: speed of sound and density in the temperature range 5–30 °C, Int. J. Food Sci. Technol. 49 (11) (2014) 2441–2448.
[10] E.P. Papadakis, Buffer-rod system for ultrasonic attenuation measurements, J. Acoust. Soc. Am. 44 (5) (1968) 1437–1441.
[11] J.C. Adamowski et al., Ultrasonic measurement of density of liquids, J. Acoust. Soc. Am. 97 (1) (1995) 354–361.
[12] R.T. Higuti, F.R. Montero de Espinosa, J.C. Adamowski, Energy method to calculate the density of liquids using ultrasonic reflection techniques, Proc. IEEE Ultrason. Symp. (2001) 319–322.
[13] E. Bjørndal, K.E. Frøysa, Acoustic methods for obtaining the pressure reflection coefficient from a buffer rod based measurement cell, IEEE Trans. UFFC 55 (8) (2008) 1781–1793.
[14] E. Bjørndal, K.E. Frøysa, S.A. Engeseth, A novel approach to acoustic liquid density measurements using a buffer rod based measuring cell, IEEE Trans. UFFC 55 (8) (2008) 1794–1808.
[15] E.P. Papadakis, K.A. Fowler, L.C. Lynnworth, Ultrasonic attenuation by spectrum analysis of pulses in buffer rods: method and diffraction corrections, J. Acoust. Soc. Am. 53 (5) (1973) 1336–1343.
[16] S. Hoche et al., Time-of-f light prediction for fermentation process monitoring, Eng. Life Sci. 11 (3) (2011) 1–12.
[17] W. Marczak, Water as standard in the measurements of speed of sound in liquids, J. Acoust. Soc. Am. 102 (1997) 2776–2779.

[18] J. Balakrishnan, B.M. Fischer, D. Abbott, Sensing the hygroscopicity of polymer and copolymer materials using terahertz time-domain spectroscopy, Appl. Opt. 48 (12) (2009) 2262–2266.
[19] W.D. Drotning, E.P. Roth, Effects of moisture on the thermal expansion of poly(methylmethacrylate), J. Mater. Sci. 24 (1989) 3137–3140.
[20] A.S. Khimunin, Numerical calculation of the diffraction corrections for the precise measurement of ultrasound absorption, Acustica 27 (4) (1972) 173–181.
[21] E.P. Papadakis, Correction for diffraction losses in the ultasonic field of a piston source, J. Acoust. Soc. Am. 31 (2) (1959) 150–152.
[22] J.C. Adamowski, C. Buiochi, R.A. Sigelmann, Ultrasonic measurement of density of liquids flowing in tubes, IEEE Trans. Ultrason. Ferroelectr. Freq. Control 45 (1) (1998) 48–56.
[23] J. Deventer, J. Delsing, An ultrasonic density probe, in: IEEE ULTRASONICS SYMPOSIUM, 1997, pp. 871–875.
[24] D.J. McClements, P. Fairly, Frequency scanning ultrasonic pulse echo reflectometer, Ultrasonics 30 (1992) 403–405.
[25] C.J. Burton, A study of ultrasonic velocity and absorption in liquid mixtures, J. Acoust. Soc. Am. 20 (2) (1947) 186–199.
[26] S.G. Brunn, P.G. Sørensen, A. Hvidt, Ultrasonie properties of ethanol–water mixtures, Acta Chem. Scand. A 28 (10) (1974) 1047–1054.
[27] G. D'Arrigo, A. Paparelli, Sound propagation in water–ethanol mixtures at low temperatures. II. Dynamical properties, J. Chem. Phys. 88 (12) (1988) 7687–7697.

2.2.4 Ultrasound based, in-line monitoring of anaerobe yeast fermentation: model, sensor design and process application.

Ultrasound-based, in-line monitoring of anaerobe yeast fermentation: model, sensor design and process application

Sven Hoche,[1] Daniel Krause,[1] Mohamed A. Hussein[1]* & Thomas Becker[2]

1 Bio-PAT (Bio-Process Analysis Technology), Technische Universität München, Weihenstephaner Steig 20, Freising 85354, Germany
2 Chair of Brewing and Beverage Technology, Technische Universität München, Weihenstephaner Steig 20, Freising 85354, Germany

(Received 22 August 2015; Accepted in revised form 5 November 2015)

Summary In order to implement process analytical technology in beer manufacturing, an ultrasound-based in-line sensor was developed which is capable to determine sound velocity and density via the multiple reflection method. Based on a systematic study of the ternary system water–maltose–ethanol, two models were established to estimate the critical process parameters: sugar and ethanol mass fraction. The sound velocity-based model showed unreasonable high errors although temperature variations and deviations due to dissolved CO_2 were corrected. In contrast, the sound velocity–density–temperature model provided an average root mean square error of 0.53%g/g sugar and 0.26%g/g ethanol content for the main fermentation. Method, sensor and model showed the capability to capture the process signature which may be related to product and process quality.

Keywords Density, multiple reflection method, process analytical technology, reflection coefficient, ultrasound velocity.

Introduction

The estimation of critical quality attributes (CQA), such as component concentrations based on critical process parameters (CPP), for example sound velocity, requires preferably the knowledge of the complete relationship within relevant process conditions. Former investigations showed that a unique characterisation of sufficiently pure, binary mixtures by two variables is possible (Contreras *et al.*, 1992; Gepert & Moskaluk, 2007; Schöck & Becker, 2010), generally realised through a temperature–density (T–ρ) or a temperature–sound velocity (T–USV) relationship. The composition is often predicted through the linear combination of properties of the pure components according to their fractional content, for example in case of the sound velocity the Urick equation (Urick, 1947; Resa *et al.*, 2009). In fact, real systems often deviate significantly from the predictions, particularly in case of mixtures of polar substances.

Hence, as a first step of process analytical technology implementation in beer manufacturing, a systematic study of the ternary system water–maltose–ethanol has been performed at normal pressure with respect to the critical process parameters density, speed of sound and temperature by Hoche *et al.* (2014) – further on this relationship will be denoted as WME model. Aiming a noninvasive, online monitoring of the CPPs in tanks as commonly utilised in beverage industries reduces the number of applicable measurement methods. Although oscillating U-tube systems often provide feasible density accuracy and included sound velocity (USV) and temperature determination, the method also requires a bypass implementation and a minimum flow rate. A more simple applicability is offered by the so-called buffer-rod techniques (BRT). As explained detailed in Hoche *et al.* (2013), the description of ultrasound signals in terms of plane wave propagation through reference materials (buffer) of known properties and across one or more interfaces which are in direct contact with the liquid of interest, provides the determination of the reflection coefficient from medium 1 (buffer) to medium 2 (fluid), r_{12}. Together with the liquid's sound velocity, the buffer's sound velocity and the buffer's density the liquid's density can be calculated:

$$\rho_2 = \frac{\rho_1 \mathrm{USV}_1}{\mathrm{USV}_2} \frac{(1 + r_{12})}{(1 - r_{12})}, \qquad (1)$$

whereby ρ represents the density and USV the ultrasound velocity. The indices define the corresponding medium: 1 – buffer material, 2 – sample liquid; or a specific medium combination at the interphase.

In case of a process application in beverage industries, moderate attenuation, inconstant process conditions and temperature gradients may be considered. So, from the four basic BRT principles, the multiple reflection method (MRM) was found to be the most promising. The method considers the variable and

*Correspondent: Fax: +49 8161 713883;
e-mail: mohamed.hussein@tum.de

sound absorptions in the different media and provides the determination of the liquid's sound velocity via the pulse-echo method:

$$\mathrm{USV}_2 = \frac{2l_2}{\mathrm{TOF}_2}, \tag{2}$$

whereby TOF is the signal's time-of-flight within the sample liquid and l_2 the calibrated distance between buffer and reflector.

The proposed method was validated based on the calibration data and the calibration set-up under ideal laboratory conditions presented by Hoche *et al.* (2015). The found root mean square errors (RMSE) were 0.515E-3 (0.15%) in reflection coefficient and 0.05 m s^{-1} in sound velocity resulting in a 1.201E-3 g cm^{-3} (±0.12%) density RMSE. The aims of the actual work are the design of a suitable sensor frame for inline application of the proposed method and the development of feasible concentration models based upon the results of the first calibration data. Finally, both were evaluated under industrial process conditions. Following we will present the evaluation of the models to estimate the ethanol and sugar concentrations, the consequential accuracy requirements, the sensor design resulting from the validation conclusions and the results of process application trials.

Materials and methods

Estimation of ethanol and sugar concentration – the direct approach

Schöck & Becker (2010) have shown that clear concentration determination of ternary system requires at least the property determination at two different temperatures, a significant third variable (e.g. density, refractive index or pH value) or constant process conditions (Resa *et al.*, 2009). The most comprehensive approach in matters of a process application is the characterisation through three variables. Practically, the temperature may not be constant under industrial conditions and the simultaneous measurement at two different temperatures requires again a bypass solution.

Nevertheless, the existing data (Hoche *et al.*, 2014) – altogether a systematic study of 271 different combinations of maltose concentrations, ethanol concentration and temperature including 100 values of all relevant variables at each combination – still provide several opportunities to realise a sugar and ethanol estimation model. Basically, it is assumed that the main sugar type (maltose) governs the property behaviour of malt-based sugar solutions (wort). Besides sound velocity and density the specific acoustic impedance, Z of the liquid or the reflection coefficient to the applied reference material, r_{12} can be measured by the proposed method and could be applied as a 3rd variable.

Consequently, the complete data field of additional variables was calculated within the available range of concentrations and temperatures according to the data presented by Hoche *et al.* (2014) and following equations:

$$Z_2 = \mathrm{USV}_2 \cdot \rho_2 = \rho_1 \mathrm{USV}_1 \frac{(1 + r_{12})}{(1 - r_{12})} \tag{3}$$

$$r_{12} = \frac{Z_2 - Z_1}{Z_2 + Z_1} \tag{4}$$

The reflection coefficient was calculated for the reference material PMMA (polymethyl methacrylate). Additionally, the property deviations, ΔP to water as reference liquid (Spieweck & Bettin, 1992; Marczak, 1997), were calculated at the particular temperature and the reference temperature:

$$\Delta P_{\mathrm{rT}} = P_S(T) - P_{\mathrm{H_2O}}(T) \tag{5}$$

$$\Delta P_{\mathrm{r20}} = P_S(T) - P_{\mathrm{H_2O}}(20\,^{\circ}\mathrm{C}), \tag{6}$$

aiming a linearisation and a reduction of error influences. Summarising exemplary for maltose, models of the variable combinations as presented in Table 1 were tested.

Basically, an adequate model type had to be chosen first. Therefore, models of varying order were generated based upon a stepwise linear regression. First, all values were scaled before adding or removing systematically terms from the multilinear model of defined order based on their statistical significance. At each regression step, the significance of the model (F-statistics) and the probability value are calculated according to the analysis of variance to decide if a term is added or removed. A detailed overview of the applied statistics is given in the evaluation of the CPPs by Hoche *et al.* (2014). The database was split into a calibration and a validation data set and each model was analysed with regard to the following presented quality indicators to evaluate the model suitability to represent the data:

Table 1 Overview of the generated maltose models and the corresponding variable combinations

Notation	Type	Model variables
M1D	Absolute values	USV-T-ρ
M1R		USV-T-r_{12}
M1Z		USV-T-Z
M2D	Deviation to water at particular temperature	$\Delta\mathrm{USV}_{\mathrm{rT}}$-$\Delta T_{\mathrm{rT}}$-$\Delta\rho_{\mathrm{rT}}$
M2R		$\Delta\mathrm{USV}_{\mathrm{rT}}$-$\Delta T_{\mathrm{rT}}$-$\Delta r_{12\mathrm{rT}}$
M2Z		$\Delta\mathrm{USV}_{\mathrm{rT}}$-$\Delta T_{\mathrm{rT}}$-$\Delta Z_{\mathrm{rT}}$
M3D	Deviation to water at 20 °C	$\Delta\mathrm{USV}_{\mathrm{r20}}$-$\Delta T_{\mathrm{r20}}$-$\Delta\rho_{\mathrm{r20}}$
M3R		$\Delta\mathrm{USV}_{\mathrm{r20}}$-$\Delta T_{\mathrm{r20}}$-$\Delta r_{12\ \mathrm{r20}}$
M3Z		$\Delta\mathrm{USV}_{\mathrm{r20}}$-$\Delta T_{\mathrm{r20}}$-$\Delta Z_{\mathrm{r20}}$

R^2	Coefficient of determination
F_{emp}/F_{crit}	Ratio of empirical *F* coefficient to critical *F* coefficient
RMSE; RMSEV	Root mean square error (*V – validation RMSE)
SSRC/SSRCV	Ratio of SSRCs: sum of squares due to regression coefficient
CND	Correlation of residues to normal distribution

Summarised, the second-order model showed the most optimal indicators. Although the RMSE and RMSEV still decrease with increasing model order, all other indicators already start to veer away from the optimum. Subsequent, the second-order models of all variable combinations were generated and evaluated. Basically, all models showed very good results ($R^2 > 0.99$ and RMSE < 0.1), but in comparison the M × D models (see Table 1) and the M3× models showed the best results. But, concerning the practical feasibility, not only the suitability to represent the data counts, but also the effect of expectable variable errors are of immense importance. Corresponding to the research work of Hoche *et al*. (2015), standard errors (SE, see Table 2) were defined for all input variables and their impact was determined via propagation of error by determining the partial derivatives of the models. Following, the results are summarised: The overall error of maltose and ethanol mass fraction due to the SE errors of the M2× and M3× models was twice as in case of the M1× models. A detailed analysis of the single error contribution showed that particularly the temperature-caused error contribution increased unreasonably: 0.1 °C deviation would cause already 0.2%g/g mass ratio deviation. Within the M1x model, the error impact of sound velocity and temperature deviation was reasonably low: the SEs caused a mass ratio deviation of <0.02%g/g only. In contrast, the density SE already causes a deviation of 0.2%g/g mass ratio.

In conclusion, the USV-T-ρ model will be used to estimate the component contents ($c_{component}$ in %g/g) online. The USV-T-ρ model is reasonably insensitive to temperature errors, but at the same time sufficiently suitable to represent the data. Furthermore, a recalculation of data and model coefficients, as it is required in case of reflection coefficient based models as soon as the reference material is changed, is not necessary. The coefficients of the finally applied model according to eqn 2 are shown in Table 3.

Table 2 Errors as they may be expected from the accuracy of the proposed multiple reflection method (MRM) according to Hoche *et al*. (2015)

Model variable	USV	T	ρ	r_{12}	Z
Standard error (SE)	0.1 m s^{-1}	0.1 °C	1.2E-3 g cm^{-3}	5.E-04	1.8 E3 kg/(s m^2)$^{-1}$

$$C_{component} = \sum_{i=0}^{n} b_i V_i \quad (7)$$

Estimation of ethanol and sugar concentration – the indirect approach

In the same way, the results of Hoche *et al*. (2014) show that a unique interpretation of sugar and alcohol content of sufficiently pure mixtures is possible via the USV-T-ρ relationship, and they also clarify that the relation between USV and the two component concentrations at a certain temperature is undetermined. But, regarding the fact that only specific substrate–product combinations come into consideration during the anaerobic batch fermentation with yeast (*Saccharomyces cerevisiae*) might turn the USV-T combination to applicable estimation parameters. In contrast to the research works of Resa *et al*. (2004, 2009), not only the enzymatic reaction but also the formation of new cells or cell components was considered. The commonly accepted description of the relation is the Balling equation presented in the book of Balling (1865) which states that 1 part of fermented extract is turned into 0.48391 parts by weight of alcohol. Nevertheless, the relation remains rather complex. Depending on beer type and recipe the initial extract, MI and the temperature may vary which leads to varying USV changes for similar grades of sugar decomposition (see Fig. 1).

While the sound velocity increases for temperatures below 25 °C, it decreases for temperatures above (see Fig. 1). For temperatures around 25 °C, the relationship is quite insignificant or even undetermined, which is basically proven by the results presented by Lamberti (2009). Considering further process variations, for example temperature (see Fig. 3), one can imagine that the resulting errors may be quite unreasonable. Eventually, a data field ranging from 10 to 16%g/g initial extract and 10–20 °C was established and a stepwise

Table 3 Coefficients, RMSE, and RMSEV of the applied models to estimate online the sugar and ethanol mass fraction c in %g/g ($R^2 = 0.99$); ρ in g cm^{-3}, USV in m s^{-1} and T in °C

Variable, V_i		Coefficients, b_i	$c_{maltose}$	$c_{ethanol}$
V_0	Intercept	b_0	−514.630426	−267.273839
V_1	ρ	b_1	478.054025	196.077648
V_2	ρ^2	b_2	−181.081037	12.45763
V_3	USV	b_3	0.20226393	0.21478278
V_4	USV*ρ	b_4	0.07045321	−0.19840763
V_5	USV^2	b_5	−8.37E-05	1.84E-05
V_6	T	b_6	−1.7863069	−2.58673776
V_7	T*ρ	b_7	−0.46874098	−0.50888565
V_8	T*USV	b_8	0.00144833	0.0019039
V_9	T^2	b_9	−0.00031452	−0.00175868
	RMSE		0.0298	0.0783
	RMSEV		0.0244	0.0647

linear regression was applied (see Section Estimation of ethanol and sugar concentration – the direct approach) whereby temperature, initial extract and the USV difference to the start value (ΔUSV, assuming constant temperature) were the regressors and the extract decomposition the regressand – further on denoted as USV-*T* model. A reasonable coefficient of determination was reached for a third-order model (allowing higher orders for variable combinations; see Table 4).

Sensor system and electronic hardware

The ultrasound signals were recorded by an analogue–digital converter with variable gain amplifier (VGA: AD8330), 14 bit vertical resolution and 50 MHz time resolution. The VGA includes a 0.1 MHz high-pass filter and provides a maximal gain of 50 dB. The ultrasound transducer (piezo-electric material: Lead Meta-Niobate (PMN), centre frequency: ca. 2 MHz, effective diameter: 10 mm) was excited by a rectangular 100 V excitation of 250 ns. For each combination of VGA, transducer and sensor, the optimal gain was chosen by maximising the signal to noise ratio (SNR) which basically means to reach the maximum signal amplitude within the analogue digital converter (ADC) range and the expected process variation. Generally, the chosen gain was in the range 20–22 dB.

The developed sensor is based upon a VARINLINE® mounting flange (GEA Tuchenhagen GmbH, Büchen, Germany). Concluding from the calibration

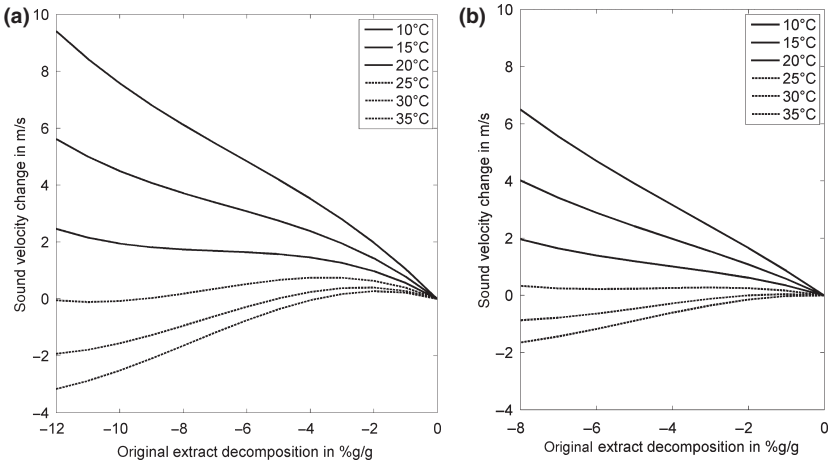

Figure 1 Sound velocity changes which can be expected at particular constant temperatures for alcoholic beer fermentation (batch) for (a) initial extract of 16%g/g and (b) initial extract of 12%g/g.

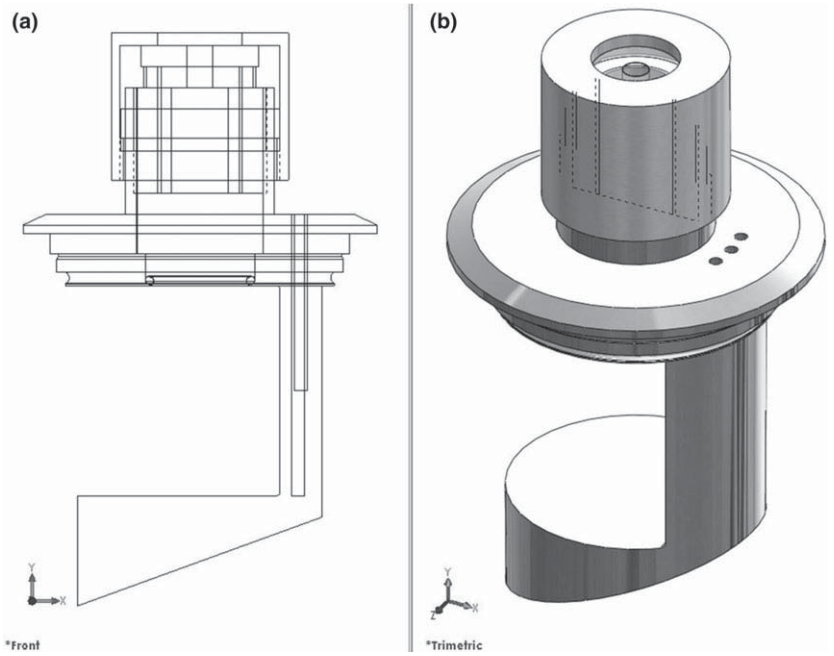

Figure 2 Wireframe front view (a) and trimetric shaded with edges view of the sensor design (b), showing the bore holes for the temperature measurements and the mounting equipment to fixate buffer and sound transducer.

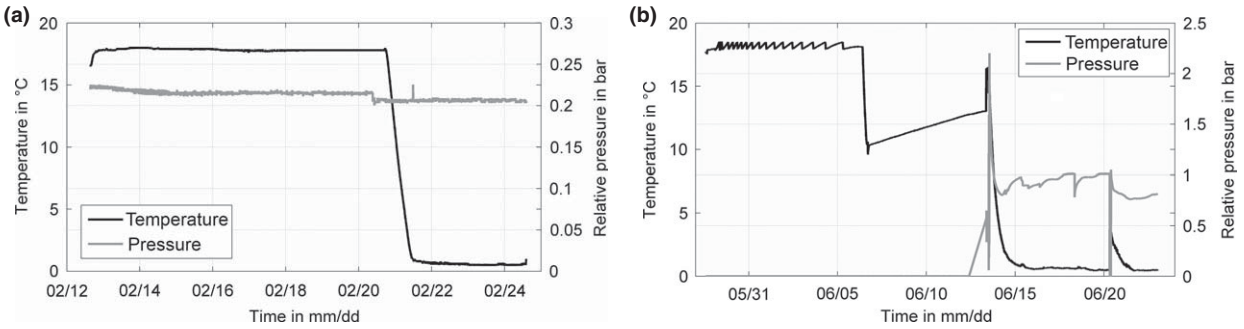

Figure 3 Temperature and pressure course over process time for (a) VPS1 trial1 (cylindrical trial fermenter) and (b) VPS7 trial3 (cylindrico-conical tank).

Table 4 Coefficients of the USV-T model to estimate online the sugar decomposition in %g/g ($R^2 = 0.99$); MI in %g/g, dUSV in m s^{-1} and T in °C

Variable, V_i		Coefficients, b_i		Variable, V_i		Coefficients, b_i	
V_0	Intercept	b_0	6.7085E-01	V_9	dUSV*T^3*MI^2	b_9	−6.9087E-06
V_1	MI^2	b_1	−9.3955E-03	V_{10}	dUSV*T^3*MI^3	b_{10}	1.5269E-07
V_2	T*MI^2	b_2	−6.3763E-04	V_{11}	dUSV^2*T^2*MI	b_{11}	−2.1657E-05
V_3	T*MI^3	b_3	7.2604E-05	V_{12}	dUSV^2*T^3	b_{12}	−7.3289E-05
V_4	dUSV	b_4	1.7071E-01	V_{13}	dUSV^3*MI	b_{13}	−1.0127E-05
V_5	dUSV*T	b_5	−1.2820E-01	V_{14}	dUSV^3*T*MI^2	b_{14}	4.6311E-05
V_6	dUSV*T*MI^3	b_6	−2.6317E-05	V_{15}	dUSV^3*T^2*M	b_{15}	−7.2962E-05
V_7	dUSV*T^2*MI^2	b_7	1.0160E-04	V_{16}	dUSV^3*T^3	b_{16}	4.5381E-05
V_8	dUSV*T^3	b_8	1.8812E-04				

and validation trials presented in Hoche *et al*. (2015), it was decided to reduce the reflector distance to 50 mm and to use an acoustically hard reflector material. Furthermore, to deflect backscattered signals from the reflector backside, the reflector was shaped angular. The resulting design (VPS: VARINLINE process sensor) is shown in Fig. 2. Altogether, six sensors (named VPS1 and VPS3-7) were manufactured, calibrated in the laboratory and tested in standard alcoholic fermentations in the chair's research brewery. The laboratory calibrations include the determination of the exact reflector distance at 20 °C and the temperature-dependent sound velocity of the reference (buffer) material. During the process trials, the temperature was measured electrically via industrial Pt100 thermometer.

Trial details, sampling and reference analytics

As shown in the schematic diagram (see Fig. 4), five of the sensors (VPS3-7) were implemented in five standard cylindro-conical tanks (CCT, total height: 3.11 m, cone height: 0.885 m, sampling valve height: 1 m, VARINLINE height: 1.06 m, diameter of cylindrical part: 1.05 m, max. volume: 2140 L) of the local research brewery, while VPS1 was implemented in a cylindrical trial fermenter (CTF: 1 m height, 0.28 m diameter, approx. 60 L volume). In case of the CCT, the fermentation was only monitored and cyclic sampling was conducted manually through sampling valves near the sensor. In case of the CTF, the temperature was regulated through a heating and cooling thermostat and the pressure through a pressure sensor – valve control circuit. The CTF trials were always executed parallel to one of the CCT trials, whereby it was tried to reproduce the standard fermentation as good as possible which means: the whort was diverted from the standard fermentation, a similar, initial yeast cell count was used and the temperature and pressure set points were chosen according to the CCT fermentation recipe. In both cases, every 15 s the ultrasound signals, the temperature and the pressure were recorded and logged. During day time (08:00 a.m. to 04:00 p.m.), samples of 150 mL were taken and immediately deep frozen (−15 °C) approximately every 2 h. As soon as the main fermentation finished, the sampling was reduced to 1–2 samples per day. Two days after beginning of the maturing phase, the trials were stopped. After unfreezing, the samples were homogenised and for 8 min at 5000 min^{-1} centrifuged. The reference analysis was conducted via the Alcolyzer Beer Analyzing System (with DMA 4500 M densitometer; Anton Paar GmbH, Anton-Paar Str, Kärntner Straβe, Austria): alcohol 0.01%v/v, extract 0.01%w/w, density 0.00001 g cm^{-3}.

Data analysis and corrections

The signals were analysed offline via a particularly developed signal processing algorithm in MATLAB®. First the echo amplitudes of the relevant signal parts were analysed in frequency domain via the spectral density according to the l2-norm within the bandwidth 1.5–2.7 MHz. Before calculating the reflection coefficient, the amplitudes were diffraction corrected as described by Khimunin (1972) and Papadakis (1959). The time-of-flight of the signal path in the liquid is determined between the first two echo signals via pulse-echo method, cross correlation and zero crossing approximation. A detailed description of all relevant signal processing steps is provided in previous publications (Hoche *et al*., 2011, 2015). The required reference properties and the liquid's sound velocity were calculated from the temperature-dependent calibration data via the process temperature and finally, the liquid's density was calculated according to the eqn 3.

In Section Estimation of ethanol and sugar concentration – the indirect approach, it was already stated that the USV-T model requires a constant temperature. In contrast, the temperature is practically not constant (as visible in Fig. 3) but one of the most important control parameters. Consequently, the temperature-dependent differences were estimated iterative from the partial temperature derivatives of the WME model:

$$\Delta \mathrm{USV}_{\mathrm{T(t_i)}} = \Delta T \cdot \mathrm{mean}\left[\frac{\partial \mathrm{WME}(T(t_1), c_M(t_i), c_E(t_i))}{\partial T}; \frac{\partial \mathrm{WME}(T(t_i), c_M(t_i), c_E(t_i))}{\partial T}\right], \tag{8}$$

whereby t_i represents an arbitrary process time and t_1 the start time. The initial values for the 1st iteration are the values at process start.

Further impact factors are discussed by Resa *et al*. (2009). It was shown that the sound velocity is not only affected by component concentration changes and temperature but also by dissolved CO_2, yeast cell concentration and bubbles. Concerning the bubble influence, the maximum resonant frequency of long-lasting bubbles (>10 μm) was determined to be around 0.6 MHz (Resa *et al*., 2009). In consequence, measurements at higher frequencies can be considered to be mostly unaffected by bubbles. The yeast cell concentration may be neglected as well. The maximum fluctuation during alcoholic beer fermentation – from main fermentation (temperature and concentration gradient driven circulation) to maturing (sedimentation of the yeast cells) – is expected to be in the range of 1–50 mio.cells mL^{-1} and is in great contrast to the sound velocity variation of approximately 0.5 m s^{-1} per 100 mio.cells mL^{-1} (Resa *et al*., 2009). In case of dissolved CO_2, the situation is different. Although Resa *et al*. (2009) reported a USV change of only <0.5 m s^{-1} for sucrose solutions, 30 °C, and 2 bar absolute pressure (closed tank, CO_2 atmosphere), the situation might be different for alcoholic beer fermentation. Depending on the beer type and recipe, the temperatures are generally lower. To reach the target CO_2 content during maturing, the temperature even drops to 0 °C and the pressure can reach up to 3 bar. According to Henry's law, the gas absorption depends on the partial pressure and the absorption coefficient in which the absorption coefficient is liquid specific and temperature dependent. An exact description to calculate the CO_2 content for malt-based sugar solutions can be found in the dissertation thesis of Rammert (1993). The relation between dissolved CO_2 in water and sound velocity was investigated by (Liu, 1998). So, for the investigated process the expected variation in the range 0.5–7 g_{CO2} l^{-1} can easily cause deviations of up to 15 m s^{-1}. Consequently, the analysed USV was corrected for the CO_2-caused deviation according to Rammert (1993) and Liu (1998) to achieve the unaffected USV as it is required by the USV-T-ρ model. For the sake of completeness, also the USV-pressure dependency was regarded. According to Wilson (1959) and Fine & Millero (1973), the pressure-caused USV variation within the relevant pressure range is <0.05 m s^{-1} and can be neglected.

After calculating the sugar and ethanol content via the USV-T-ρ model, the root mean square error compared with the laboratory results was calculated.

$$\mathrm{RMSE}_{\mathrm{lab}} = \sqrt{\frac{\sum_{k=1}^{n\mathrm{lab}} (c_{\mathrm{lab}}(t_k) - c_{\mathrm{US}}(t_k))^2}{n}}, \tag{9}$$

whereby c_{lab} is the laboratory result, c_{US} the result determined by the ultrasound sensor system and t the time at which the sample was taken. Additionally, the course of the component concentrations was estimated to expand the laboratory data via the fit functions and to determine a more realistic RMSE for the entire process:

$$\mathrm{RMSE}_{\mathrm{fit}} = \sqrt{\frac{\sum_{k=1}^{n\mathrm{US}} (c_{\mathrm{fit}}(t_k) - c_{\mathrm{US}}(t_k))^2}{n}} \tag{10}$$

Finally, to characterise the error of the described sensor system for the main fermentation in which pressure and temperature is more or less constant, the $\mathrm{RMSE}_{\mathrm{fitM}}$ was determined:

$$\mathrm{RMSE}_{\mathrm{fitM}} = \sqrt{\frac{\sum_{k=1}^{n\mathrm{US\_main}} (c_{\mathrm{fit}}(t_k) - c_{\mathrm{US}}(t_k))^2}{n}}. \tag{11}$$

Results

USV correction

The conformity of the CO_2 corrected USV and the expected, 'ideal' USV is shown in Fig. 5. The corresponding process data are shown in Fig. 3. Generally, deviations of 2–3 m s^{-1} were observed at process start (approx. 18 °C, normal pressure) that increased to deviations of 4–12 m s^{-1} at process end (approx.. 0–3 °C, 1 bar). Over the main fermentation, the mean deviation of the CO_2 corrected USV to the WME-USV was <0.5 m s^{-1}, but could reach up to 1.5 m s^{-1} deviation in the maturing. According to the propagation of error deviations, up to 0.5 m s^{-1} are unproblematic for component concentrations of acceptable error via the USV-T-ρ model.

Taking a more thoroughly look to the process data reveals a few interesting details. The temperature is the key parameter in matters of the USV course. Even the saw tooth profile caused by the 2-point temperature regulation of the CCT perfectly matches the USV course and superimposes the USV change due to anaerobic yeast fermentation (decrease in sugar and increase in ethanol content) and the increased USV variation in the main fermentation (the first 4–5 days). Generally, the USV variation is around ±0.05 m s^{-1} but increases to ±0.5 m s^{-1} due to passing bubbles and yeast cells. And finally, comparing the data with the results of Resa *et al.* (2009) confirms the theoretical considerations concerning the component concentration via USV only (see Section Estimation of ethanol and sugar concentration – the indirect approach). While in the research work of Resa *et al.* (2009), an overall drop of 6 m s^{-1} is reported for 30 °C, the actual investigations showed a 10–12 m s^{-1} rise of the USV at mean temperatures around 18 °C.

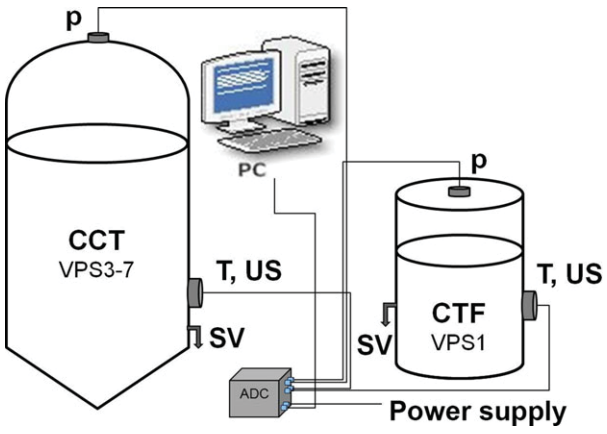

Figure 4 Schematic trial set-up of sensors and data acquisition in the research brewery, T, temperature, p, pressure, US, ultrasound signals, CCT, cylindrico-conical tank, CTF, cylindrical trial fermenter, SV, sampling valve, ADC, analogue digital converter, VPS, Varinline process sensor.

Determination of component concentrations – the USV-T model

Some results of the USV-T model-based estimations of the sugar content are presented in Fig. 6. In both cases, the shown process part did not exceed ±1 °C temperature variation. The observed RMSEs were in the range 2.3–2.8%g/g sugar content. For higher temperature variations, the error became unreasonable. Nevertheless, the results show that the superimposed temperature influence can be adjusted via the proposed correction and that a basic estimation of the sugar content is possible in principle. Even the refill due to a double brew (see start of Fig. 6b) is represented adequately.

Determination of component concentrations – the USV-T-ρ model

Process results of the relevant key parameters to calculate the component concentrations via the USV-T-ρ model: reflection coefficient, USV, the resulting density and the temperature are shown in Figs 3, 5 and 7. The component concentrations which are calculated via Table 3 and eqn 7 and the related reference results are presented in Fig. 7, lower images. The results illustrate clearly the dependency of the density from the reflection coefficient. Each small reflection coefficient deviation results in a significant density deviation which furthermore transfers the error to the component concentrations. Although the sensor was specifically designed to show a high sensitivity to small changes of the liquids density, the reflection coefficient range that has to be resolved with high accuracy is rather small. Notably at process start and at each strong process change, particularly high concentration errors were noticed. The determined RMSE related to different references are shown in Table 5.

Discussion

Overall, six sensors were tested in fourteen anaerobic fermentations of varying rare materials – the beer type varied from Pilsner over Pale Ale to Stout. The estimation of component concentrations based on sound velocity only as introduced in the research paper of Resa *et al.* (2009) showed only limited practicability. The actual study illustrates that immense errors are possible even though the sound velocity variation within relevant boundary conditions was not estimated but known exactly. As well variations due to temperature and dissolved CO_2 were considered. Of course, model improvements are possible by limiting the

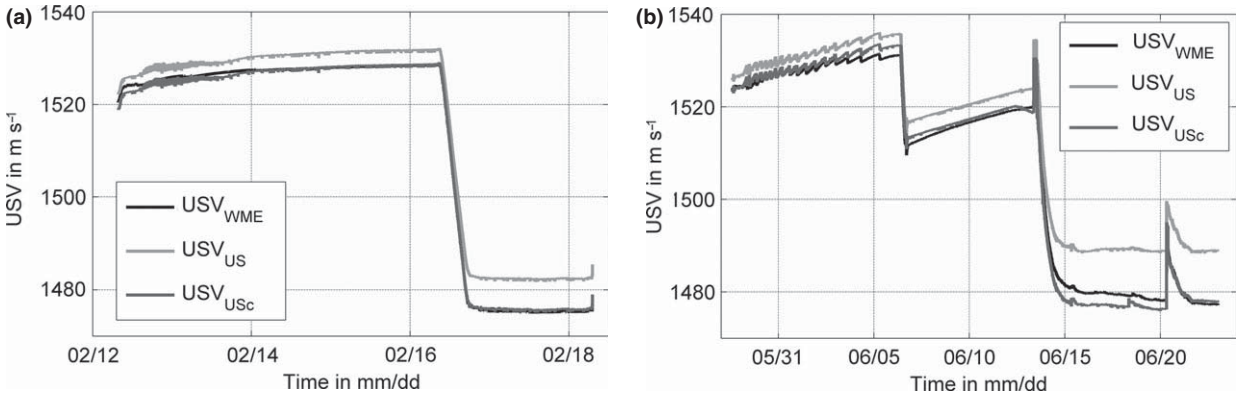

Figure 5 Sound velocity (USV) course over process time for (a) VPS1 trial1 (cylindrical trial fermenter) and (b) VPS7 trial3 (cylindrico-conical tank); USV_{WME}... USV as it was expected according to temperature and component concentration (Hoche *et al.*, 2014), USV_{US}... USV determined from TOF and temperature-dependent sound propagation path, USV_{USc}... CO_2 corrected USV_{US}.

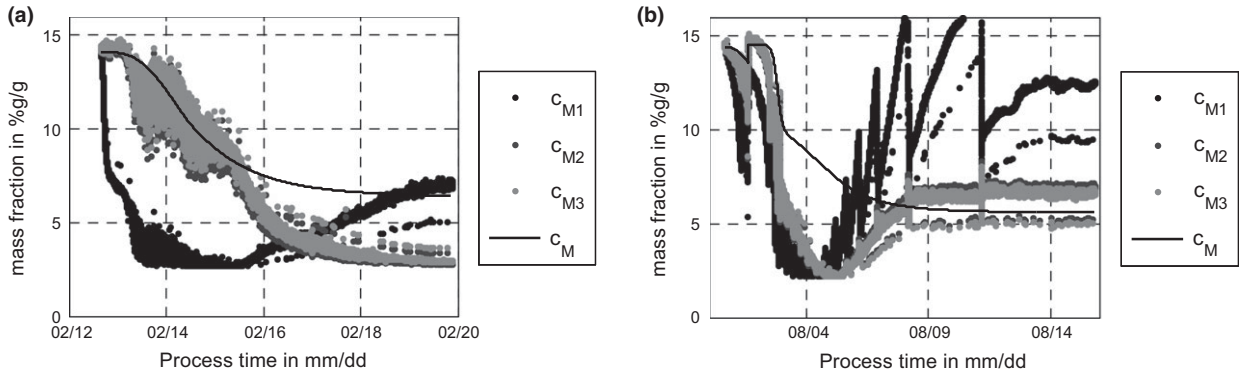

Figure 6 Sugar content, determined by the introduced sensor and the USV-*T* model for (a) VPS1 trial1 (cylindrical trial fermenter) and (b) VPS7 trial5 (cylindrico-conical tank); indices: M... expanded reference data, M1... no sound velocity (USV) correction, M2... only temperature correction according to 2.2, M3... temperature and CO_2 correction.

temperature range, the valid initial sugar content, or by introducing variables of higher order. But for processes like beer fermentation with varying raw material qualities and compositions, which may lead to sugar-type variations and significant sound velocity variations (Contreras *et al.*, 1992;Hoche *et al.*, 2014), further estimation variables ought to be chosen. On the other hand, for processes of more constant character or with higher concentration variations, the USV-*T* approach might be practical. In contrast, the USV-*T*-ρ model showed lower errors and a much better stability to process variations. The average RMSEs for the main fermentation ($RMSE_{fitM}$) were 0.53%g/g sugar content and 0.26%g/g ethanol content. In contrast, regarding the whole process ($RMSE_{fit}$), the mean RMSEs increased to 0.79%g/g sugar content and 0.39%g/g ethanol content due to temporarily higher deviations at strong changes of process conditions. As soon as the process condition stabilises again, also the error decreases.

Of course, the primary reasons of the noticed deviations are deviations of the basic model variables: sound velocity and density. One reason for deviations of the sound velocity from the expected, 'ideal' model values was already discussed explicitly and is considered in the calculations – dissolved CO_2. But, as with any correction, there are application constraints. Since the dissolved CO_2 is not measured by a sensor but estimated, mainly based on temperature and pressure, the value can differ from the true dissolved CO_2. But the true value at the point of measurement depends on time-dependent diffusion effects and the homogenisation of the tank content. So, a sudden pressure increase will not lead to a sudden increase in the dissolved CO_2 as it is assumed by the applied correction. In fact, it has to be distinguished between two main diffusion processes – the diffusion at the liquid–gas interface at the tank head volume and the diffusion from the bubble or yeast cell surface which is basically restricted to the main fermentation. As well, the CO_2 dissolution is not a purely

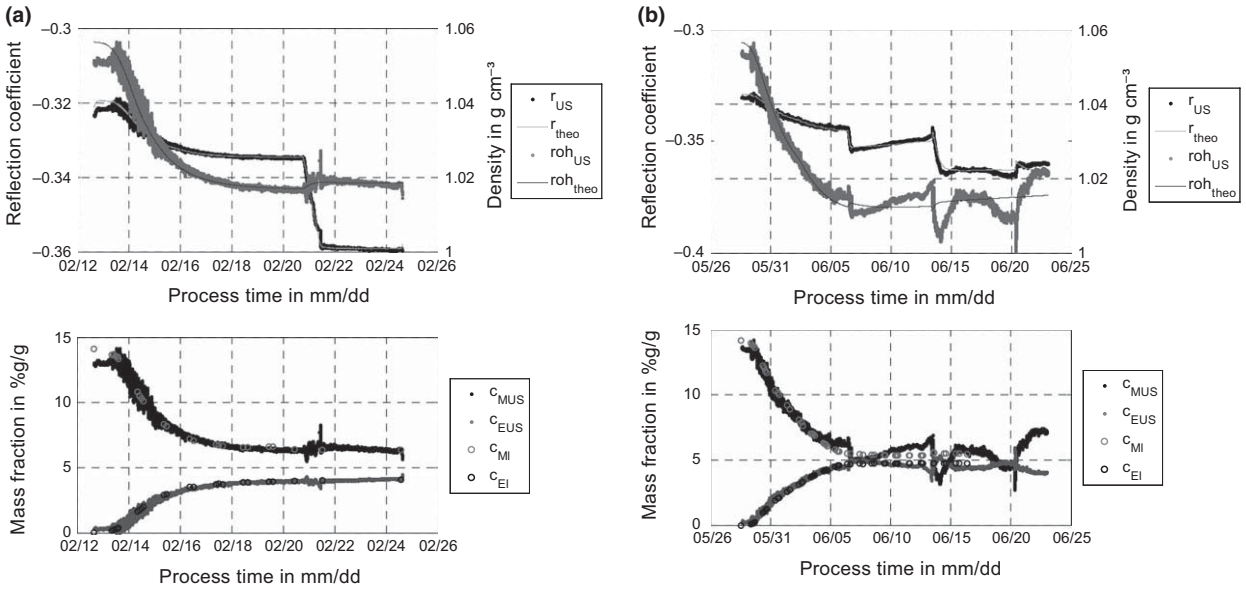

Figure 7 Reflection coefficient, density and component mass fractions determined by the introduced sensor and the USV-T-ρ model for (a) VPS1 trial1 (cylindrical trial fermenter) and (b) VPS7 trial3 (cylindrico-conical tank); r, reflection coefficient, c, mass fraction, rho, density; indices: l, laboratory results, US, measured via ultrasound sensor, theo, theoretical value according to laboratory reference and (Hoche *et al.*, 2014), E, ethanol, M, sugar.

Table 5 RMSE of sugar and ethanol content (USV-T-ρ model) in relation to the laboratory references ($RMSE_{lab}$), the expanded reference results ($RMSE_{fit}$) and to the expanded reference results but limited to the main fermentation ($RMSE_{fitM}$)

	Sugar, $RMSE_{lab}$ in %g/g						**Ethanol, $RMSE_{lab}$ in %g/g**					
Sensor	**VPS1**	**VPS3**	**VPS4**	**VPS5**	**VPS6**	**VPS7**	**VPS1**	**VPS3**	**VPS4**	**VPS5**	**VPS6**	**VPS7**
Buffer	**PMMA**	**PEEK**	**PEEK**	**PEEK**	**PMMA**	**PMMA**	**PMMA**	**PEEK**	**PEEK**	**PEEK**	**PMMA**	**PMMA**
Trial 1	0.37	–	–	–	–	–	0.15	–	–	–	–	–
Trial 2	0.63	–	–	–	–	–	0.30	–	–	–	–	–
Trial 3	0.65	1.03	0.74	0.64	1.15	0.48	0.28	0.51	0.29	0.38	0.47	0.20
Trial 4	0.51	2.27	1.73	0.78	0.46	0.71	0.19	0.60	0.91	0.34	0.23	0.27
	Sugar, $RMSE_{fit}$ in %g/g						**Ethanol, $RMSE_{fit}$ in %g/g**					
Trial 1	0.33	–	–	–	–	–	0.13	–	–	–	–	–
Trial 2	0.56	–	–	–	–	–	0.31	–	–	–	–	–
Trial 3	0.56	0.94	0.64	0.67	0.68	0.68	0.27	0.59	0.29	0.38	0.45	0.25
Trial 4	0.58	1.48	2.24	0.48	0.38	0.84	0.34	0.68	1.15	0.18	0.20	0.29
	Sugar, $RMSE_{fitm}$ in %g/g						**Ethanol, $RMSE_{fitm}$ in %g/g**					
Trial 1	0.48	–	–	–	–	–	0.19	–	–	–	–	–
Trial 2	0.53	–	–	–	–	–	0.31	–	–	–	–	–
Trial 3	0.54	0.78	0.44	0.73	0.57	0.37	0.23	0.29	0.25	0.40	0.46	0.17
Trial 4	0.52	0.36	0.47	0.72	0.58	0.45	0.15	0.17	0.27	0.26	0.30	0.22

physical dissolution due to the dissociation equilibrium as against carbonic acid. But, according to Rammert (1993), the increase in hydrogen carbonate is small compared to the rise of CO_2 concentration and can be neglected. Nevertheless, it exemplifies that a lot more concentrations of minor components can vary (basically every substance that is involved in the yeast nutrition) and that the model only considers major components. Finally, sound velocity deviations may be caused by temperature-dependent effects. Dependent on the local and seasonal conditions, varying temperature gradients may occur which can cause real sound

velocity gradients and reflector distance deviations due to faulty one-point measurements.

Although the sound velocity errors influence both the accuracy of the density and the component concentration, the main deviations originate from reflection coefficient-caused density deviations. Small reflection coefficient errors might be caused by noise or the limited signal resolution (Hoche *et al*., 2015). But the main reflection coefficient deviations occur particularly at sudden temperature changes. It is assumed that temperature gradients within the buffer material or at the interphase might cause an additional dispersion of the sound wave which is not considered by the diffraction correction. Further explanations of the noticed phenomena could be time delayed effects, for example temperature and dimension of the involved sensor parts or material, might change with a different velocity as recorded by the temperature sensor. The diffraction correction as described by Khimunin (1972) and Papadakis (1959) is based on the dimensionless characterisation of the signal's propagation path and relies on the sound velocities and the exact dimensional description.

Concerning the buffer material, both PEEK (Polyether ether ketone) and PMMA showed acceptable errors. In comparison, the results of the PMMA sensors showed better results which was expected due to a better sensitivity for density changes of the liquid. On the other hand, negative effects like property and dimensional changes due to water absorption (Hoche *et al*., 2014, 2015) could be avoided successfully by conditioning the materials in water prior to its usage. The comparison of calibration results before and after the trials showed a similar reflector distance. Furthermore, the calibration results of single sensors which showed exceptional bad results could be improved by replacing the transducer.

Concluding, the online monitoring of major component concentrations (sugar and ethanol) was applied successfully in anaerobe batch fermentation of malt-based solutions with yeast. The presented sensor system is feasible to determine all relevant variables via the MRM method with sufficient accuracy to determine the component mass fractions by the USV-T-ρ model. Overall a mass fraction error of 0.5%g/g maltose and 0.25%g/g ethanol is realistic. Lower errors can be expected at lower noise levels and higher signal resolutions. Definitely, the sensor system can be used to capture the process signature which may be related to product and process quality.

Funding

This research project was supported by the German Ministry of Economics and Technology (via AiF) and the WiFö (Wissenschaftsförderung der Deutschen Brauwirtschaft e.V., Berlin). Project AiF 16536 N.

Conflict of interest

The authors declare no conflict of interest.

References

Balling, C.J.N. (1865). Die Bierbrauerei. Prague (CHZ), Calve

Contreras, N.I., Fairly, P., McClements, D.J. & Povey, M.J.W. (1992). Analysis of the sugar content of fruit juices and drinks using ultrasonic velocity measurements. *International Journal of Food Science and Technology*, **21**, 515–529.

Fine, R.A. & Millero, F.J. (1973). Compressibility of water as a function of temperature and pressure. *The Journal of Chemical Physics*, **59**, 5529–5539.

Gepert, M. & Moskaluk, A. (2007). Acoustic and thermodynamic investigations of aqueous solutions of some corbohydrates. *Molecular and Quantum Acoustics*, **28**, 95–100.

Hoche, S., Hussein, W.B., Hussein, M.A. & Becker, T. (2011). Time-of-f light prediction for fermentation process monitoring. *Engineering in Life Sciences*, **11**, 1–12.

Hoche, S., Hussein, M.A. & Becker, T. (2013). Ultrasound-based density determination via buffer rod techniques: a review. *Journal of Sensors and Sensor Systems*, **2**, 103–125.

Hoche, S., Hussein, M.A. & Becker, T. (2014). Critical process parameter of alcoholic yeast fermentation: speed of sound and density in the temperature range 5–30 °C. *International Journal of Food Science and Technology*, **49**, 2441–2448.

Hoche, S., Hussein, M.A. & Becker, T. (2015). Density, ultrasound velocity, acoustic impedance, reflection and absorption coefficient determination of liquids via multiple reflection method. *Ultrasonics*, **57**, 65–71.

Khimunin, A.S. (1972). Numerical calculation of the diffraction corrections for the precise measurement of ultrasound absorption. *Acustica*, **27**, 173–181.

Lamberti, N. (2009). An ultrasound technique for monitoring the alcoholic wine fermentation. *Ultrasonics*, **49**, 94–97.

Liu, L. (1998). Acoustic properties of reservoir fluids. In: Department of Geophysics. Stanford University.

Marczak, W. (1997). Water as standard in the measurements of speed of sound in liquids. *The Journal of the Acoustical Society of America*, **102**, 2776–2779.

Papadakis, E.P. (1959). Correction for diffraction losses in the ultasonic field of a piston source. *The Journal of the Acoustical Society of America*, **31**, 150–152.

Rammert, M. (1993). Zur Optimierung von Hochleistungsabflülanlagen. In: Fachbereich 10, Maschinentechnik. Universität Gesamthochschule Paderborn.

Resa, P., Elvira, L. & Montero de Espinosa, F. (2004). Concentration control in alcoholic fermentation processes from ultrasonic velocity measurements. *Food Research International*, **37**, 587–594.

Resa, P., Elvira, L., de Espinosa, F.M., Gonzalez, R. & Barcenilla, J. (2009). On-line ultrasonic velocity monitoring of alcoholic fermentation kinetics. *Bioprocess and Biosystems Engineering*, **32**, 321–331.

Schöck, T. & Becker, T. (2010). Sensor array for the combined analysis of water–sugar–ethanol mixtures in yeast fermentations by ultrasound. *Food Control*, **21**, 362–369.

Spieweck, F. & Bettin, H. (1992). Review: solid and liquid density determination. *tm - Technisches Messen*, **59**, 285–292.

Urick, R.J. (1947). A sound velocity method for determining the compressibility of finely divided substances. *Journal of Applied Physics*, **18**, 983–987.

Wilson, W.D. (1959). Speed of sound in distilled water as a function of temperature and pressure. *Journal of the Acoustical Society of America*, **31**, 1067–1072.

3 Discussion

The ultrasound-based buffer methods have proven to be an adequate measurement method for non-invasive, non-destructive online process monitoring of important product attributes of the anaerobic fermentation. The relevance of the present study results from the limitations of previous research results: consideration of binary mixtures only in conjunction with the limited transferability to ternary mixtures, limited applicability of theoretical and semi-empirical models, the neglect of important process parameters and their process-specific variation, and ultimately the limited information due the scale limitation (Resa*, et al.* 2005; Contreras*, et al.* 1992; Vatandas*, et al.* 2007; Schöck and Becker 2010).

The present study combines the process and method-specific examination of relevant fluid properties with the application- and method-oriented optimisation of the sensor design. Based on intensive research work important boundary conditions for the experimental determination of the necessary properties of the ternary mixture, sugar-ethanol-water and for the validation of measurement methods could be acquired. In turn, key relations between sensor design, signal characteristic and the method's accuracy could be analyzed, based on the subsequent experiments. The conclusions of the tested sensor system and the developed models to describe the ternary mixture were decisive for the promising results of the final validation tests in pilot plant scale.

Concerning the sensor design the main methodological findings of the experimental determination of relevant fluid properties were:

- the confirmation that the calibration of the exact reflector-distance as well as the consideration of thermal dimensional changes (or the general predictability of dimensional changes) are of significant importance for the accuracy of the measurement method,
- that the combination of acoustic soft and hard materials represents a conditional necessity in the used method to guarantee optimal signal characteristics and a reasonable reflection coefficient resolution,

- and that the stability to polar liquids of all materials involved at different temperatures and dwell times should be sufficiently high.

Particularly in the interpretation of the measurement path for determining the ultrasonic velocity for many acoustically soft materials (mostly plastics) the last requirement often is an exclusion criterion. The mass transport into the material causes time depending dimensional changes which hardly can be predicted exactly. Furthermore, the inclusion of additional foreign molecules is often associated with changes of material properties. Indeed, a relevant change in density can be excluded for most of the plastics based on the available data. Nevertheless, Drotning and Roth (1989) have shown that the thermal expansion changes with water content which indicates the variation of mechanical properties and therefore as well of the sound velocity. Nevertheless, clear indications in what extend the variation of moisture content affects the acoustic properties, particularly the ultrasonic velocity, are not available. A more detailed, scientifically grounded study of this problem could not be carried out within this work. But the final, practical examinations suggest that within certain limits the use of such materials is possible by conditioning (setting a sufficiently high degree of saturation) of the hygroscopic buffer material and sufficiently constant conditions of operation.

Based on the experimental data eventually, the accuracy of the methods and sensor technology could be determined in relation to the applied reference data and analytics. In addition to the density and the ultrasound speed, the MRM buffer method also provides the determination of the reflection coefficient and the specific acoustic impedance. Thereby three measures available are available for the description of the concentration proportions of water-sugar-ethanol mixture, which in combination with temperature and ultrasonic velocity allow a unique definition of the individual component concentrations within the ternary mixture. In addition, besides the absolute characteristics of the measured variables the differences to reference values might be used for the generation of models, e.g. the difference to the variable at similar temperature but water as fluid or the difference to the variable value of water at 20 ° C in water; so all together nine models are available which allow a reasonable description of the target variables.

An overview of the indices used to describe the models is shown in Table 3-1. The mean square error of the individual parameters resulting from the validation, or in the case of temperature, the in practice expected error are summarised in Table 3-2 and are referred to as standard errors in the following paragraphs. Although the assumed error values are strictly valid only for developed measurement cell for the experimental determination of fluid properties (see 2.2.2), but for the sensor system employed in the final trial comparable, still rather lower errors are expected, so that the estimate of the total error based on the standard error is appropriate.

Table 3-1: Indices legend describing the models and the error variables considered in the error calculation; e.g.: M1DA – maltose model by means of the absolute values of temperature, ultrasonic velocity and density with error amounts of all model variables considering.

Indices	Description	Ausprägungen
C	mass fraction of a component	M – maltose mass fraction in %g/g
		E – ethanol mass fraction in %g/g
i	model-type	1 – abs: absolute values
		2 – ref: reference to water at measured temperature
		3 – r20: reference to water at 20 °C
k	modification-variable (MV)	D, R, Z (description see EV)
EV	error variable	U – ultrasound velocity
		T – temperature
		D – density
		R – reflection coefficient
		Z – specific acoustic impedance
		A – all model variables

Table 3-2: The standard error of the different measured variables as assumed for the error calculation.

model variable	U	T	MV
standard-Error, SE	0.1 m/s	0.1 °C	SE(MV)
modifications-variable (MV)	**D**	**R**	**Z**
SE(MV)	1.2E-3 g/cm³	5.E-04	1.8 E3 kg/(s·m²)

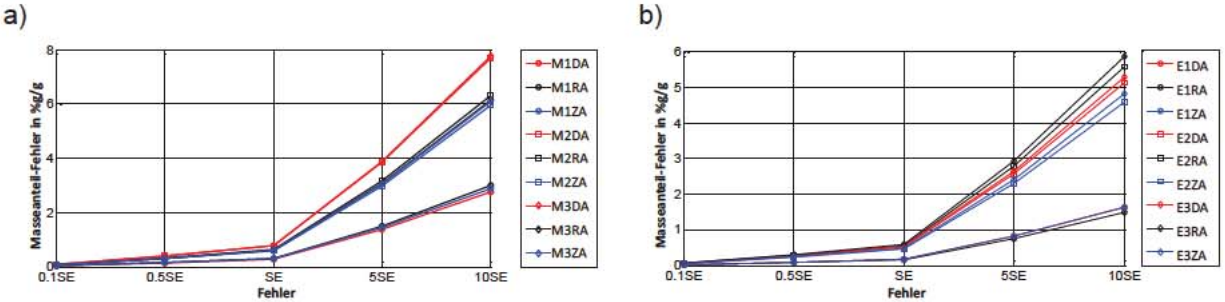

Figure 3.1: Comparison of different modeling approaches taking into account the standard error values of all model variables; a) maltose mass fraction, b) ethanol mass fraction.

By comparison (see Figure 3.1) the absolute value models show for both component concentrations, the smallest deviations. Within the absolute value models, there is no

(see Figure 3.1b E3DA vs. E3RA) or only very slight differences. A detailed comparison with respect to the error amounts of the individual variables (see Figure 3.2) shows that the density and impedance model have a greater stability to temperature errors and the density model shows better stability to deviations of the ultrasonic velocity.

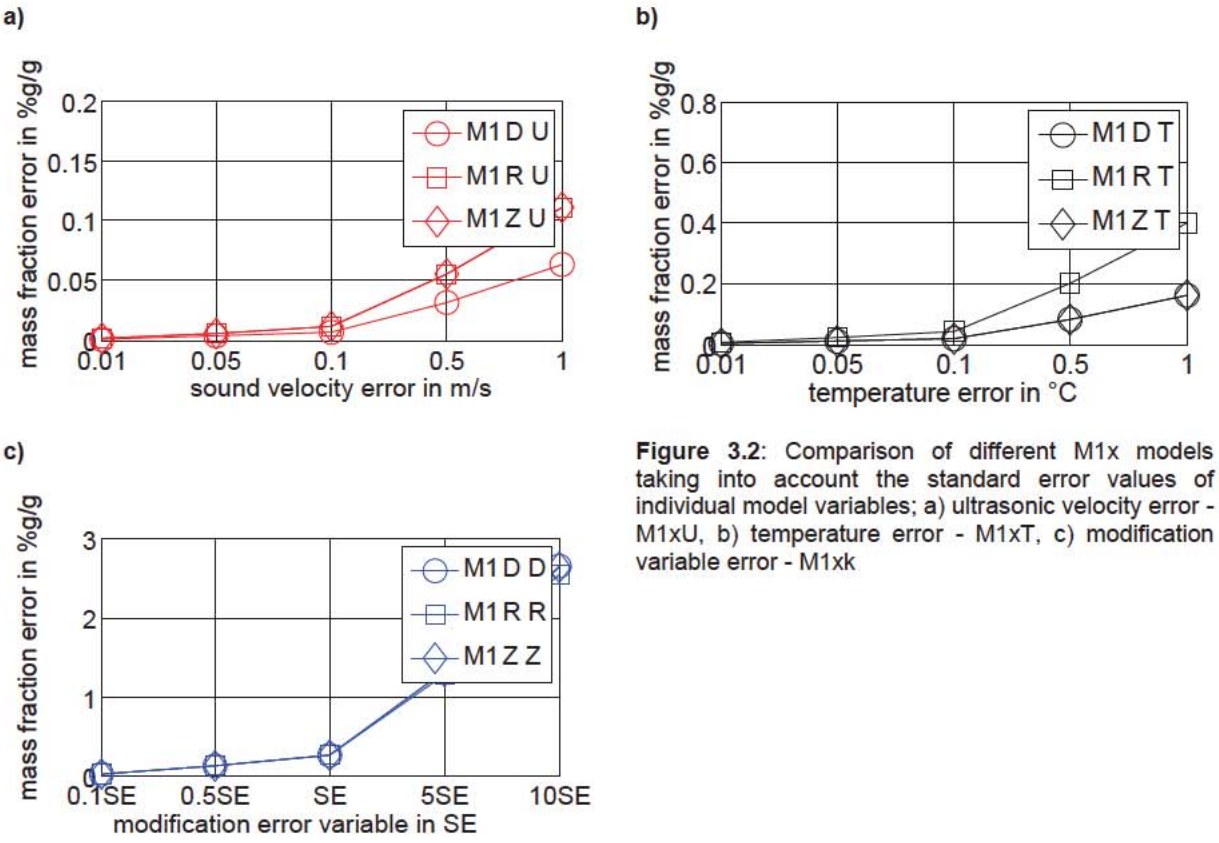

Figure 3.2: Comparison of different M1x models taking into account the standard error values of individual model variables; a) ultrasonic velocity error - M1xU, b) temperature error - M1xT, c) modification variable error - M1xk

In the end, for the final validation trials tests the absolute value models with the variables density, temperature, and ultrasonic velocity were considered to determine the component concentrations. The experimental results of the final application trials confirm the estimated errors and the immense influence of the density measurement accuracy.

In addition to the multivariate linear models, a further, from the literature known, semi-empirical approach has been studied (Becker, *et al.* 2001; Lamberti 2008; Resa, *et al.* 2004). Basically this approach is based on the prediction of the concentration ratios based on the typical reaction equilibrium that can be expected for anaerobic yeast fermentation. Based on clearly defined start conditions only uniquely defined concentration ratios may arise during the process. Therefore, it

should theoretically be possible to determine the concentration ratios uniquely on the basis of the known start conditions and the current differences of relevant process variables to its characteristics at start time. Thus, the model can be reduced to two parameters only (temperature and ultrasonic velocity).

On the one hand previously published data show unsatisfactory accuracy and on the other hand partially contradictory statements. Partial over the process time falling sound velocity trends are reported (Resa*, et al.* 2004; Lamberti 2008) and in other studies rising trends (Becker*, et al.* 2001; Hoche*, et al.* 2016). A detailed analysis for various boundary conditions (initial sugar concentration, temperature) using the multivariate model shows that both trends are theoretically possible. Fermentations of maltose solutions at a temperature of about 25 ° C show an ultrasound velocity trend which in relation to the component concentrations is nonsignificant. At temperatures above that a gradual decrease, at temperatures below a steady increase of the speed of sound is perceptible. To establish a generally applicable model of good precision is relatively difficult and the accuracy of the results correspondingly low. For limited temperature ranges with significant changes in the speed of sound (and preferably constant process temperatures) models can be implemented presumably with good accuracy.

The final practical trials in pilot plant scale demonstrate the advantages of multivariate linear model compared with the semi-empirical approach. Likewise, significant for the method accuracy critical process sections could be characterised. In particular, the drop in temperature to initialise the maturation phase shows strong deviations from the on the basis of laboratory data extrapolated, ideal characteristic of process course. At the same time the deviations are much more distinct compared with the comparative experiments with the test fermenter. Comparing both process courses, two major differences arise as potential evidence for the observed deviations. The test fermenter has significantly lower dimensions compared to the CCTs of the research brewery, so that a more homogeneous distribution and circulation in test fermenter can be expected. Likewise, technologically-related differences arose in the course of the pressure curve result. The multivariate model is indeed relatively insensitive to variations of the ultrasonic velocity compared with the standard error of the measurement system: 1 m/s deviation will cause only about

0.1% g/g difference in maltose mass fraction (see Figure 3.2). But greater deviations of the speed of sound could explain the observed deviations thoroughly. In addition, the CO_2 correction of sound speed is solely based on the theoretical estimation of the CO_2 content at prevailing process conditions and thus based on the assumption of a state of equilibrium. However, arise rapid changes in temperature or pressure, it cannot be expected that the amount of dissolved CO_2 adapts to its new state of equilibrium as quickly as the process changes. The alignment with the theoretically assumed equilibrium is significantly slower, especially considering diffusion from the gas-filled head volume in high tanks.

Another, not completely negligible aspect is the convective circulation, which can cause higher flow velocities particularly in the vicinity of the tank wall during strong cooling processes (compare with Papanicolaou and Belessiotis (2002); Lin and Armfield (1999)). The flow at right perpendicular to the propagation direction of the sound causes a displacement of the sound beam (Lynnworth 2013). Similar to the diffraction effects, not the complete portion of the reflected energy reaches the receiver and according to the theory results in an unconsidered deviation which causes amplitude and therefore reflection coefficient errors. Ultimately, however, both sources of error are of importance for fast, dynamic process changes only. With progressive process time and convergence to the equilibrium state the error amounts reduce.

In general, the discussed phenomena are only of subordinated importance for the aimed industrial application. The monitoring of the main fermentation is possible with adequate accuracy, so that an online fermentation monitoring can be provided which is conform to the hygiene standards.

4 References

Annemüller, G. & Manger, H. J. (2009). Gärung und Reifung des Bieres: Grundlagen, Technologie, Anlagentechnik. VLB.

Becker, T., Mitzscherling, M. & Delgado, A. (2001). Ultrasonic Velocity - A Noninvasive Method for the Determination of Density during Beer Fermentation. *Engineering in Life Sciences,* **1,** 61-67.

Belogol'skii, V. A., Sekoyan, S. S., Samorukova, L. M., Stefanov, S. R. & Levtsov, V. I. Pressure dependence of the sound velocity in distilled water. *Measurement Techniques,* **42,** 406-413.

Benedetto, G., Gavioso, R. M., Giuliano Albo, P. A., Lago, S., Madonna Ripa, D. & Spagnolo, R. (2003). Speed of Sound of Pure Water at Temperatures between 274 and 394 K and Pressures up to 90 MPa. In: Fifteenth Symposium on Thermophysical Properties, . Boulder, Colorado, U.S.A.

Bhatia, A. B. (2012). Ultrasonic Absorption: An Introduction to the Theory of Sound Absorption and Dispersion in Gases, Liquids and Solids. New York, Dover Publications.

Bjørndal, E. & Frøysa, K. E. (2008). Acoustic Methods for Obtaining the Pressure Reflection Coefficient from a Buffer Rod Based Measurement Cell. *IEEE Trans UFFC,* **55,** 1781-1793.

Brand, S. (2004). Ultraschallspectroskopie an fokussierenden Systemen unter Berücksichtigung vorgelagerter absorbierender Schichten. Otto-von-Guericke-Universität Magdeburg, Universitätsbibliothek.

Brunn, S. G., Sørensen, P. G. & Hvidt, A. (1974). Ultrasonie Properties of Ethanol-Water Mixtures. *Acta Chemica Scandinavica A,* **28,** 1047-1054.

Cheeke, J. D. N. (2012). Fundamentals and Applications of Ultrasonic Waves, Second Edition. Taylor & Francis.

Contreras, N. I., Fairly, P., McClements, D. J. & Povey, M. J. W. (1992). Analysis of the sugar content of fruit juices and drinks using ultrasonic velocity measurements. *International Journal of Food Science and Technology,* **21,** 515-529.

D'Arrigo, G., Mistura, L., and Tartaglia, P. (1974). " Sound Propagation in the Binary System Aniline-Cyclohaxane in the Critical Region. *Physical review A,* **1,** 286-295.

D'Arrigo, G. & Paparelli, A. (1988). Sound propagation in water–ethanol mixtures at low temperatures. I. Ultrasonic velocity. *Journal of Chemical Physics,* **88,** 405-415.

Drotning, W. D. & Roth, E. P. (1989). Effects of moisture on the thermal expansion of poly(methylmethacrylate). *Journal of Materials Science,* **24,** 3137-3140.

Dukhin, A. S. & Goetz, P. J. (2002). Ultrasound for Characterizing Colloids: Particle Sizing, Zeta Potential, Rheology. Elsevier.

Fine, R. A. & Millero, F. J. (1973). Compressibility of water as a function of temperature and pressure. *The Journal of Chemical Physics,* **59,** 5529-5539.

Flood, A. E., Addai-Mensah, J., Johns, M. R. & White, E. T. (1996). Refractive Index, Viscosity, Density, and Solubility in the System Fructose + Ethanol + Water at 30, 40, and 50 °C. *J. Chem. Eng. Data,* **41,** 418-421.

US. Food and Drug Administration (2004). Guidance for Industry, PAT - a framework for innovative pharmaceutical development, manufacturing, and quality assurance.

Gepert, M. & Moskaluk, A. (2007). Acoustic and thermodynamic investigations of aqueous solutions of some corbohydrates. *Molecular and Quantum Acoustics,* **28,** 95-100.

Henning, B., Prange, S., Dierks, K., Daur, C. & Hauptmann, P. (2000). In-line concentration measurement in complex liquids using ultrasonic sensors. *Ultrasonics,* **38** 799–803.

Hoche, S., Hussein, M. A. & Becker, T. (2014). Critical process parameter of alcoholic yeast fermentation: speed of sound and density in the temperature range 5–30 °C. *International Journal of Food Science and Technology,* **49,** 2441–2448.

Hoche, S., Krause, D., Hussein, M. A. & Becker, T. (2016). Ultrasound-based, in-line monitoring of anaerobe yeast fermentation: model, sensor design and process application. *International Journal of Food Science & Technology,* **51,** 710-719.

Kell, G. S. (1975). Density, Thermal Expansivity, and Compressibility of Liquid Water from 0° to 150°C: Correlations and Tables for Atmospheric Pressure and Saturation Reviewed and Expressed on 1968 Temperature Scale. *Journal of Chemical and Engineering Data,* **20,** 97-105.

Kell, G. S. (1977). Effects of isotopic composition, temperature, pressure and dissolved gases on the density of liquid water. *J. Phys. Chem. Ref. Data,* **6,** 1109–1131.

Khimunin, A. S. (1972). Numerical calculation of the diffraction corrections for the precise measurement of ultrasound absorption. *Acustica,* **27,** 173-181.

Kinsler, L. E. (2000). Fundamentals of acoustics. Wiley.

Lamberti, N. (2008). An ultrasound technique for monitoring the alcoholic wine fermentation. *Ultrasonics*.

Liley, P. E., Thomson, G. H., Friend, D. G., Daubert, T. E. & Buck, E. (1997). Physical and chemical data. In: Perry's Chemical Engineers' Handbook (edited by PERRY, R. H., GREEN, D. W. & MALONEAY, J. O.). Pp. 204. New York: McGraw-Hill.

Lin, W. & Armfield, S. (1999). Direct simulation of natural convection cooling in a vertical circular cylinder. *International Journal of Heat and Mass Transfer,* **42,** 4117-4130.

Litovitz, T. A. & Davis, C. M. (1965). 5 - Structural and Shear Relaxation in Liquids. In: Physical Acoustics (edited by WARREN P, M.). Pp. 281-349. Academic Press.

Liu, L. (1998). Acoustic properties of reservoir fluids. In: Department of Geophysics. Stanford University.

Lynnworth, L. C. (2013). Ultrasonic measurements for process control: theory, techniques, applications. Academic press.

MEBAK (2012). Würze, Bier, Biermischgetränke: Methodensammlung der Mitteleuropäischen Brautechnischen Analysenkommission. Freising-Weihenstephan, Jacob, F.

Narziss, L. & Back, W. (2009). Die Bierbrauerei: Band 2: Die Technologie der Würzebereitung. Wiley.

Natta, G. & Baccaredda, M. (1948). Sulla velocità di propagazione degli ultrasuoni nelle miscele ideali. *Atti Accad. Nazionale di Lincei Roma,* **4**.

Nomoto, O. (1958). Empirical formula for sound velocity in liquid mixtures. *Journal of the Physical Society of Japan,* **13,** 1528-1532.

Papadakis, E. P., Fowler, K. A. & Lynnworth, L. C. (1973). Ultrasonic attenuation by spectrum analysis of pulses in buffer rods: Method and diffraction corrections. *The Journal of the Acoustical Society of America,* **53,** 1336-1343.

Papanicolaou, E. & Belessiotis, V. (2002). Transient natural convection in a cylindrical enclosure at high Rayleigh numbers. *International Journal of Heat and Mass Transfer,* **45,** 1425-1444.

Resa, P., Elvira, L., de Espinosa, F. M., Gonzalez, R. & Barcenilla, J. (2009). On-line ultrasonic velocity monitoring of alcoholic fermentation kinetics. *Bioprocess and Biosystems Engineering,* **32,** 321–331.

Resa, P., Elvira, L. & Montero de Espinosa, F. (2004). Concentration control in alcoholic fermentation processes from ultrasonic velocity measurements. *Food Research International,* **37,** 587-594.

Resa, P., Elvira, L., Montero de Espinosa, F. & Gomez-Ullate, Y. (2005). Ultrasonic velocity in water-ethanol-sucrose mixtures during alcoholic fermentation. *Ultrasonics,* **43,** 247-252.

Schöck, T. & Becker, T. (2010). Sensor array for the combined analysis of water–sugar–ethanol mixtures in yeast fermentations by ultrasound. *Food Control,* **21,** 362-369.

Urick, R. (1947). A sound velocity method for determining the compressibility of finely divided substances. *Journal of Applied Physics,* **18,** 983-987.

Vatandas, M., Koc, A. B. & Koc, C. (2007). Ultrasonic velocity measurements in ethanol–water and methanol–water mixtures *European Food Research and Technology,* **225,** 525-532.

Weyns, A. (1980a). Radiation field calculations of pulsed ultrasonic transducers: Part 1: Planar circular, square and annular transducers. *Ultrasonics,* **18,** 183-188.

Weyns, A. (1980b). Radiation field calculations of pulsed ultrasonic transducers: Part 2: spherical disc-and ring-shaped transducers. *Ultrasonics,* **18,** 219-223.

Wilson, W. D. (1959). Speed of Sound in Distilled Water as a Function of Temperature and Pressure. *Journal of the Acoustical Society of America,* **31,** 1067-1072.

Zemanek, J. (1971). Beam behavior within the nearfield of a vibrating piston. *The Journal of the Acoustical Society of America,* **49,** 181-191.